NASA CR-121089
AE-71-023-9

VISCOSEAL PERFORMANCE WITH RAREFIED-GAS SEALANT

by Mancil W. Milligan

UNIVERSITY OF TENNESSEE

prepared for

NATIONAL AERONAUTICS AND SPACE ADMINISTRATION

NASA Lewis Research Center
Grant NGL 43-001-023

1 Report No	2 Government Accession No	3 Recipient's Catalog No
NASA CR-121089		

4 Title and Subtitle	5 Report Date
VISCOSEAL PERFORMANCE WITH RAREFIED-GAS SEALANT	April 1973
	6 Performing Organization Code

7 Author(s)	8 Performing Organization Report No
Mancil W. Milligan	AE-71-023-9
	10 Work Unit No

9 Performing Organization Name and Address	11 Contract or Grant No
University of Tennessee Knoxville, Tennessee	NGL 43-001-023
	13 Type of Report and Period Covered
12 Sponsoring Agency Name and Address	Contractor Report
National Aeronautics and Space Administration Washington, D. C. 20546	14 Sponsoring Agency Code

15 Supplementary Notes

Project Manager, Lawrence P. Ludwig, Fluid System Components Division, NASA Lewis Research Center, Cleveland, Ohio

16 Abstract

A fundamental study of viscoseals having a rarefied gas as the sealant has been conducted. Both experimental and analytical investigations are reported. Three different analytical models have been formulated and are described in detail. An experimental investigation has been conducted on multiple grooved two-inch diameter viscoseals over a wide range of gas densities and shaft speeds up to 30 000 rpm. Comparisons are presented between actual viscoseal performance and the theoretical predictions for both sealing coefficient and net leakage parameters as functions of the degree of gas rarefication. Recommendations are presented for the use of the analytical models.

17 Key Words (Suggested by Author(s))	18 Distribution Statement
Molecular seal Low density gas flow Rarefied flow	Unclassified - unlimited

19 Security Classif (of this report)	20 Security Classif (of this page)	21 No of Pages	22 Price*
Unclassified	Unclassified	114	$3.00

* For sale by the National Technical Information Service, Springfield, Virginia 22151

TABLE OF CONTENTS

NOMENCLATURE

a	Groove aspect ratio, b'/h
a'	Hypothetical groove aspect ratio
A	Groove cross sectional area
A'	Rotor induced flow coefficient
A_c	Annulus flow coefficient
A_L	Dimensionless annulus flow coefficient
A_{LC}	Continuum limit of A_L
A_m	Manometer cross section area
A_p	Groove pressure flow coefficient
A_u	Rotor induced flow coefficient
b	Groove axial width
b'	Groove normal width, $b \cos \alpha$
B	Groove flow coefficient
c	Radial seal clearance
$\bar{c}$	Mean radial clearance
D	Shaft diameter
G	Slip coefficient constant of proportionality
h	Groove depth
H	Manometer total deflection
H_1, H_2	Manometer deflections
K, k	Boltzmann constant
K'	Seal radius ratio, $1 - 2c/d$
ℓ	Flow passage length coordinate
ℓ'	Tube length coordinate
ℓ_g	Groove length coordinate

ℓ_L	Land length coordinate
ℓ_t	Total groove length on seal
L	Seal axial length
m	Sealant mass per molecule
$\dot{m}$	Sealant mass flow rate
M	Sealant molecular weight
n	Molecular density, N/V
n_ℓ	Number of thread lands in seal section
N	Number of molecules
$\dot{N}$, $\dot{n}$	Sealant molecular flow rate
$\overline{N}$	Seal speed, rpm
N_K	Knudsen number, λ/c
N_{Kg}	Groove Knudsen number, λ/b'
N_{Kh}	Knudsen number based on groove depth, λ/h
N_s	Number of groove starts
N_t	Total turns of spiral on seal
P	Absolute pressure
$\overline{P}$	Average seal pressure, $(P_1 + P_2)/2$
P_o	Atmospheric pressure
P_T, P_2	Upstream seal pressure
P_b, P_1	Downstream seal pressure
ΔP	Differential pressure across seal, $P_T - P_b$
Q	Sealant volumetric flow rate
Q'	Volume flow rate at unit pressure, V'P
Q'_g	Volume flow rate at unit pressure in groove
Q'_L	Volume flow rate at unit pressure over land

Q'_N	Net volume flow rate at unit pressure
Q'_R	Rotor induced volume flow rate at unit pressure
r_1	Inner radius of annulus (shaft)
r_2	Outer radius of annulus (housing)
r_p	Seal pressure ratio, P_T/P_b or P_2/P_1
R	Distance ratio, r/b'
RR	Distance ratio, rr/b'
R_o	Universal gas constant
t	Tangent of helix angle α
Δt	Flow measurement time increment
T	Absolute temperature
u,v,w	Velocity components in ξ, η, z coordinates
$\bar{u}$	Average rotor induced velocity
U	Surface velocity
u'	Dimensionless groove flow velocity
U_e	Effective rotor velocity
v'	Groove flow velocity
v_R	Rotor induced flow velocity
v'_R	Rotor induced flow velocity in hypothetical groove
V	Volume
$\bar{V}$	Mean molecular speed
V'	Volume flow rate
V_g	Total groove volume flow rate
V'_g	Volume flow rate in a single groove
V'_{gc}	Continuum limit of V'_g
V_L	Land leakage volume flow rate

V_o	Calibrated volume
V_T	Total volume flow rate in seal
w	Land axial width
w'	Land normal width, w cos α
W	Manometer fluid specific weight
α	Seal helix angle, $\sin^{-1}\left[\frac{n_s(b' + w')}{\pi D}\right]$
α_n	Eigenvalue
β	Seal geometric parameter, (h + c)/c
β'	Tube flow coefficient
γ	Seal geometric parameter, b/(a + b)
γ'	Tube flow coefficient
ζ	Coefficient of slip
λ	Mean free path
Λ	Sealing coefficient
μ	Absolute viscosity
μ_{Hg}	Pressure unit, micron of mercury
ρ	Density
σ	Ratio of molecular collisions
τ	Elemental volume
ψ	Rarefied viscoseal parameter
ω	Solid angle
Ω	Angular velocity

Special Subscripts

r	Refers to land
g	Refers to groove
ξr	Refers to ξ direction in region of land

ηr	Rerers to η direction in region of land
ξg	Refers to ξ direction in region of groove
ηg	Refers to η direction in region of groove
y	Refers to axial component

1. INTRODUCTION

An investigation of rarefied, internal gas dynamics with emphasis on shaft sealing applications was initiated on May 1, 1966 at the University of Tennessee in the Department of Mechanical and Aerospace Engineering. The investigation was conducted for the National Aeronautics and Space Administration under Research Grant 43-001-023. This report is the final report of this investigation with major emphasis on the rarefied-gas viscoseal.

The initial efforts were directed at a number of basic problems. The results of these investigations have previously been documented and only the references will be repeated here. These investigations concerned rarefied flow through short tubes (1,2), annuli (3,4), long square tubes (5), and other basic geometries (6-8). From these investigations a more complete understanding of rarefied flow has provided the basis for analysis of more complex applications.

The major effort of this study has been directed to developing analytical models which can be used to predict the performance of viscoseals operating with a rarefied gas as the sealant. Since no experimental data were available which were adequate for establishing the validity of analytical models a significant portion of this effort has been devoted to the development of such data. This report details the analytical models which were developed and also the experimental procedures and results. Conclusions are presented based on the comparison of results from analytical models with experimental results.

2. ANALYTICAL MODELS

Three different analytical models have been developed in this investigation and will be presented in detail. The first is based on

Hodgson's (9) work and is called the modified Hodgson Model. The next model is based on the work of Boon and Tal (10) and is called the Slip Modified Boon and Tal Model. The third model is based on a superposition of the groove and annulus flow components and is called the Annulus-Groove Model.

2.1 Modified Hodgson Model

In Hodgson's (9) investigation only seals with a single thread start were considered. The development presented follows closely that of Hodgson but the analysis has been generalized to include multiple thread start seals and also a technique is presented for solving the specific molecular flow rate equation for a sealed condition.

Hodgson chose to analyze the particular configuration where a smooth shaft rotates within a grooved housing. It will be shown later that the analysis for the grooved shaft and smooth housing is identical to this configuration. This being the case, Hodgson's model is not as restricted in this respect as it might appear.

Hodgson considers the flow in the viscoseal to be composed of three basic components: (1) the pressure induced flow along the groove, (2) the pressure induced flow over the lands, and (3) the rotor induced flow in the groove. This treatment of the flow is quite common and is exactly the way King (11) chose to divide the flow for analytical considerations. Figure 1 shows a representation of the flow components, Q'_L, Q'_R, and Q'_g represent the pressure induced land flow, the rotor induced groove flow and the pressure induced groove flow, respectively. Hodgson also restricts his considerations to a seal with a single thread start.

In his development of the two pressure induced flow components, he takes the semi-empirical approach of Knudsen (12) in describing the flow throughout the entire regime from continuum to free-molecule flow. In his long tube work Knudsen found that his experimental data could be described by an equation of the form

$$Q' = [\gamma' P + \beta' \frac{1 + \nu P}{1 + \xi P}] \frac{dP}{d\ell'} \qquad (1)$$

In the continuum limit Knudsen reduced Equation (1) to $Q' = \gamma' P \frac{dP}{d\ell'}$, and by equating this to the known continuum solution, he was able to determine γ'. In a similar manner as the free-molecule limit was approached he reduced Equation (1) to $Q' = \beta' \frac{dP}{d\ell'}$, and by equating this to the known free-molecule solution he determined β'. By considering the slip flow regime, Knudsen was able to determine the ratio ν/ξ' by noting that Equation (1) becomes $Q' = (\gamma' P + \beta' \frac{\nu}{\xi'}) \frac{dP}{d\ell'}$, and equating this to the known continuum with slip solution. Next Knudsen determined the difference $\xi' - \nu$ from a consideration of nearly free molecule flow and thus was able to determine both ξ' and ν. He then applied experimentally determined corrections to ξ' and ν so that the experimentally observed minimum in the $Q'/\Delta P$ versus P curve would be correctly predicted. Knudsen applied the analysis above to a long circular tube. In his analysis Hodgson applies the identical procedure to his treatment of the pressure induced flow in the groove (a long rectangular duct) and the pressure induced flow over the lands which he takes to be a narrow slit.

2.11 Pressure Induced Flow in the Seal Groove. Hodgson assumes that the pressure varies continuously along the axis of the seal groove from a value of P_2 at the high pressure end to P_1 at the other end. In order to determine the pressure gradient

gradient along the groove axis, it is necessary to relate the length of the groove, ℓ_g, to the seal length, L. A development of a viscoseal is shown in Figure 2. Hodgson only considered seals with a single thread. The development that follows is generalized to any number of thread starts, n_s.

In Figure 2 line $\overline{AB}$ is drawn perpendicular to the grooves. The number of turns of spiral that $\overline{AB}$ crosses is equal to the total number, N_t, of complete turns on the seal which can be expressed as

$$N_t = \frac{L \cos \alpha}{w' + b'} .$$

The length of groove per turn of spiral is $\pi D/\cos \alpha$. The total groove length on the seal is

$$\ell_T = \frac{\pi D}{\cos \alpha} \cdot \frac{L \cos \alpha}{w' + b'} = \frac{L\pi D}{w' + b'} .$$

The length of each groove is then

$$\ell_g = \frac{\ell_T}{N_s} = \frac{L\pi D}{N_s(w' + b')} .$$

It follows that

$$\frac{dP}{d\ell_g} = \frac{dP}{D\left[\frac{L\pi D}{N_s(w' + b')}\right]} = \frac{N_s(w' + b')}{\pi D} \frac{dP}{dL} .$$

Hodgson indicates that the groove pressure gradient in a single threaded seal is

$$\frac{dP}{d\ell_g} = \frac{w' + b'}{\pi D} \frac{dP}{dL}$$

from which it follows that the flow in a groove of a multi-threaded seal is N_s times the flow in the groove of a single threaded seal of the same groove width, land width and diameter. Since there are N_s of

these grooves, the total groove flow in the multi-threaded seal is N_s^2 time the flow in a comparable single threaded seal. The total groove flow is then

$$Q'_g = N_s^2[(BP + C\frac{1 + C_1P}{1 + C_2P})\frac{dP}{dL}], \tag{2}$$

where the bracketed term is the single threaded groove flow developed by Hodgson. The constants B, C, C_1, and C_2 depend on the geometry of the seal and the properties of the sealant and are given in Appendix A. Appendix A also contains a discussion of the flow models used by Hodgson to obtain these constants.

2.12 Pressure Induced Flow Over the Lands. Based on the assumption that the pressure varies continuously along the helical groove, Hodgson shows that the effective pressure gradient for the land flow is

$$\frac{dP}{d\ell_L} = \frac{w' + b'}{w'} \cos \alpha \frac{dP}{dL} .$$

This pressure gradient applies equally well to both the single and multi-threaded seal. The land leakage flow for a seal of any number of threads is then

$$Q'_L = [D'P + E\frac{1 + C_3P}{1 + C_4P}]\frac{dP}{dL} \tag{3}$$

where the constants D', E, C_3 and C_4 also depend on the seal geometry and the properties of the sealant and are given in Appendix A along with a discussion of their origin.

2.13 Rotor Induced Flow. Hodgson takes a simplified approach to the prediction of the rotor induced flow. In Figure 3 a groove cross section is shown with the rotor moving over the top of the groove. Hodgson develops the rotor induced flow on a molecular basis, but as he

points out a continuum approach yields the same result. It is assumed that the rotor induced flow is the same as the flow obtained in a long rectangular duct of width b' and height h in which the upper wall moves with velocity U cos α (the component of the circumferential velocity of the rotor along the axis of the groove). Rather than solve the describing differential equation for parallel flow, Hodgson chooses to compute the volume flow based on an area-weighted average velocity. This average velocity is

$$\bar{u} = \frac{(U \cos \alpha)b' + (2h + b')(0)}{2(b' + h)} = \frac{Ub'}{2(b' + h)} \cos \alpha.$$

The total rotor induced flow is thus

$$Q'_R = N_s \left[\frac{Ub^2h}{2(b' + h)} \cos \alpha\right] P = N_s A' P \qquad (4)$$

where Q'_R is generalized to a multi-threaded seal.

2.14 Total Seal Flow. The flow rates given by Equations (2, 3, and 4) are superimposed to give the total flow in the seal which can be expressed as

$$Q'_N = - N_s^2 \left[BP + C \frac{1 + C_1P}{1 + C_2P}\right] \frac{dP}{dL} - \left[D'P + E \frac{1 + C_3P}{1 + C_4P}\right] \frac{dP}{dL} - N_s A' P \qquad (5)$$

where flow in the direction of decreasing pressure is considered positive.

2.15 Solution of the Modified-Hodgson Equation. Unlike Hodgson's basic equation, Equation (5) is applicable to a seal with any number of threads. There are three solutions to Equation (5) which are of particular interest. These three cases are: (1) the flow rate through a non-rotating seal, (2) the flow rate through a rotating seal, and (3) the pressure difference across a rotating seal when the net flow is zero.

Flow Rate in a Static Seal

The volume flow rate at unit pressure, $Q' = V'P$, is related to the molecular flow rate, $\dot{n}$, by

$$\dot{n} = \frac{Q'}{kT}$$

For the case of a non-rotating seal ($Q_R = 0$), Equation (5) can be integrated to obtain the specific molecular flow rate

$$\frac{\dot{n}}{\Delta P} = \frac{1}{kTL}\{(N_s^2 B + D')\bar{P} + N_s^2 C \frac{C_1}{C_2} + E\frac{C_3}{C_4} + N_s^2 C \frac{2}{2C_2^2 \bar{P}}(\frac{r_p}{r_p - 1}) \ln[\frac{r_p(1 + 2C_2\bar{P}) + 1}{r_p + 2C_2\bar{P} + 1}] + E\frac{C_4 - C_3}{2C_4^2\bar{P}}(\frac{r_p + 1}{r_p - 1}) \ln[\frac{r_p(1 + 2C_4\bar{P}) + 1}{r_p + 2C_4\bar{P} + 1}]\} \quad (6)$$

Flow Rate in a Rotating Seal

Assuming a constant pressure gradient along the groove, the total rotor induced flow on a molecule basis is

$$\frac{\dot{n}}{\Delta P} = -\frac{N_s A'\bar{P}}{kT\Delta P} = -\frac{N_s A'}{2kT}[\frac{r_p + 1}{r_p - 1}]. \quad (7)$$

The net flow through a rotating seal is found by combining the rotor induced flow of Equation (7) with the flow in the static seal, Equation (6). The net specific molecular leakage is

$$\frac{\dot{n}}{\Delta P} = \frac{1}{kTL}\{(N_s^2 B + D')\bar{P} + N_s^2 C \frac{C_1}{C_2} + E\frac{C_3}{C_4} + \frac{1}{2}[\frac{r_p + 1}{r_p - 1}][N_s^2 C \frac{C_2 - C_1}{C_2^2 \bar{P}} \ln(\frac{r_p(1 + 2C_2\bar{P}) + 1}{r_p + 2C_2\bar{P} + 1}) + E\frac{C_4 - C_3}{C_4^2 \bar{P}} \ln(\frac{r_p(1 + 2C_4\bar{P}) + 1}{r_p + 2C_4\bar{P} + 1})] - N_s A'L\}. \quad (8)$$

Pressure Difference at Zero Net Leakage

Since a rarefied viscoseal, in the ideal case of a true space environment, will normally operate with $P_1 = 0$, it would be impossible to maintain a zero net flow. However, the condition of zero net flow is of interest as far as experimentation and comparison to continuum performance are concerned, and in non-space applications where $P_1 \neq 0$.

The maximum pressure difference under which a seal can maintain a zero net flow is found by solving the modified-Hodgson model equation subject to the condition that $Q_N' = 0$. Integrating Equation (5) subject to this condition one obtains

$$\left[\frac{2\bar{P} + \Delta P}{2\bar{P} - \Delta P}\right]^{N_s^2 C + E} \left[\frac{2 + C_2(2\bar{P} + \Delta P)}{2 + C_2(2\bar{P} - \Delta P)}\right]^{N_s^2 C\left(\frac{C_1}{C_2} - 1\right)} \left[\frac{2 + C_4(2\bar{P} + \Delta P)}{2 + C_4(2\bar{P} - \Delta P)}\right]^{E\left(\frac{C_3}{C_4} - 1\right)}$$

$$= \exp\left[N_s A'L - (N_s^2 B + D')\Delta P\right]. \tag{9}$$

In general Equation (9) cannot be solved explicitly for ΔP. For the special case of continuum flow $2\bar{P} >> \Delta P$, the continuum ΔP can be obtained from Equation (9) as

$$\Delta P = \frac{N_s A'L}{n_s^2 B + D}. \tag{10}$$

At the other extreme, free-molecule flow, Equation (5) can be reduced to its free-molecule limit,

$$Q_N' = -(N_s^2 C + E)\frac{dP}{dL} - N_s A'P. \tag{10a}$$

Since in the free-molecule limit P is very small, the last term in Equation (10a) could presumably be very small; but since efficient seal performance requires that the rotor induced flow be of the same order of magnitude as the pressure induced flow, this term is retained.

Solving Equation (10a) subject to the condition that $Q_N = 0$, the free-molecule pressure ratio becomes

$$r_p = \exp[N_s A'L/(N_s^2 C + E)]. \tag{11}$$

The ΔP across the seal can be expressed as

$$\Delta P = 2\overline{P}\ \frac{r_p - 1}{r_p + 1}. \tag{12}$$

Combining Equations (11) and (12), the ΔP in the free-molecule regime is

$$\Delta P = 2\overline{P}\ \frac{\exp\,[N_s A'L/(N_s^2 C + E)] - 1}{\exp[N_s A'L/(N_s^2 C + E)] + 1}. \tag{13}$$

Since no explicit solution to Equation (9) can in general be obtained, some approximate solution technique must be employed. Since Newton's method of approximating roots is generally a rapidly converging iterative method, it is employed in solving Equation (9). Newton's method requires that the given relationship be differentiable. Equation (9) can certainly be differentiated. Another very important requirement is the ability to make a close initial approximation to the solution. This requirement is particularly important with a complicated relationship such as Equation (9).

In order to make a close approximation to the roots of Equation (9), one needs to know as much as possible before hand about the character of the solution. At this point two characteristics are known: (1) the continuum limit, Equation (10), and (2) the free-molecule limit, Equation (13). The solution of Equation (9) will simply define the behavior over the entire range of average pressures and approach the continuum and free-molecule limits at the two extremes. In order to

make a close approximation to the value of ΔP which satisfies Equation (9) for a given $\overline{P}$, a high average pressure, $\overline{P}_1$, is chosen initially such that the continuum solution from Equation (10) is a good approximation to the root of Equation (9). Using this initial approximation for ΔP, Newton's method is employed to solve Equation (9) for the ΔP at $\overline{P}_1$. An incremental decrease, $\Delta\overline{P}$, in the average pressure is then taken and the ΔP obtained from the previous iteration at $\overline{P}_1$ is used as the initial estimate of the solution for ΔP at $\overline{P}_2$ and the iteration process is repeated to obtain ΔP. The entire process is repeated to obtain ΔP at $\overline{P}_3$, $\overline{P}_4$, etc.

Essentially the above process could be continued until the entire spectrum of pressures had been traversed, but the process encounters difficulties near the intersection of the continuum and free-molecule asymptotes. In the near continuum region, the ΔP versus $\overline{P}$ solution of Equation (9) is fairly flat, thus making the solution at $\overline{P}_{n-1}$ a good approximation to the root at $\overline{P}_n$. In the intersection region, however, the rate of change is so large that the method used above for the initial estimation of the solution is not sufficiently accurate. Two simple modifications to the above method can help to ensure a close approximation of the root at $\overline{P}_n$. An obvious modification would be to reduce the step size, $\Delta\overline{P}$. Since all previous points $\overline{P}_1$ through $\overline{P}_{n-1}$ have been determined, these points can be used to extrapolate to an initial approximation at $\overline{P}_n$. Essentially an extrapolation of order $n - 2$ could be made, but experience has shown that a linear extrapolation combined with successive reductions in $\Delta\overline{P}$ is sufficient to ensure convergence at $\overline{P}_n$.

After passing through the critical region in the vicinity of the intersection of the asymptotes, the curve essentially assumes the straight line predicted by Equation (13). The solution is thus complete.

The Fortran programs for the solution of Equation (5) for the three cases outlined above are presented in Reference 13. The flow rate in a static seal is simply a special case ($Q'_R = 0$) of the rotating solution. Consequently only one program is needed for the flow rate solutions.

The modified-Hodgson model provides a convenient means of predicting the performance of a given viscoseal. The limiting conditions of Equations (10) and (13) can conveniently be used to predict optimum seal geometries in the purely continuum and purely free-molecule regimes, respectively. In the transition regime, however, Equation (9) would be very difficult to use in an optimization study because of the time consuming solution method.

2.2 Slip Modified Boon and Tal Model

In 1959 Boon and Tal published (10) a significant analysis of the viscoseal in the laminar continuum regime for a constant density fluid. The viscoseal geometry was approximated by two flat plates, one of which was grooved,moving parallel to each other. The flow field was developed from a superposition of Couette flows along and across the grooves. The resulting velocity distributions were integrated to obtain the volumetric flow rate, and the pressure generation for zero net leakage conditions was developed. Subsequent investigations by Stair (14) using liquids as the sealant showed very good agreement with the analysis of Boon and Tal. The data of Hodgson and Milligan (15) using air as the

sealant also substantiated this analysis for laminar continuum operation with gases.

The Slip Modified Boon and Tal Model has been developed by formulating "rarefied" corrections to the laminar continuum equations developed by Boon and Tal. This approach is similar to that used in previous investigations (3, 4, 16, 17) of internal rarefied flow that have indicated that a single model for gas flow through tubes and annuli, applicable to the flow regime extending from continuum to free molecular flow can be derived by the inclusion of rarefied effects on the continuum model.

Consider a screw formed on a shaft located concentrically within a cylindrical housing with a radial clearance c. The annular space is filled with a gas and the shaft is moving relative to the housing with an angular velocity, Ω. Figure 4 shows a developed view of the viscoseal geometry. The (x, y) axes are along and normal to the direction of relative motion and the (ξ, η) axes are parallel and normal to the grooves. The (x, y) and (ξ, η) coordinates systems are related by:

$$\xi = x \cos \alpha + y \sin \alpha$$

$$\eta = y \cos \alpha - x \sin \alpha.$$

Previous investigators (10, 18) have reduced the describing partial differential momentum equations to the Reynolds lubrication equations. These analyses were based on the flat plate model of Figure 2 and assumed steady, isothermal, two-dimensional, laminar flow. Further, these analyses assumed inertia forces to be negligible in comparison to viscous forces and neglected body forces and end effects. The describing mathematical model is taken as:

$$\frac{d^2u}{dz^2} = \frac{1}{\mu}\frac{\partial P}{\partial \xi} \tag{14}$$

$$\frac{d^2v}{dz^2} = \frac{1}{\mu}\frac{\partial P}{\partial \eta}\,. \tag{15}$$

Integration of (14) and (15) gives:

$$u = \frac{1}{2\mu}\frac{\partial P}{\partial \xi}\,z^2 + C_1 z + C_2 \tag{16}$$

$$v = \frac{1}{2\mu}\frac{\partial P}{\partial \eta}\,z^2 + C_3 z + C_4. \tag{17}$$

The integration constants are determined by the boundary conditions. To account for the non-continuum effects, slip boundary conditions are introduced as derived by Kennard (19). For a monatomic gas, flowing within two parallel boundaries, the slip boundary condition can be written in the following general form:

$$u_{gas}\big|_{z=0} = u_{wall} + G\lambda\left(\frac{\partial u}{\partial z}\right)\Big|_{z=0}$$

$$+ \frac{3}{4}\frac{\mu}{\rho T}\left(\frac{\partial T}{\partial x}\right)\Big|_{z=0} + O(\lambda^2), \tag{18}$$

where u is the velocity in the tangential x direction, z is the direction normal to the motion, and G is a proportionality constant. If the temperatures of the surfaces are assumed constant and equal to the gas temperature then the slip boundary condition reduces in general form to

$$u_{gas} = u_{wall} + G\lambda\left(\frac{\partial u}{\partial z}\right)_z = 0. \tag{19}$$

For the particular geometry under study, the slip boundary conditions are:

Along the lands:

$$u_r\big|_{z=0} = U\cos\alpha + G\lambda\frac{du_r}{dz}\Big|_{z=0} \equiv u_1$$

$$u_r\big|_{z = h_r} = - G\lambda \frac{du_r}{dz}\Big|_{z = h_r} \equiv u_2$$

Along the groove:

$$u_g\big|_{z = 0} = U \cos \alpha + G\lambda \frac{du_g}{dz}\Big|_{z = o} \equiv u_3$$

$$u_g\big|_{z = h_g} = - G\lambda \frac{du_g}{dz}\Big|_{z = h_g} \equiv u_4.$$

Across the lands:

$$v_r\big|_{z = 0} = - U \sin \alpha + G\lambda \frac{dv_r}{dz}\Big|_{z = 0} \equiv v_1$$

$$v_r\big|_{z = h_r} = - G\lambda \frac{dv_r}{dz}\Big|_{z = h_r} \equiv v_2.$$

Across the groove:

$$v_g\big|_{z = 0} = - U \sin \alpha + G\lambda \frac{dv_g}{dz}\Big|_{z = 0} \equiv v_3$$

$$v_g\big|_{z = h_g} = - G\lambda \frac{dv_g}{dz}\Big|_{z = h_g} \equiv v_4.$$

Using the above boundary conditions the following velocity components are determined:

Along the lands:

$$u_r = \frac{1}{2\mu} \frac{\partial P}{\partial \xi} (z^2 - h_r z) + \left(\frac{u_2 - u_1}{h_r}\right) z + u_1. \tag{20}$$

Along the grooves:

$$u_g = \frac{1}{2\mu} \frac{\partial P}{\partial \xi} (z^2 - h_g z) + \left(\frac{u_4 - u_3}{h_g}\right) z + u_3. \tag{21}$$

Across the lands:

$$v_r = \frac{1}{2\mu} \frac{\partial P}{\partial \eta} (z^2 - h_r z) + \left(\frac{v_2 - v_1}{h_r}\right) z + v_1. \tag{22}$$

Across the grooves:

$$v_g = \frac{1}{2\mu} \frac{\partial P}{\partial \eta} (z^2 - h_g z) + \left(\frac{v_4 - v_3}{h_g}\right) z + v_3. \tag{23}$$

The slip velocities at the walls can now be determined, and the following velocity distribution equations obtained:

$$u_r = \frac{1}{2\mu}\frac{\partial P}{\partial \xi}(z^2 - h_r z) + \left(\frac{-U\cos\alpha}{1 + 2G\lambda/h_r}\right)\frac{z}{h_r} + U\cos\alpha\left(\frac{1 + G\lambda/h_r}{1 + 2G\lambda/h_r}\right) - \frac{1}{2\mu}\frac{\partial P}{\partial \xi}h_r^2\frac{G\lambda}{h_r} \tag{24}$$

$$u_g = \frac{1}{2\mu}\frac{\partial P}{\partial \xi}(z^2 - h_g z) + \left(\frac{-U\cos\alpha}{1 + 2G\lambda/h_g}\right)\frac{z}{h_g} + U\cos\alpha\left(\frac{1 + G\lambda/h_g}{1 + 2G\lambda/h_g}\right) - \frac{1}{2\mu}\frac{\partial P}{\partial \xi}h_g^2\frac{G\lambda}{h_g} \tag{25}$$

$$v_r = \frac{1}{2\mu}\frac{\partial P}{\partial \eta}(z^2 - h_r z) + \left(\frac{U\sin\alpha}{1 + 2G\lambda/h_r}\right)\frac{z}{h_r} - U\sin\alpha\left(\frac{1 + G\lambda/h_r}{1 + 2G\lambda/h_r}\right) - \frac{1}{2\mu}\frac{\partial P}{\partial \eta}h_r^2\frac{G\lambda}{h_r} \tag{26}$$

$$v_g = \frac{1}{2\mu}\frac{\partial P}{\partial \eta}(z^2 - h_g z) + \left(\frac{U\sin\alpha}{1 + 2G\lambda/h_g}\right)\frac{z}{h_g} - U\sin\alpha\left(\frac{1 + G\lambda/h_g}{1 + 2G\lambda/h_g}\right) - \frac{1}{2\mu}\frac{\partial P}{\partial \eta}h_g^2\frac{G\lambda}{h_g}. \tag{27}$$

Noting that the axial velocity components are:

$$u_y = u\sin\alpha \tag{28}$$

$$v_y = v\cos\alpha \tag{29}$$

the axial flow rate components $Q_{\xi r}$, $Q_{\xi g}$, $Q_{\eta r}$ and $Q_{\eta g}$ may be determined. The width of the flow path for the ξ land flow component is $(1 - \gamma)\pi D$ and the path width for the ξ groove flow is $\gamma\pi D$. The ratio of the groove width to the groove plus land width is defined as γ. The axial component of the ξ coordinate land flow is:

$$Q_{\xi r} = (1 - \gamma)\pi D\int_0^{h_r} U_{ry}\,dz = (1 - \gamma)\pi D\int_0^{h_r} U_r\sin\alpha\,dz. \tag{30}$$

Substituting Equation (24) into Equation (30) and integrating gives

$$Q_{\xi r} = (1 - \gamma)\pi D \sin \alpha[\frac{1}{2\mu} (\frac{\partial P}{\partial \xi})_r h_r^3(- \frac{G\lambda}{h_r} - \frac{1}{6}) + U \cos \alpha \frac{h_r}{2}]. \quad (31)$$

In a similar manner:

$$Q_{\xi g} = D \sin \alpha[\frac{1}{2\mu} (\frac{\partial P}{\partial \xi})_g h_g^3 (- \frac{G\lambda}{h_g} - \frac{1}{6}) + U \cos \alpha \frac{h_g}{2}] \quad (32)$$

$$Q_{\eta r} = (1 - \gamma)\pi D \cos \alpha[\frac{1}{2\mu}(\frac{\partial P}{\partial \eta})_r h_r^3(- \frac{G\lambda}{h_r} - \frac{1}{6}) - U \sin \alpha \frac{h_r}{2}] \quad (33)$$

$$Q_{\eta g} = \gamma\pi D \cos \alpha[\frac{1}{2\mu} (\frac{\partial P}{\partial \eta})_g h_g^3(- \frac{G\lambda}{h_g} - \frac{1}{6}) - U \sin \alpha \frac{h_g}{2}]. \quad (34)$$

The pressure gradients in Equations (31) through (34) may be replaced by the more convenient axial gradients by noting that

$$\frac{\partial P}{\partial \xi} = \frac{\partial P}{\partial y} \sin \alpha , \quad (35)$$

and

$$(1 - \gamma)(\frac{\partial P}{\partial \eta})_r + (\frac{\partial P}{\partial \eta})_g = \frac{\partial P}{\partial y} \cos \alpha . \quad (36)$$

From the continuity of mass, the flow across the groove in the η direction must equal the flow across the land in this direction. Thus it can be shown that

$$[\frac{1}{2\mu} (\frac{\partial P}{\partial \eta})_r h_r^3 (- \frac{G\lambda}{h_r} - \frac{1}{6}) - U \sin \alpha \frac{h_r}{2}] =$$

$$[\frac{1}{2\mu} (\frac{\partial P}{\partial \eta})_g h_g^3 (- \frac{G\lambda}{h_g} - \frac{1}{6}) - U \sin \alpha \frac{h_g}{2}]. \quad (37)$$

The total flow is given by

$$Q = Q_{\xi r} + Q_{\xi g} + Q_{\eta r} + Q_{\eta h}. \quad (38)$$

Using Equations (31) through (38), the expression for the axial flow is:

$$Q = - \frac{1}{12\mu} \frac{\partial P}{\partial y} \frac{c^3\pi D}{(1 + t^2)} [t^2(1 - \gamma)(1 + \frac{6G\lambda}{c}) + (1 + \frac{6G\lambda}{\beta c})(\beta^3)(\gamma t^2 + \frac{1}{\psi})]$$

$$+ \frac{Uc\pi D}{2} \frac{t(1-\gamma)(\beta-1)}{1+t^2}\left[\frac{\beta^3(1+\frac{6G\lambda}{\beta c})}{\psi(1+\frac{6G\lambda}{c})} - 1\right], \tag{39}$$

where

$$\beta = \frac{h+c}{c}$$

$$\gamma = \frac{b}{w+b}$$

$$\psi = (1-\gamma)\beta^3\left(\frac{1+\frac{6G\lambda}{\beta c}}{1+\frac{6G\lambda}{c}}\right) + \gamma$$

$$t = \tan\alpha$$

The Knudsen number for the viscoseal is defined as

$$N_K \equiv \frac{\lambda}{c}, \tag{40}$$

where seal radial clearance, c, has been selected as the characteristic system dimension because of the manner of its appearance in Equation (39) in relation to the mean free path λ.

Equation (40) can be rewritten in terms of molecular flow rate rather than volumetric flow rate as

$$\dot{n} = -\frac{P}{12\mu KT}\frac{\partial P}{\partial y}\frac{c^3\pi D}{(1+t^2)}\left[t^2(1-\gamma)(1+\frac{6G\lambda}{c}) + (1+\frac{6G\lambda}{\beta c})(\beta^3)(\gamma t^2 + \frac{1}{\psi})\right] + \frac{Uc\pi D}{2}\frac{t(1-\gamma)(\beta-1)}{1+t^2}\left[\frac{\beta^3(1+\frac{6G\lambda}{\beta c})}{\psi(1+\frac{6G\lambda}{c})} - 1\right], \tag{41}$$

Further consideration now needs to be given to the slip coefficient constant of proportionality "G". Various investigators have developed expressions for this proportionality constant ranging from 2/3 (20) to (2 - f)/f (19) where f is the fraction of their tangential momentum which molecules give up upon striking a solid boundary. Published values of f by Kennard (19) range from 0.79 for air flowing over fresh

shellac to 1.00 for air or CO_2 over machined brass. A value of f equal to one is taken to be realistic for the flow of gases over machined surfaces. Thus the value of the slip coefficient G was taken to be unity.

Knudsen number as defined in Equation (40) indicates the degree of rarefication since it becomes large as the mean free path, λ, becomes large. When the Knudsen value becomes small and approaches zero, corresponding to continuum conditions, then Equation (30) reduces to the continuum, no slip, solution shown by Stair (18).

For isothermal flow the mean free path, λ, is a function of the pressure and gas properties. The Chapman relationship (19) can be used to express this dependence.

$$\lambda = \frac{\mu(2\pi\frac{kT}{m})^{1/2}}{2p} \tag{42}$$

This relationship will be used to express the right hand side of Equation (41) in terms of pressure.

2.21 Variable Mean Free Path Solution. In order to solve Equation (41) for the flow rate in terms of the seal length and the ΔP across the seal a numerical scheme must be employed. Before integrating the equation is rearranged. Let P_o be the pressure at which $\lambda = C/6G$. Then

$$P_o = \frac{6G\lambda P}{C} = \frac{6G}{C} \frac{\mu(2\pi\frac{kT}{m})^{1/2}}{2}$$

Now Equation (41) may be written in terms of pressure

$$\dot{n} = -\frac{P_o^2 P' c^3 \pi D}{12\mu kT(1+t^2)} \frac{dP'}{dy} [t^2(1-\gamma)(1+\frac{1}{P'}) + (1+\frac{1}{\beta P'})\beta^3(\gamma t^2 + \frac{1}{\psi})]$$
$$+ \frac{UcP_o P'\pi Dt(1-\gamma)(\beta-1)}{2kT(1+t^2)} [\frac{\beta^3(1+\frac{1}{\beta P'})}{\psi(1+\frac{1}{P'})} - 1] \tag{43}$$

where

$$P' + P/P_o$$

and

$$\psi = (1 - \gamma)\beta^3 \frac{(1 + \frac{1}{\beta P'})}{(1 + \frac{1}{P'})} + \gamma$$

Non-dimensionalizing the length coordinate, y, by using the seal length, L, i.e., $y' = y/L$ and $dy = Ldy'$ we can write

$$n = f(P') \frac{dP'}{dy'} + g(P') \tag{44}$$

where

$$f(P') = - \frac{P_o^2 c^3 \pi D}{12\mu kT\ (1 + t^2)L} [t^2(1 - \gamma)(P' + 1)$$

$$+ (P' + \frac{1}{\beta})\beta^3(\gamma t^2 + \frac{1}{\psi})]$$

$$g(P') = \frac{cUP_o \pi Dt(1 - \gamma)(\beta - 1)}{2kT\ (1 + t^2)} [\beta^3 \frac{(P' + 1/\beta)}{\psi(1 + 1/P')} - P']$$

Simplifying Equation (44) by defining a new flow rate parameter $\bar{\dot{n}}$ we obtain

$$\bar{\dot{n}} \equiv \bar{f} \frac{dP'}{dy'} + \Lambda_f \bar{g} \tag{45}$$

where

$$\Lambda_f = \frac{6\mu UL}{c^2 P_o}$$

$$\bar{f} = \bar{f}(P', \beta, \gamma, t) = - \frac{1}{(1 + t^2)} [t^2(1 - \gamma)(P' + 1) + (P' + \frac{1}{\beta})$$

$$\beta^3(\gamma t^2 + \frac{1}{\psi})]$$

$$\bar{g} = \bar{g}(P', \beta, \gamma, t) = \frac{t(1 - \gamma)(\beta - 1)}{(1 + t^2)} [\beta^3 \frac{(P' + \frac{1}{\beta})}{\psi(1 + \frac{1}{P'})} - P']$$

Separating variables in Equation (45) and integrating over the seal length gives

$$1 = \int_{P_1'}^{P_2'} \frac{\bar{f}(P')}{\bar{\dot{n}} - \Lambda_f \bar{g}(P')} dP' \tag{46}$$

For a given physical condition, i.e., P_1', P_2', β, γ, t, Λ_f, the problem reduces to solving Equation (46) for $\bar{\dot{n}}$. Newton's method was used by letting

$$F = 1 - \int_{P_1'}^{P_2'} \frac{\bar{f}(P')}{\bar{\dot{n}} - \Lambda \bar{g}(P')} dP' = 0 \tag{47}$$

Newton's method predicts successive approximations to the solution of Equation (45) through the following relationship:

$$\bar{\dot{n}}_{n+1} = \bar{\dot{n}}_n - F/F'|n$$

where

$$F' = \frac{dF}{d\bar{\dot{n}}} = \int_{P_1'}^{P_2'} \frac{\bar{f}(P')}{(\bar{\dot{n}} - \Lambda_f \bar{g}(P'))^2} dP'$$

Since the most useful situation for the viscoseal as a sealing device would be to have the net flow rate equal to zero a similar technique was used to solve Equation (41) for the ΔP which results for $\dot{n} = 0$. A widely used parameter in sealing work is defined for no net flow in the form of sealing coefficient, Λ.

$$\Lambda \equiv \frac{6\mu UL}{\Delta P_c^2} \tag{48}$$

Results for the variable mean free path will be presented for both net leakage and for no net leakage (sealing coefficient) values.

2.22 Mean-Value Solution. If the mean value of seal pressure is used in Equation (42) to calculate a mean value of mean free path, then Equation (39) can be approximated by replacing the local mean free path by an average value. This permits the simple integration of Equation (39) to give

$$Q = -\frac{1}{12\mu}\frac{\Delta P}{QL}\frac{c^3\pi D}{(1+t^2)}f_1(N_K) + \frac{Uc\pi D}{2(1+t^2)}f_2(N_K). \tag{49}$$

where

$$f_1(N_K) = t^2(1-\gamma)(1+6GN_K) + (1+\frac{6GN_K}{\beta})(\beta^3)(\gamma t^2+\frac{1}{\psi}),$$

and

$$f_2(N_K) = t(1-\gamma)(\beta-1)[\frac{\beta^3(1+\frac{6GN_K}{\beta})}{\psi(1+6GN_K)} - 1],$$

For no net flow the sealing coefficient can be written as

$$\Lambda \equiv \frac{6\mu UL}{\Delta Pc^2} = \frac{f_1(N_K)}{f_2(N_K)}. \tag{50}$$

Results will be presented using this mean-value type solution.

2.23 Particle Slip Correction. In the previous section where the slip-modified Reynolds solution was derived, slip boundary conditions were applied to account for the decreased intermolecular momentum transport at the walls. The analysis attributed a slip velocity relative to the walls for all the molecules adjacent to these surfaces. For the case of stationary walls, this implies that every molecule, on the average, will possess additional flow velocity due to the slip flow contribution. The preponderance of evidence presented by Weber (16), Kennard (19), Present (20), and Fryer (21) indicate that molecules whose last collision was at the wall can have no slip velocity since such

molecules are diffusely reflected from the walls. Thus only those molecules coming from collisions with other molecules can possess a slip velocity. A correction will now be developed to account for those molecules which do not experience slip boundary conditions due to their collisions with the walls. The correction will be established by determining the ratio of the molecule-to-molecule collisions to the total number of collisions, or the sum of the molecule-to-wall plus the molecule-to-molecule collisions. This ratio, σ, represents the fraction of molecules present which experience the slip boundary condition.

The number of molecules striking the wall per unit time and unit area is (20) $\frac{n\bar{V}}{4}$ where $\bar{V}$ is the mean molecular speed. If one considers the unwrapped viscoseal geometry of Figure 4, the seal surface area is approximated by

$$2\pi DL + 2h \frac{\pi D}{\cos \alpha} \left(\frac{L}{w + b}\right)$$

where the right hand term is the surface area contributed by the groove side walls. Thus the number of molecule-to-wall collisions in unit time is

$$\frac{n\bar{V}}{2} \pi DL\left[1 + \frac{h}{\cos \alpha(w + b)}\right].$$

The total number of molecule-to-molecule collisions per unit time and unit volume is (20) $\frac{n\bar{V}}{\lambda}$. The volume of the viscoseal is the volume of the annular space plus the volume of the grooves. Thus the total number of molecule-to-molecule collisions per unit time is

$$\frac{n\bar{V}}{\lambda} \left[\pi L(r_2^2 - r_1^2) + \frac{\pi DL \cdot h \cdot b}{(w + b)}\right].$$

Since

$$(r_2^2 - r_1^2) = (r_2 + r_1)(r_2 - r_1),$$

and, due to the small clearance of the normal viscoseal geometry,

$r_1 + r_2 \approx D$ and $r_2 - r_1 = c$,

then the expression simplifies to

$$\frac{n\bar{V}}{\lambda} \pi DL \left[c + \frac{h \cdot b}{w + b}\right].$$

Hence, the proportion of the molecules which experience slip is

$$\sigma = \frac{1/N_K \left[1 + \gamma(\beta - 1)\right]}{1/N_K \left[1 + \gamma(\beta - 1)\right] + \frac{1}{2}\left[1 + \frac{h}{\cos \alpha(w + b)}\right]} \quad (51)$$

with

$$\beta \equiv \frac{h + c}{c} \qquad \lambda \equiv \frac{b}{w + b}$$

$$N_K \equiv \frac{\lambda}{c} \quad \text{and} \quad \frac{h}{c} = (\beta - 1).$$

In the solution of the slip-modified Reynolds equation, it will be recalled that boundary conditions were not permitted on the groove side walls. Thus it is more in keeping with the manner of this analysis to omit the molecule-to-wall collisions which occur on these surfaces and contribute the $h/\cos \alpha(a + b)$ term in the denominator of Equation (51). With this restriction, the equation becomes

$$\sigma = \frac{1}{1 + N_K/2\left[1 + (\beta - 1)\gamma\right]} \quad (52)$$

In the analysis of slip flow through long tubes by Weber (16), Fryer (21), and Milligan (17), the resulting flow equation could be manipulated into two separate terms. One of these terms is the continuum Poiseuille flow term while the second term is the slip flow contribution which results from application of the slip boundary conditions. Equivalent type terms were obtained by Milligan, Cowling, and

Wilkerson (4) in the analysis of rarefied flow in a long concentric annulus. For both of these geometries, the correction for the particles which do not experience slip was made by multiplying the slip flow contribution by σ, since it is this uncorrected term which implies that all the molecules possess the additional slip velocity. Thus when σ is applied in this manner the resulting slip contribution term has been corrected for the particles which experience wall collisions and thus possess no slip velocity. When this correction is made to Equation (49) the following equation is obtained:

$$Q = -\frac{1}{12\mu}\frac{\Delta P}{L}\frac{c^3\pi D}{(1+t^2)} f_3(N_K) + \frac{Uc\pi D}{2(1+t^2)} f_4(N_K). \tag{53}$$

where

$$f_3(N_K) \equiv \sigma f_1(N_K) + C_5(1-\sigma),$$

and

$$f_4(N_K) \equiv \sigma f_2(N_K) + C_6(1-\sigma),$$

$$C_5 \equiv \frac{\gamma t^2(1-\gamma)(\beta^3-1)^2 + \beta^3(1+t^2)}{\beta^3(1-\gamma)+\gamma}$$

$$C_6 \equiv \frac{\gamma t(1-\gamma)(\beta^3-1)(\beta-1)}{\beta^3(1-\gamma)+\gamma}$$

In a similar manner to that of Equation (50), the sealing coefficient for the mean-value slip-modified Reynolds solution with corrections for particles which do not experience slip is

$$\Lambda = \frac{6\mu UL}{\Delta P c^2} = \frac{f_3(N_K)}{f_4(N_K)}. \tag{54}$$

Often it is more desirable to express results in terms of molecular flow rates rather than volumetric flow rates. Equation (49) for the Mean-Value Slip Modified Boon and Tal solution with no correction due to particles which do not experience slip is

$$\frac{\dot{n}}{\Delta P} = -\left(\frac{\pi}{2mKT}\right)^{1/2} \left(\frac{c^2\pi D}{N_K\,(1 + t^2)L}\right) f_1(N_K)$$

$$+ \left(\frac{r_p + 1}{r_p - 1}\right) \frac{Uc\pi D}{4KT\,(1 + t^2)}\, f_2(N_K), \tag{55}$$

where the relationship that

$$\Delta P = 2\bar{P}\left(\frac{r_p - 1}{r_p + 1}\right), \tag{56}$$

has been written in terms of the pressure ratio, r_p, across the seal in the right hand term. Similarly, the specific leakage flow rate with the correction for the particles that do not experience slip is

$$\frac{\dot{n}}{\Delta P} = -\left(\frac{\pi}{2mKT}\right)^{1/2} \left(\frac{c^2\pi D}{N_K(1 + t^2)L}\right) f_3(N_K)$$

$$+ \left(\frac{r_p + 1}{r_p - 1}\right)\frac{Uc\pi D}{4KT(1 + t^2)}\, f_4(N_K). \tag{57}$$

It should be noted that for a fixed seal geometry and a given gas at a specified temperature, the specific molecular flow rates of Equations (55) and (57) are functions only of Knudsen number, the speed U, and the viscoseal pressure ratio, r_p. As the pressure ratio becomes high, then $(r_p + 1)/(r_p - 1)$ approaches unity and the specific flow rate is a function of the speed and the Knudsen number only.

This same technique can be used to evaluate the particle slip correction for the variable mean-free path solution by correcting Equation (43) before using a numerical scheme to solve the equation.

2.24 Self-Diffusion. The term diffusion, as used here, refers to the molecular transfer which occurs due to a concentration gradient. If the gas is a pure unmixed gas, then the diffusion is one of self-diffusion. In their work concerning low density flow of gases in a capillary, Pollard and Present (22) suggested that at low pressures the total transport can be described by the superposition of the diffusive transport and a drift component. In his study of flow through long tubes, Weber (16) applied the idea of the superposition of a diffusive component, a slip contribution, and the viscous component. Weber demonstrated that his solution has the correct limiting values for continuum and free molecule flows and adequately describes Knudsen's data for long tubes (23). Milligan experimentally verified, with excellent agreement, the analysis technique of Weber for rarefied flow in long tubes (17). Lund and Berman (24) developed empirical relations for the flow and self-diffusion of gases in both long and short capillaries by the superposition of the diffusive and drift components. They developed an algebraic expression which permits the direct computation of the Weber diffusion coefficient at any pressure and thus avoided the numerical integration inherent in the Pollard and Present treatment of self-diffusion. Lund and Berman demonstrated the adequacy of their model for describing self-diffusion and flow in capillaries in addition to the flow between flat plates. Milligan, Cowling, and Wilkerson (14) extended the superposition analysis technique of Weber to long annuli with continuing success.

In this section, the self diffusion flow in both the grooves and annular space of the viscoseal will be discussed and evaluated using the Pollard and Present treatment as applied by Weber.

Annular Space Self-Diffusion

The self-diffusion flow in the clearance space of the rarefied-gas viscoseal was obtained by considering this flow to be that of a concentric annulus. The molecular transfer was determined by evaluating the net number of molecules crossing a plane normal to the annulus. The evaluation was done by considering separately the molecules which come from the outer and the inner walls with the grooved inner wall taken as being smooth and of diameter D as shown in Figure 1. The details of this derivation are presented in Reference (3) and the procedure used was essentially that given by Weber (16). The following equations were numerically integrated to obtain the diffusion contribution in the annular space:

$$\dot{N}_{\text{net outer wall}} = -2\bar{V}\lambda \frac{dn}{dy}(r_2 - r_1)^2 \int_{R_1}^{R_2} \int_0^{\phi_o} \int_0^{\pi/2} (R). \sin\theta \cos^2\theta(1 - e^{-R/N_K})\, dR'\, d\phi\, d\theta \qquad (58)$$

$$\dot{N}_{\text{net inner wall}} = -2\bar{V}\lambda \frac{dn}{dy}(r_2 - r_1)^2 \int_{R_1}^{R_2} \int_{\phi_o}^{\pi} \int_0^{\pi/2} (R'). \sin\theta' \cos^2\theta'(1 - e^{-R/N_K})\, dR'\, d\phi\, d\theta'. \qquad (59)$$

The total self-diffusion flow in the annular space is the sum of Equations (58 and 59) and may be arranged into specific molecular flow rate form using

$$\frac{dn}{dy} = \frac{d}{dy}\left(\frac{P}{KT}\right) = \frac{1}{KT}\frac{dP}{dy} \approx \frac{1}{KT}\frac{P}{L}$$

and

$$\bar{V} = 2\left[\frac{2KT}{\pi m}\right]^{1/2}$$

to obtain

$$\frac{\dot{N}}{\Delta P} = -4\left(\frac{2}{\pi mKT}\right)^{1/2} \frac{(r_2 - r_1)^3}{L} N_K \,[\text{SUM (O.W.)} + \text{SUM (I.W.)}], \quad (60)$$

where SUM (O.W.) and SUM (I.W.) designates the numerical integration of the integrals of Equations (58 and 59), respectively.

Groove Self-Diffusion

The self-diffusion flow in the grooves of the shaft was obtained in a similar manner to that of the diffusive flow in the annular space. The flow in the groove was determined by considering this transport to be that of a long groove of rectangular cross section. This neglects any curvature effects of the helical groove and becomes increasingly in error as the groove dimensions become of the order of magnitude of the seal diameter. The development work of the numerical scheme is presented in complete detail in Reference (25).

The groove diffusion flow involves the numerical solution of the following type of equation:

$$N = -\frac{\bar{V} N_{Kg}}{2\pi} \frac{dn}{d\xi} \int_0^h \int_0^{b'} \int_0^h \int_0^{\infty} \left\{ \frac{(b' - \eta)b'}{r^5} (1 - e^{-R/N_{Kg}}) \right.$$

$$\left. + \frac{\eta b'}{rr^5} (1 - e^{-RR/N_{Kg}}) \right\} \xi^2 \, dz' \, (d\eta dz d\xi), \quad (61)$$

where

$$N_{Kg} = \frac{\lambda}{b'}$$

is the Knudsen number of the groove flow with the groove width, b', being taken as the characteristic dimension. Again

$$\bar{V} = 2\left[\frac{2KT}{\pi m}\right]^{1/2}$$

and

$$\frac{dn}{d\xi} = \frac{d}{d\xi}\left(\frac{P}{KT}\right) = \frac{1}{KT}\frac{dP}{d\xi} \sim \frac{1}{KT}\frac{\Delta P}{\ell} ,$$

where ℓ is now the groove length. The relation between the length of one groove and the axial seal length is

$$\ell = \frac{1}{N_S}\frac{\pi D}{\cos \alpha}\frac{L}{(w + b)} = \frac{L}{\sin \alpha} ,$$

where N_S is the number of grooves. For a multiple grooved shaft the total groove diffusion flow is N_S times the flow of a single groove. Thus the total specific molecular flow due to the diffusion is

$$\frac{\dot{N}}{\Delta P} = -\frac{N_S \sin \alpha}{\pi L}\left(\frac{2}{\pi mKT}\right)^{1/2} [\text{SUM (Walls)}], \tag{62}$$

where SUM (Walls) designates the numerical integration of the integral terms of Equation (61) to include the total walls of the grooves.

2.25 Composite Solution. The total specific molecular flow for the composite solution is obtained by adding the continuum solution plus the slip flow contribution after correction for the molecules which do not experience slip plus the self-diffusion flows in the annular space and the grooves. Thus for the mean-value solution

$$\left(\frac{\dot{N}}{\Delta P}\right)_{\text{composite}} = \text{Eq. (57)} + \text{Eq. (60)} + \text{Eq. (62)} \tag{63}$$

It should be noted in summating the flows that the contributions of each equation must be evaluated at the same physical gaseous state. In the development of the groove self-diffusion the Knudsen number, N_{Kg}, was based on the groove width, b', rather than the seal radial clearance, c. Thus the corresponding value of groove Knudsen number for a given clearance Knudsen number is

$$N_{Kg} = N_K\left(\frac{c}{b'}\right). \tag{64}$$

This same technique can be used to formulate the composite solution for the variable mean free path analysis and other models such as the annulus-groove model.

2.3 Annulus-Groove Model. In this section a simpler model than the Modified-Hodgson Model will be developed which will lend itself to a less arduous solution in the transition regime and will also correctly predict the continuum performance. The model also predicts the rotor induced flow in a more rigorous manner.

The basic model will be essentially the same as the one used by Hodgson and which is basically the same as the simplified screw extruder theory presented by Carley, et al. (26). The assumptions inherent in these models are:

(1) the total flow in the seal can be treated as the superposition of the leakage flow in the grooves, the leakage flow over the lands and the rotor induced flow in the grooves,

(2) the pressure varies continuously along the groove and is constant over the cross section of a particular groove,

(3) the groove depth is small compared to the diameter of the seal, thus allowing curvature effects to be neglected in the groove flow development,

and

(4) the flow in a seal with a grooved housing is identical to the flow in a seal with a grooved shaft (13).

Assumption 1 obviously neglects the convective coupling of the flow components. The solution without this assumption is extremely complicated for even purely continuum flow (27). Its exclusion would

certainly lead to an even more complex analysis when non-continuum boundary conditions are applied. Since the objective is the development of a simplified theory, the inclusion of assumption 1 is a necessity. One important assumption that is usually made which is not made here is that the groove sidewall effects are negligible. This assumption is one of the prime distinctions between this analysis and the Slip-Modified Boon and Tal Model in which this assumption is made.

The assumptions governing the development of the component flows are:

(1) the flow is steady, constant viscosity, fully developed, isothermal and Newtonian with negligible body forces,

(2) the Navier-Stokes equations with non-continuum boundary conditions are applicable,

and

(3) the non-continuum boundary conditions can be expressed as (19)

$$v|_{wall} \sim \lambda \left.\frac{\partial v}{\partial n}\right|_{wall} .$$

In the development of the flow components, flow models which have been experimentally verified will be used and reference made to their verification.

2.31 Flow in the Groove

Although most previous investigators have initially treated the groove flow in two parts, this analysis will initially treat the groove flow as a single flow from which the two previously mentioned groove flows are eventually obtained.

Based on the assumptions stated above, the Navier-Stokes equations reduce to the single z-momentum equation

$$\frac{\partial^2 v}{\partial \bar{x}^2} + \frac{\partial^2 v}{\partial \bar{y}^2} = \frac{1}{\mu} \frac{dP}{dz} \quad . \tag{65}$$

The applicable slip boundary conditions shown in Figure 5 are:

$$\frac{\partial v}{\partial \bar{x}} (0, \bar{y}) = 0 \tag{66a}$$

$$v(b'/2, \bar{y}) = - G\lambda \frac{\partial v}{\partial \bar{x}} (b'/2, \bar{y}) \tag{66b}$$

$$v(\bar{x}, 0) = G\lambda \frac{\partial v}{\partial \bar{y}} (\bar{x}, 0) \tag{66c}$$

and

$$v(\bar{x}, h) = - U \cos \alpha - G\lambda \frac{\partial v}{\partial \bar{y}} (\bar{x}, h) \tag{66d}$$

where advantage has been taken of the symmetry about the $\bar{y}$-axis. The slip coefficient, G, is usually taken as unity as will be done here.

It is convenient at this point to non-dimensionalize the velocity and the coordinates and introduce an index of rarefication. The non-dimensionalized variables are taken as

$$x = \bar{x}/(b'/2) \qquad y = \bar{y}/h \quad \text{and} \quad u = \frac{v}{U \cos \alpha}.$$

A common index of rarefication, the Knudsen number is taken as

$$N_{Kh} = \lambda/h.$$

Introducing these new variable into Equations (65) and (66) one obtains

$$\frac{\partial^2 u}{\partial x^2} + \left(\frac{a}{2}\right)^2 \frac{\partial^2 u}{\partial y^2} = \frac{(b')^2}{4\mu U \cos \alpha} \frac{dP}{dz} = \frac{R'}{U} \tag{67}$$

where

$$R' \equiv \frac{(b')^2}{4\mu \cos \alpha} \frac{dP}{dz}$$

and the boundary conditions are

$$\frac{\partial u}{\partial x} (0, y) = 0 \tag{68a}$$

$$u(1, y) = - \frac{2N_{Kh}}{a} \frac{\partial u}{\partial x} (1, y) \tag{68b}$$

$$u(x, 0) = N_{Kh} \frac{\partial u}{\partial y} (x, 0) \tag{68c}$$

and

$$u(x, 1) = - 1 - N_{Kh} \frac{\partial u}{\partial y} (x, 1). \tag{68d}$$

Many techniques have been used to solve non-homogeneous problems of the type presented above. The least arduous is a modified form of the method of variation of parameters (28). This method has been employed successfully by Ebert and Sparrow (29) to solve Equation (65) with four homogeneous boundary conditions. In the case considered here Equation (68d) presents a non-homogeneous boundary condition, but the method used by Ebert and Sparrow still leads to a solution.

The method of variation of parameters is a generalization of the method of separation of variables, and as such, experience gained from employing the latter is helpful when applying the former method. In the method of separation of variables, the sign of the separation constant is taken so that the trigonometric solution is obtained for the homogeneous direction. In the method of variation of parameters the same reasoning is used in the assumption that the solution has the form

$$u(x, y) = \sum_{n = 1}^{\infty} \phi_n(y)(\cos \alpha_n x + C_7 \sin \alpha_n x) \tag{69}$$

where the x-direction is the homogeneous direction determined by an inspection of Equations (68). The function ϕ_n (y) is a yet unknown function of y. One now proceeds to determine ϕ_n, α_n, and C_7.

Substituting Equation (69) into the boundary condition of Equation (68a) one obtains

$$\sum_{n=1}^{\infty} \phi_n(y)[C_7\alpha_n \cos(0) - \alpha_n \sin(0)] = 0$$

which implies that $C_7 = 0$ and that

$$u(x, y) = \sum_{n=1}^{\infty} \phi_n(y) \cos \alpha_n x. \tag{70}$$

Substituting Equation (70) into Equation (68b) gives

$$\sum_{n=1}^{\infty} \phi_n(y)[\cos \alpha_n - \frac{2N_{Kh}\alpha_n}{a} \sin \alpha_n] = 0$$

from which it follows that for a non-trivial solution

$$\cos \alpha_n - \frac{2N_{Kh}\alpha_n}{a} \sin \alpha_n = 0$$

or

$$\alpha_n \tan \alpha_n = \frac{a}{2N_{Kh}} . \tag{71}$$

The eigenvalues, α_n, of the eigenfunctions, cos $\alpha_n x$, are the roots of the transcendental relationship of Equation (71).

The problem now reduces to determining $\phi_n(y)$. Substituting Equation (70) into Equation (67) yields

$$-\sum_{n=1}^{\infty} \alpha_n^2 \phi_n(y) \cos \alpha_n x + (\frac{a}{2})^2 \sum_{n=1}^{\infty} \phi_n''(y) \cos \alpha_n x$$

$$= \frac{R'}{U} \sum_{n=1}^{\infty} \Omega_n \cos \alpha_n x \tag{72}$$

where Ω_n satisfies the Fourier series

$$1 = \sum_{n=1}^{\infty} \Omega_n \cos \alpha_n x. \tag{73}$$

The Fourier cosine series coefficient, Ω_n, must be

$$\Omega_n = \frac{2 \sin \alpha_n}{\alpha_n + \sin \alpha_n \cos \alpha_n} = \frac{2}{\alpha_n} [\frac{\sin \alpha_n}{1 + \frac{2K_h \sin^2 \alpha_n}{a}}] \tag{74}$$

where the last step comes from Equation (71).

In order for $\phi_n(y)$ to satisfy Equation (72), it must be that

$$\phi_n''(y) - \left(\frac{2\alpha_n}{a}\right)^2 \phi_n(y) = \frac{4R'\Omega_n}{Ua^2} . \tag{75}$$

The determination of ϕ_n thus reduces to the solution of a non-homogeneous second-order ordinary differential equation. The boundary conditions on $\phi_n(y)$ are obtained from Equations (68c) and (68d). From Equation (68c), one boundary condition is

$$\phi_n(0) = N_{Kh}\phi_n'(0). \tag{76a}$$

Substituting Equation (73) for the unity term in Equation (68d) leads to the second boundary condition,

$$\phi_n(1) = -\Omega_n - N_{Kh}\phi_n'(1). \tag{76b}$$

The solution of Equation (75) subject to the boundary conditions in Equations (76) is

$$\phi_n(y) = (C_{1np} + C_{1nu})e^{-\theta_n y} + (C_{2np} + C_{2nu})e^{-\theta_n y} - \frac{R'\Omega_n}{U\alpha_n^2} \tag{77}$$

where

$$\theta_n = \frac{2\alpha_n}{a}$$

$$C_{1np} = \frac{R'\Omega_n}{U\alpha_n^2}\left[\frac{(1 - N_{Kh}\theta_n)e^{-\theta_n} - (1 + N_{Kh}\theta_n)}{(1 - N_{Kh}\theta_n)^2 e^{-\theta_n} - (1 + N_{Kh}\theta_n)^2 e^{\theta_n}}\right]$$

$$C_{1nu} = \frac{\Omega_n(1 + N_{Kh}\theta_n)}{(1 - N_{Kh}\theta_n)^2 e^{-\theta_n} - (1 + N_{Kh}\theta_n)^2 e^{\theta_n}}$$

$$C_{2np} = \left[\frac{(1 - N_{Kh}\theta_n) - (1 + N_{Kh}\theta_n)e^{\theta_n}}{(1 - N_{Kh}\theta_n)^2 e^{-\theta_n} - (1 + N_{Kh}\theta_n)^2 e^{\theta_n}}\right]\frac{R'\Omega_n}{U\alpha_n^2}$$

$$C_{2nu} = - \frac{\Omega_n (1 - N_{Kh}\theta_n)}{(1 - N_{Kh}\theta_n)^2 e^{-\theta_n} - (1 + N_{Kh}\theta_n)^2 e^{\theta_n}} .$$

By substituting Equation (77) back into Equation (70) the dimensionless velocity distribution becomes, after considerable simplification,

$$u(x, y) = \frac{(b')^2}{2\mu U \cos\alpha} \frac{dP}{dz} \sum_{n=1}^{\infty} \left[\frac{\sin\alpha_n}{1 + \frac{2N_{Kh}}{a}\sin^2\alpha_n}\right] \cdot$$

$$\left[\frac{\cos\alpha_n x}{\alpha_n^3}\right] \left[\frac{\cosh\frac{2\alpha_n y}{a} - \tanh\frac{\alpha_n}{a}\sinh\frac{2\alpha_n y}{a}}{1 + \frac{2N_{Kh}\alpha_n}{a}\tanh\frac{\alpha_n}{a}} - 1\right]$$

$$- \sum_{n=1}^{\infty} 2 \left[\frac{\sin\alpha_n}{1 + \frac{2N_{Kh}}{a}\sin^2\alpha_n}\right] \left[\frac{\cos\alpha_n x}{\alpha_n}\right] \cdot$$

$$\left[\frac{\sinh\frac{2\alpha_n y}{a} + \frac{2N_{Kh}\alpha_n}{a}\cosh\frac{2\alpha_n y}{a}}{\left[1 + \left(\frac{2N_{Kh}\alpha_n}{a}\right)^2\right]\sinh\frac{2\alpha_n}{a} + \frac{4N_{Kh}\alpha_n}{a}\cosh\frac{2\alpha_n}{a}}\right] . \qquad (78)$$

The volume flow rate in the groove is obtained by integrating the velocity distribution over the area of the groove. The volume flow rate thus obtained is

$$V'_g = \frac{(b')^3 h}{2\mu}\frac{dP}{dz} \sum_{n=1}^{\infty} \frac{a}{\alpha_n^5} \left[\frac{\sin^2\alpha_n}{1 + \frac{2N_{Kh}}{a}\sin^2\alpha_n}\right] \left[\frac{\tanh\alpha_n/a}{1 + \frac{2N_{Kh}\alpha_n}{a}\tanh\frac{\alpha_n}{a}} - \frac{\alpha_n}{a}\right]$$

$$= Ub'h\cos\alpha \sum_{n=1}^{\infty} \frac{a}{\alpha_n^3} \left[\frac{\sin^2\alpha_n}{1 + \frac{2N_{Kh}}{a}\sin^2\alpha_n}\right] \left[\frac{\tanh\alpha_n/a}{1 + \frac{2N_{Kh}}{a}\tanh\frac{\alpha_n}{a}}\right] . \qquad (79)$$

The first summation term represents the pressure induced flow in the groove whereas the second term represents the rotor induced flow.

The linearity of Equation (65) has been demonstrated in the analysis above since the solution of Equation (79) can be shown to be the sum of two solutions. The first term is in agreement with the expression obtained by Ebert and Sparrow (29) for slip flow in a rectangular duct with stationary walls. Milligan and Patterson (5) have experimentally verified the solution of Ebert and Sparrow. The last term is the solution of $\nabla^2 v = 0$ with the boundary conditions given in Equation (66). It is thus demonstrated that it is permissible to obtain the two solutions mentioned above independently and then to add them together to arrive at the same result as Equation (79).

At this point it is interesting to determine V'_g when the Knudsen number approaches zero, the continuum flow regime. The solution for the eigenvalues becomes

$$\cos \alpha_n = 0$$

or

$$\alpha_n = \frac{n\pi}{2} \qquad n = 1, 3, 5, 7 \ldots$$

With these eigenvalues and with $N_{Kh} \to 0$, V'_g becomes

$$V'_{gc} = \frac{16(b')^3 h}{\pi^5 \mu} \frac{dP}{dz} \sum_{n=1}^{\infty} \frac{a}{n^5}\left[\tanh \frac{n\pi}{2a} - \frac{n\pi}{2a}\right] - \frac{8Ub'h \cos \alpha}{\pi^3} \sum_{n=1}^{\infty} \frac{a}{n^3} \tanh \frac{n\pi}{2a} \qquad (80)$$

$n = 1, 3, 5, 7 \ldots$

2.32. Correction to Rotor Induced Flow. In the analysis above it was assumed that the rotor velocity, U cos α, acted at the top of the groove ($\bar{y} = h$). No attempt was made to account for the fact that the rotor is not located at $\bar{y} = h$ but rather at $\bar{y} = h + c$. Since an exact analysis of the region above the

groove, $h \leq \bar{y} \leq h + c$, has been shown to be very complex even for continuum flow (27), some sort of approximation must be made to obtain a simple solution. The following assumptions are made: (1) the flow induced by the rotor in the region $h \leq \bar{y} \leq h + c$ does not contribute to the seal discharge and (2) an effective inducing velocity less than $U \cos \alpha$ acts at $\bar{y} = h$ as a result of the clearance region $h \leq \bar{y} \leq h + c$. This effective inducing velocity, U_e, will be determined by calculating the average velocity in the plane $\bar{y} = h$ of a hypothetical groove of depth $h + c$ and width b with the upper boundary moving at $U \cos \alpha$ and with slip boundary conditions on all surfaces. The hypothetical groove and associated boundary conditions are shown in Figure 6. The brackets in Figure 6 indicate the portion of the boundary over which each boundary condition is applied.

From Equation (78) the velocity distribution induced by the rotor is

$$v_R = U \cos \alpha \sum_{n=1}^{\infty} \frac{2}{\alpha_n} \left[\frac{\sin \alpha_n \cos \alpha_n x}{1 + \frac{2N_{Kh}}{a} \sin^2 \alpha_n}\right] \cdot \left[\frac{\sinh \frac{2\alpha_n y}{a} + \frac{2N_{Kh}\alpha_n}{a} \cosh \frac{2\alpha_n y}{a}}{\left[1 + \left(\frac{2N_{Kh}\alpha_n}{a}\right)^2\right] \sinh \frac{2\alpha_n}{a} + \frac{4N_{Kh}\alpha_n}{a} \cosh \frac{2\alpha_n}{a}}\right]. \quad (81)$$

If Equation (81) is applied to a groove of depth $h + c$, the resulting distribution is

$$v_R' = U \cos \alpha \sum_{n=1}^{\infty} \frac{2}{\alpha_n} \left[\frac{\sin \alpha_n \cos \alpha_n x}{1 + \frac{2N_{Kh'}}{a'} \sin^2 \alpha_n}\right] \cdot \left[\frac{\sinh \frac{2\alpha_n y'}{a'} + \frac{2N_{Kh'}\alpha_n}{a'} \cosh \frac{2\alpha_n y'}{a'}}{\left[1 + \left(\frac{2N_{Kh'}\alpha_n}{a'}\right)^2\right] \sinh \frac{2\alpha_n}{a'} + \frac{4N_{Kh'}\alpha_n}{a'} \cosh \frac{2\alpha_n}{a'}}\right],$$

where

$$a' = \frac{b'}{h + c} = \frac{a}{1 + c/h}$$

$$N_{Kh'} = \frac{\lambda}{h + c} = \frac{N_{Kh}}{1 + c/h}$$

$$y' = \frac{\bar{y}}{h + c} .$$

The eigenvalues of Equation (71) are still the same because

$$\frac{a}{2N_{Kh}} = \frac{a'}{2N_{Kh'}} .$$

The average velocity at the plane $\bar{y} = h$ or $y' = \frac{h}{h + c}$ is

$$U_e = \int_0^1 v_R'(x, h/(h + c))dx.$$

Carrying through the integration, U_e becomes

$$U_e = 2U \cos \alpha \sum_{n=1}^{\infty} \frac{1}{\alpha_n^2} \left[\frac{\sin^2 \alpha_n}{1 + \frac{2N_{Kh}}{a} \sin^2 \alpha_n} \right] \left[\frac{\sinh \frac{2\alpha_n}{a} + \frac{2N_{Kh}\alpha_n}{a} \cosh \frac{2\alpha_n}{a}}{\left[1' + \frac{2N_{Kh}\alpha_n}{a}\right)^2] \sinh \frac{2\alpha_n}{a'} + \frac{4N_{Kh}\alpha_n}{a} \cosh \frac{2\alpha_n}{a'}} \right] \quad (82)$$

or

$$U_e = [U \cos \alpha] \Sigma_c \quad (83)$$

where the Σ_c is equal to twice the summation in Equation (82). The corrected groove flow is now obtained by replacing U cos α in Equation (79) with $[U \cos \alpha]\Sigma_c$. The total groove flow now becomes

$$V_g' = - \frac{(b')^3 h}{2\mu} \frac{dP}{dz} \Sigma_p - U b'h \cos \alpha [\Sigma_c \Sigma_u] \quad (84)$$

where

$$\Sigma_p = \sum_{n=1}^{\infty} \frac{a}{\alpha_n^5} \left[\frac{\sin^2\alpha_n}{1 + \frac{2N_{Kh}}{a}\sin^2\alpha_n}\right]\left[\frac{\tanh\frac{\alpha_n}{a}}{1 + \frac{2N_{Kh}\alpha_n}{a}\tanh\frac{\alpha_n}{a}} - \frac{\alpha_n}{a}\right] \quad (85a)$$

$$\Sigma_u = \sum_{n=1}^{\infty} \frac{a}{\alpha_n^3} \left[\frac{\sin^2\alpha_n}{1 + \frac{2N_{Kh}}{a}\sin^2\alpha_n}\right]\left[\frac{\tanh\frac{\alpha_n}{a}}{1 + \frac{2N_{Kh}\alpha_n}{a}\tanh\frac{\alpha_n}{a}}\right] \quad (85b)$$

and

$$\Sigma_c = \sum_{n=1}^{\infty} \frac{2}{\alpha_n^2} \left[\frac{\sin^2\alpha_n}{1 + \frac{2N_{Kh}}{a}\sin^2\alpha_n}\right].$$

$$\frac{\sinh\frac{2\alpha_n}{a} + \frac{2N_{Kh}\alpha_n}{a}\cosh\frac{2\alpha_n}{a}}{\left[1 + \left(\frac{2N_{Kh}\alpha_n}{a}\right)^2\right]\sinh\frac{2\alpha_n}{a'} + \frac{4N_{Kh}\alpha_n}{a}\cosh\frac{2\alpha_n}{a'}}\Bigg]. \quad (85c)$$

In terms of the viscoseal geometry

$$\frac{dP}{dz} = \frac{dP}{d\ell_g} = \frac{N_s(b' + w)}{\pi D}\frac{dP}{dL} = \sin\alpha\frac{dP}{dL}, \quad (86)$$

and since the pressure gradient in the viscoseal is assumed to be constant,

$$\frac{dP}{dz} = -\sin\alpha\frac{\Delta P}{L}. \quad (87)$$

The total groove flow is obtained by multiplying Equation (84) by N_s. Noting that $N_s = (\pi D)\sin\alpha/(b' + w)$ the total groove flow becomes

$$V_g = N_s V_g' = \frac{\pi D(b')^3 h\Delta P \sin^2\alpha}{2\mu L(b' + w)}\Sigma_p - \frac{U\pi Db'h\cos\alpha\sin\alpha}{(b' + w)}\Sigma_u\Sigma_c. \quad (88)$$

2.3 Land Leakage Flow

The land leakage flow is taken as flow through a long annulus. Milligan et al. (4) have developed an expression for slip flow in an annulus and have obtained excellent experimental confirmation of the expression. The expression derived by Milligan is

$$V_L = - \frac{\pi D^4}{128\mu} \frac{dP}{d\ell_L} A_L \tag{89}$$

where

$$A_L = [(1 - K'^4) + \frac{(1 - K'^2)^2}{\ln K'}] + [\frac{2N_K(1 - K'^2)}{K' \ln K' - N_K(1 - K'^2)} \cdot$$

$$[2K'(K'^2 - 1) - 2K'(\ln K')(K'^2 - K' + 1) - \frac{(1 - K'^2)^2}{2 \ln K'}$$

$$+ 2(1 - K'^2)(1 - K')^2 N_K], \tag{90}$$

and $\frac{dP}{d\ell_L}$ is the effective land pressure gradient. For a single-threaded seal, Hodgson (9) showed based on assumption (2) at the beinning of this chapter that

$$\frac{dP}{d\ell_L} = \frac{w' + b'}{w'} \cos \alpha \frac{dP}{dL} . \tag{91}$$

As was shown in Reference (13), Equation (91) remains valid for a multi-threaded seal.

Combining Equations (89) and (91) the land leakage flow becomes

$$V_L = \frac{\pi D^4 (w' + b') \cos \alpha}{128\mu w'} A_L \frac{dP}{dL} = \frac{\pi D^4 (w' + b') \cos \alpha}{128\mu w' L} A_L \Delta P \tag{92}$$

2.3 Total Seal Flow and Sealing Coefficient

The total seal flow is obtained by combining Equations (88) and (92). The result is

$$V_T = \frac{\Delta P}{\mu L} [A_p \Sigma_p + A_c A_L] - \frac{6U}{c^2} [A_u \Sigma_c \Sigma_u] \tag{93}$$

where

$$A_p = \frac{\pi D (b')^3 h \sin^2 \alpha}{2(w' + b')}$$

$$A_c = \frac{\pi D^4 (b' + w') \cos \alpha}{128\, w'}$$

and

$$A_u = \frac{\pi D b' h c^2 \cos \alpha \sin \alpha}{6(w' + b')}$$

The specific molecular flow rate is

$$\frac{\dot{n}}{\Delta P} = \frac{V_T}{\Delta P} \left(\frac{\overline{P}}{kT}\right)$$

or

$$\frac{\dot{n}}{\Delta P} = \frac{\overline{P}}{\mu L k T} \left[A_p \Sigma_p + A_c A_L\right] - \frac{3U}{c^2 kT} \left[\frac{r_p + 1}{r_p - 1}\right] \left[A_u \Sigma_c \Sigma_u\right] \tag{94}$$

where Equation (12) is used to eliminate ΔP.

A common dimensionless viscoseal performance index is called the sealing coefficient and is defined by

$$\Lambda \equiv \frac{6\mu U L}{c^2 \Delta P} \tag{95}$$

where ΔP is the pressure difference at zero flow. By equating V_T to zero in Equation (93), the sealing coefficient is obtained as

$$\Lambda = \frac{A_p \Sigma_p + A_c A_L}{A_u \Sigma_c \Sigma_u} . \tag{96}$$

A digital computer was used to compute the specific molecular flow rate from Equation (94) and the sealing coefficient from Equation (96). In order to evaluate the summations, Σ_p, Σ_c, and Σ_u, it is necessary to determine the eigenvalues which satisfy Equation (71). Newton's method of approximating roots was employed to solve Equation (71) for these eigenvalues at each Knudsen number.

3. EXPERIMENTAL INVESTIGATION

Since no reliable performance data were available for viscoseals having a rarefied gas as the sealant it was necessary to conduct an experimental investigation. The object was to obtain performance data which could be used to evaluate the theoretical models. These investigations were conducted on multiple groove two-inch diameter viscoseals operating over a wide range of shaft speeds and gas densities. Data were obtained with no leakage through the seal which permitted the evaluation of sealing coefficients. In addition data were obtained for a wide range of net leakage conditions. All rarefied data were obtained using argon as the sealant. Continuum sealing coefficient data were obtained using air as the sealant.

3.1 Viscoseal Test Section

The experimental apparatus was designed to investigate viscoseal performance in the gas flow regime between continuum and free molecule flow.

The viscoseal test section, Figure 7, consists of an outer housing with its associated vacuum pumping system surrounding a rotating grooved shaft. The shaft is a hollow eight-inch cantilever extension of a high speed spindle shaft which is belt-driven through an intermediate spindle by a direct current motor. The drive system is capable of seal shaft speeds from zero to 35,000 rpm. The speed control for the motor is self-regulating and maintains a selected speed within $\pm$ 0.1 percent. Since the entire test section operates under vacuum, a rubbing contact graphite ring seal is provided where the rotating shaft penetrates the housing. The ring seal is a series B-103032, Type E, manufactured by the Cleveland Graphite Bronze Division of the Clevite Corporation. Cooling water and air are supplied at the ring seal end of the spindle

to minimize thermal growth due to the rubbing seal friction under dynamic conditions. A Conflat vacuum flange is provided between the housing and its support for purposes of sealing and two provide minor adjustment capabilities for housing-shaft alignment. Other vacuum seals are obtained by the use of "O" rings in addition to vacuum sealants for threaded connections. The maintenance of a high quality vacuum system with essentially no atmospheric leakage, except at the shaft seal, was assured by the frequent use of a helium leak detector throughout the experimental program.

Experimental data were obtained for two different viscoseal geometries consisting of a grooved shaft inside a smooth housing. Pertinent specifications of the rarefied viscoseals are contained in Table I.

Table I. Dimensional Specifications of Viscoseals (All Dimensions are in Inches)

Parameter	Seal No. 1	Seal No. 2
Housing diameter ($\pm$ 0.0003)	2.0088	2.0088
Shaft diameter ($\pm$ 0.0001)	2.0005	2.0005
"Cold" radial clearance ($\pm$ 0.0002)	0.00418	0.00418
Axial length ($\pm$ 0.005)	4.530	4.530
Groove axial width	0.03111 $\pm$ 0.0003	0.1691 $\pm$ 0.012
Land axial width	0.03235 $\pm$ 0.0003	0.2016 $\pm$ 0.012
Groove depth	0.03065 $\pm$ 0.0003	0.0144 $\pm$ 0.0005
Groove helix angle	9.30°	19.474°
Aspect ratio, $(b \cos \alpha)/h$	1.002	11.071

A schematic diagram of the overall experimental test apparatus is shown in Figure 8.

3.2 Vacuum Pumping System

It was necessary to develop a vacuum pumping system capable of providing the desired low pressures and gas flow rates. This task was accomplished by connecting two independent vacuum pumping systems in parallel to a common reservoir, Figure 8. One of these pumping systems consisted of a single stage rotary oil-sealed mechanical pump mated with a three-stage high vacuum oil diffusion pump. This part of the pumping system was connected to the reservoir with a large diameter open-or-close vacuum valve. The second pumping system was composed of another single stage rotary oil-sealed mechanical pump mated with a positive displacement roots blower type vacuum pump. This portion of the pumping system was connected to the reservoir througha throttlable high vacuum valve. Through manipulation of the two connecting valves it was possible to regulate the pumping speed over a suitable range of downstream test section pressures. The complete vacuum pumping system was capable of attaining pressures to 10^{-5} millimeters of mercury with a blanked-off system.

3.3 Instrumentation

The radial alignment of the shaft within the housing was determined by the use of five proximity detectors manufactured by the Bentley-Nevada Corporation. These probes were located near either end of the viscoseal section. When viewed from the shaft drive end of the test section, the probes of the first set were located at 12, 3, and 6 o'clock positions, and the probes of the second set were located at 12 and 3 o'clock positions. The arrangement of the probes permitted the shaft to be aligned within the housing to a value of eccentricity ratio (shaft centerline deviation/mean radial

clearance) on the order of 0.05. The probes were also used to determine the thermal growth of the shaft caused by the graphite ring seal friction when the shaft was rotating. In addition, the probes permitted the measurement of all vibrational movements of the shaft. The output gains of the detector amplifiers were individually adjusted and calibrated to ensure a linear output voltage of the probes as a function of the clearance gap.

Pressure measurements upstream and downstream of the viscoseal were obtained using both McLeod gauges and absolute aneroid type gauges. The McLeod gauge is normally considered to be a primary standard (30), but after previous attempts (31) to use thermocouple gauges, ionization gauges and cold cathode gauges, it was apparent that McLeod gauges were the only instruments capable of giving the desired accuracy and reproducibility. The McLeod gauges utilized were the GM-100A gauge manufactured by the Consolidated Vacuum Corporation and are described in detail in Reference (31).

Temperature measurements of the argon entering the high pressure end of the viscoseal test section were made early in the experimental program using a thermocouple. A comparison of the measured gas temperature with the ambient (room) temperature revealed that the error involved in using room temperature instead of the actual gas temperature was less than one percent. Therefore the gas temperature was taken to be 297°K in all data calculations.

Speed measurements of the viscoseal shaft were made using a magnetic pickup located near the attachment nut for the drive belt pulley on the high speed spindle. The pulses from the pickup were registered using an electronic counter to obtain shaft rpm. The speed

measurements were independently verified using a calibrated hand held tachometer in the low rpm range and a calibrated strobotac over the entire speed range of 0 to 35,000 rpm.

The molecular flow rate through the viscoseal test section was determined using a variation of a constant pressure method developed by J. R. Downing (30) for the measurement of pumping speeds of vacuum pumps. The technique consists of applying the perfect gas equation of state to known gas volumes at two different time periods. In brief, the flow measurement is obtained by adjusting the indexed valve of Figure 8 to a desired setting and waiting for steady state to be achieved in the test section as indication by pressure and proximity probe measurements. The shut-off valve leading from the constant pressure gas reservoir is then closed and the rate of rise of manometer fluid in the right hand side of the manometer is observed. With knowledge of the manometer cross sectional area, the rate of fluid rise, the value of the calibrated volume, the initial and final pressures in the calibrated volume, and the gas temperature, the molecular flow rate is calculated in the following manner.

Consider the flow measurement diagram of Figure 9. Let

V_o = calibrated volume including tank and manometer down to the zero deflection line, "0"

P_o = atmospheric pressure

H_1 = initial manometer deflection

H_2 = final manometer deflection

A_m = cross section area of manometer tube

W = specific weight ofmanometer fluid

From fluid statics:

$$P_1 = P_o + 2WH_1$$

$$P_2 = P_o - 2WH_2.$$

The corresponding gas volumes are:

$$V_1 = V_o + H_1A_m$$

$$V_2 = V_o - H_2A_m.$$

Applying the perfect gas equation of state,

$$PV = NKT, \tag{97}$$

on a molecular basis to determine the number of molecules within the system at time (1) and time (2), then,

$$\Delta N = N_1 - N_2 = \frac{P_1V_1}{KT_1} - \frac{P_2V_2}{KT_2}. \tag{98}$$

Assuming isothermal conditions and substituting for the pressures and volumes, Equation (98) simplifies to,

$$\Delta N = \frac{H_1 + H_2}{KT}\{A_m[P_o + 2W(H_1 - H_2)] + 2WV_o\}. \tag{99}$$

The flow measurement system was operated experimentally such that

$$H_1 = H_2.$$

Letting

$$H = H_1 + H_2$$

and Δt be the time period for the total deflection H, then the molecular flow rate is

$$\dot{N} = \frac{\Delta N}{\Delta t} = \frac{H}{\Delta tKT}\{A_mP_o + 2WV_o\}. \tag{100}$$

The basic premise for the measurement system rests in the fact that while the pressure in the calibrated volume does change slightly, less than $\pm$ 1%, it still remains very close to atmospheric pressure.

Thus, the change in flow rate through the valve is negligibly affected by the slight decrease in the pressure within the calibrated volume during the course of a measurement.

3.4 Experimental Procedure

Experimental data of two different types were obtained for the operation of the viscoseals in the rarefied regime. These may be described as net flow leakage data and sealing coefficient data. The operational procedure utilized in gathering the data differed only in respect to shutting off the argon gas supply when obtaining sealing coefficient data.

All data were acquired by the coordinated adjustment of the gas supply rate, the vacuum pumping speed, and the seal shaft drive speed followed by a time period sufficient to obtain a steady-state condition. Following achievement of steady state, final readings of the gas flow rate, pressures upstream and downstream of the viscoseal, and the proximity probes were made. The proximity probes were used to record the seal clearance which decreases slightly with increasing shaft speed due to the friction of the graphite ring vacuum seal.

3.5 Data Treatment

The viscoseal performance data for both the net flow leakage tests and the sealing coefficient tests were correlated versus an index of the flow rarefication, Knudsen number. The mean radial clearance, $\bar{c}$, was selected as the viscoseal characteristic dimension. Thus using the Chapman relationship for the mean free path, the experimental values for Knudsen number were determined using the following equation.

$$N_K = \frac{\lambda}{\bar{c}} = \frac{\mu(2\pi \frac{R_o}{M} T)^{1/2}}{2\bar{P}\,\bar{c}} \qquad (101)$$

The mean free path was based on the average seal section pressure

$$\bar{P} = \frac{P_T + P_b}{2} . \tag{102}$$

The molecular flow rates for the net flow leakage data were calculated using Equation (100). These data were revised to specific molecular flow rates by dividing by the pressure drop, ΔP, across the viscoseal, or

$$\frac{\dot{N}}{\Delta P} = \frac{H[A_m P_o + 2WV_o]}{(P_T - P_b)\Delta t K T} . \tag{103}$$

The sealing coefficient data were calculated from the zero net leakage tests using

$$\Lambda = \frac{6\mu UL}{\Delta P \bar{c}^{-2}} = \frac{6\mu UL}{(P_T - P_b)\bar{c}^{-2}} . \tag{104}$$

3.6 Experimental Uncertainty. A detailed analysis was performed to estimate the propagated uncertainty in the final performance parameters based on the individual uncertainties of all measured variables. The analysis was performed using standard statistical techniques after postulating a normal distribution in the uncertainty of each variable. This method of analysis assumes all errors are random in nature. Considerable effort was expended during the experimental investigation to minimize any error of a systematic nature.

The propagated uncertainties, in general, are not constant and vary with the degree of rarefication. The uncertainty in the specific molecular flow rate, $\dot{N}/\Delta P$, of Equation (103) is $\pm$ 5.1 percent at an Inverse Knudsen Number of 27 where the calibrated volume, V_o, contribution is 84 percent of the total. The uncertainty in the specific molecular flow rate increases to $\pm$ 8.9 percent at an Inverse

Knudsen Number of 0.50 where the uncertainty in the differential pressure, ΔP, contributes 72 percent of the total. The ability to determine the Inverse Knudsen Number of Equation (101) is estimated at $\pm$ 4.8 percent for $1/N_K$ equal to 27 and increases to $\pm$ 5.7 percent for $1/N_K$ equal to 0.50. The propagated uncertainty estimate in the sealing coefficient, Λ, of Equation (104) is insensitive to the degree of rarefication and remains at essentially $\pm$ 9.6 percent. The uncertainty in the radial clerance, c, contributes approximately 99 percent of the propagated uncertainty estimate for Λ. It should be noted that the clearance uncertainty is controlled by the ability to establish the diameters of the seal shaft and housing and not by any limitations of the proximity probe system.

All uncertainties are stated to a confidence level of 95 percent.

3.7 Investigations Conducted

Sealing coefficient performance data and net leakage performance data were obtained for each of the two geometries. Sealing coefficient data were obtained over a wide range of sealant gas rarefication for shaft speeds of zero, 5000, 10,000, and 30,000 rpm. Net leakage data were also obtained over comparable ranges of rarefication and shaft speeds. These data are presented and discussed in Section 4 and the reduced data are tabulated in Appendix B.

4. RESULTS

Two types of results will be presented for each of the three analytical models. Net leakage and sealing coefficients will be given as a function of the degree of rarefication. The inverse Knudsen number is used as the parameter indicating the degree of rarefication.

4.1 Net Leakage

The net leakage flow occurs from the high pressure end to the low pressure end of the viscoseal when the viscous pumping action is insufficient to overcome the pressure induced flow in the grooves and through the annular clearance space. The net leakage data are shown in Figures 10 through 15. These data are presented in the form of specific leakage rate (units of molecules per sec-μHg) versus Inverse Knudsen Number. The experimental data for viscoseal Seal No. 1 are shown in Figures 10, 11, and 12. The theoretical specific leakage values as predicted by the Modified Hodgson Model are shown in Figure 10. These theoretical values were obtained by using Equation (6) for the zero rpm case and Equation (8) for the 5000; 10,000; and 30,000 rpm cases. The Slip Modified Boon and Tal Model was used to determine the theoretical values shown on Figure 11. Two solutions for this model are presented. The mean-value values were calcualted using Equation (55). The variable-mean-free-path values were obtained by solving Equation (46). In Figure 12 theoretical values for the Annulus-Groove Model are presented. Equation (94) was used to determine the theoretical values shown in Figure 12.

The experimental data for Viscoseal No. 2 are presented in Figures 13, 14, and 15. These figures contain data for one additional speed, 2500 rpm. The theoretical specific leakage values shown on these figures were determined in the same manner as described above for Viscoseal No. 1.

In Section 2.25 a composite type solution was discussed for the Slip Modified Boon and Tal Model. This type of composite solution is

obtained by the superposition of the corrected continuum-slip flow contribution with the self-diffusion flows in the annular space and the grooves. The corrected continuum-slip flow is determined by taking into account the fact that all the molecules cannot experience the slip boundary condition. This procedure is explained in detail in Section 2.23. A detailed procedure for calculating the self-diffusion flows is given in Section 2.24. Tables II through VII present composite solution results and the uncorrected continuum-slip results. In each table the first column on the left is Inverse Knudsen Number. Moving to the right in the tables the second column is the uncorrected continuum-slip solution. The third column is the particle-slip corrected solution. The fourth column is the self-diffusion through the annular clearance space, the fifth column is the self-diffusion through the grooves, and the last column is the composite solution.

Table II shows specific leakage results from the Slip-Modified Boon and Tal Model for Seal No. 1 at zero rpm. Table III is the same except that these results are for 5000 rpm. Tables IV and V contain specific leakage as predicted by the Boon and Tal Model for Seal No. 2 at zero and 2500 rpm, respectively. Tables VI and VII contain results for the Annulus-Groove Model. Table VI is for Seal No. 2 at zero rpm and Table VII is for the same seal at 2500 rpm. These are typical composite solution results. The particular results shown in Tables II through VII were chosen because they were the cases which gave the largest deviations between the composite solution and the simpler non-corrected continuum-slip solution.

Table II. Slip Modified Boon and Tal Model

Net Leakage Solutions x 10^{-14} for Seal No. 1 at Zero rpm

$1/N_K$	$\check{N}/\Delta P$	$\check{N}/\Delta P$ Composite Solution - Eq. (63)			
	Cont. + slip No. Part. Corr.	Cont. + slip Part. Corr.	Annulus Diffusion	Groove Diffusion	Composite Flow 1 + 2 + 3
1×10^{-2}	2.22	0.198	1.92	0.48	2.60
3×10^{-2}	2.24	0.514	1.69	0.42	2.62
7×10^{-2}	2.30	0.951	1.41	0.34	2.70
1×10^{-1}	2.33	1.18	1.30	0.30	2.78
3×10^{-1}	2.58	1.99	0.87	0.17	3.03
7×10^{-1}	3.08	2.78	0.57	0.086	3.44
1×10^{0}	3.45	3.23	0.45	0.053	3.73
3×10^{0}	5.92	5.84	0.19	0.022	6.05
7×10^{0}	10.8	10.8	0.090	0.0096	10.9
1×10^{1}	14.5	14.5	0.064	0.0068	14.6
3×10^{1}	39.2	39.2	0.022	0.0023	39.2
7×10^{1}	88.4	88.4	0.0094	0.0010	88.4
1×10^{2}	125.0	125.0	0.0065	0.0007	125.0

Table III. Slip Modified Boon and Tal Model

Net Leakage Solutions x 10^{-14} for Seal No. 1 at 5000 rpm

$1/N_K$	$\dot{N}/\Delta P$	$\dot{N}/\Delta P$ Composite Solution - Equation (63)			
	No. Part. Corr.	Part Corr. 1	Annulus Diff. 2	Groove Diffusion 3	Composite Flow 1 + 2 + 3
1×10^{-2}	-8.36	-10.36	1.55	0.48	-8.33
3×10^{-2}	-8.35	-10.04	1.45	0.42	-8.17
7×10^{-2}	-8.31	- 9.60	1.22	0.34	-8.04
1×10^{-1}	-8.28	- 9.37	1.11	0.29	-7.97
3×10^{-1}	-8.07	- 8.61	0.76	0.16	-7.69
7×10^{-1}	-7.61	- 7.87	0.49	0.08	-7.30
1×10^{0}	-7.26	- 7.44	0.39	0.059	-6.99
2×10^{0}	-6.04	- 6.14	0.22	0.031	-5.89
3×10^{0}	-4.81	- 4.87	0.16	0.020	-4.69
4×10^{0}	-3.57	- 3.62	0.12	0.015	-3.49
5×10^{0}	-2.33	- 2.37	0.10	0.012	-2.26
6×10^{0}	-1.08	- 1.11	0.086	0.010	-1.01
7×10^{0}	+0.16	+ 0.13	0.075	0.009	+0.21
1×10^{1}	3.90	3.88	0.054	0.0063	3.94
3×10^{1}	28.84	28.83	0.019	0.0021	28.85
7×10^{1}	78.73	78.72	0.0082	0.00092	78.73
1×10^{2}	116.10	116.10	0.0056	0.00065	116.11

Table IV. Slip Modified Boon and Tal Model

Net Leakage Solutions x 10^{-14} for Seal No. 2 at Zero rpm

	$\dot{N}/\Delta P$	$\dot{N}/\Delta P$ Composite Solution - Equation (63)			
$1/N_K$	Cont. + slip No. Part. Corr.	Cont. + Slip Part. Corr. 1	Annulus Diffusion 2	Groove Diffusion 3	Composite Flow 1 + 2 + 3
1×10^{-2}	2.09	0.110	1.92	0.72	2.75
3×10^{-2}	2.11	0.303	1.69	0.49	2.48
7×10^{-2}	2.14	0.609	1.41	0.31	2.33
1×10^{-1}	2.17	0.790	1.30	0.24	2.33
3×10^{-1}	2.33	1.518	0.87	0.11	2.49
7×10^{-1}	2.66	2.21	0.57	0.05	2.83
1×10^{0}	2.91	2.57	0.45	0.035	3.05
3×10^{0}	4.54	4.41	0.19	0.012	4.61
7×10^{0}	7.78	7.72	0.09	0.005	7.82
1×10^{1}	10.21	10.17	0.064	0.0036	10.24
3×10^{1}	26.41	26.39	0.022	0.0012	26.41
7×10^{1}	58.80	58.80	0.0094	0.0005	58.81
1×10^{2}	83.10	83.09	0.0065	0.00036	83.10

Table V. Slip Modified Boon and Tal Model

Net Leakage Solutions x 10^{-14} for Seal No. 2 at 2500 rpm

$1/N_K$	$\dot{N}/\Delta P$	$\dot{N}/\Delta P$ Composite Solution - Equation (63)			
	Cont.+Slip No. Part. Corr.	Cont. + Slip Part. Corr. 1	Annulus Diffusion 2	Groove Diffusion 3	Composite Flow 1 + 2 + 3
1×10^{-2}	-2.26	-4.36	1.75	0.71	-1.90
3×10^{-2}	-2.25	-4.15	1.52	0.47	-2.16
7×10^{-2}	-2.22	-3.82	1.28	0.29	-2.25
1×10^{-1}	-2.20	-3.64	1.16	0.23	-2.25
3×10^{-1}	-2.07	-2.69	0.79	0.10	-1.80
7×10^{-1}	-1.80	-2.25	0.51	0.047	-1.69
1×10^{0}	-1.58	-1.91	0.41	0.033	-1.47
2×10^{0}	-0.829	-1.00	0.23	0.016	-0.75
3×10^{0}	-0.056	-0.175	0.17	0.011	+0.006
4×10^{0}	+0.726	+0.636	0.13	0.0072	0.773
5×10^{0}	1.51	1.44	0.11	0.0066	1.56
6×10^{0}	2.30	2.24	0.092	0.0056	2.34
7×10^{0}	3.09	3.04	0.080	0.0048	3.18
1×10^{1}	5.48	5.44	0.057	0.0033	5.50
3×10^{1}	21.40	21.39	0.020	0.0011	21.41
7×10^{1}	53.28	53.28	0.0085	0.00048	53.29
1×10^{2}	77.20	77.20	0.0060	0.00033	77.21

Table VI. Annulus-Groove Model

Net Leakage Solution x 10^{-14} for Seal No. 2 at Zero rpm

$1/N_K$	$\dot{N}/\Delta P$	$\dot{N}/\Delta P$ Composite Solutions			
	No. Part. Corr.	Part. Corr. 1	Annulus Diffusion 2	Groove Diffusion 3	Composite Flow 1 + 2 + 3
1×10^{-2}	1.81	0.06	1.92	0.72	2.70
3×10^{-2}	1.82	0.16	1.69	0.49	2.34
7×10^{-2}	1.84	0.34	1.41	0.31	2.06
1×10^{-1}	1.86	0.48	1.30	0.24	2.02
3×10^{-1}	1.96	0.95	0.87	0.11	1.93
7×10^{-1}	2.16	1.50	0.57	0.05	2.12
1×10^{0}	2.30	1.79	0.45	0.035	2.28
3×10^{0}	3.28	3.06	0.19	0.012	3.26
7×10^{0}	5.22	5.12	0.09	0.005	5.22
1×10^{1}	6.68	6.60	0.064	0.0036	6.67
3×10^{1}	16.39	16.36	0.022	0.0012	16.38
7×10^{1}	35.81	35.80	0.0094	0.0005	35.81
1×10^{2}	50.37	50.36	0.0065	0.00036	50.37

Table VII. Annulus Groove Model

Net Leakage Solutions x 10^{-14} for Seal No. 2 at 2500 rpm

$1/N_K$	$\dot{N}/\Delta P$	$\dot{N}/\Delta P$ Composite Solution			
	No Part. Corr.	Part. Corr. 1	Annulus Diffusion 2	Groove Diffusion 3	Composite Flow 1 + 2 + 3
1×10^{-2}	-0.26	-3.06	1.75	0.71	-0.60
3×10^{-2}	-0.32	-2.84	1.52	0.47	-0.85
7×10^{-2}	-0.41	-2.52	1.28	0.29	-0.95
1×10^{-1}	-0.47	-2.36	1.16	0.23	-0.97
3×10^{-1}	-0.67	-1.82	0.79	0.10	-0.93
7×10^{-1}	-0.74	-1.41	0.51	0.047	-0.85
1×10^{0}	-0.70	-1.21	0.41	0.033	-0.77
2×10^{0}	-0.38	-0.66	0.23	0.016	-0.41
3×10^{0}	+0.04	-0.16	0.17	0.011	+0.02
4×10^{0}	0.48	+0.32	0.13	0.0072	0.46
5×10^{0}	0.94	0.81	0.11	0.0066	0.93
6×10^{0}	1.40	1.30	0.092	0.0056	1.40
7×10^{0}	1.86	1.77	0.080	0.0048	1.85
1×10^{1}	3.27	3.21	0.057	0.0033	3.27
3×10^{1}	12.76	12.73	0.020	0.0011	12.75
7×10^{1}	31.78	31.77	0.0085	0.00048	31.78
1×10^{2}	46.04	46.05	0.0060	0.00033	46.06

4.2 Sealing Coefficient

The sealing coefficient as defined in Equation (95) is a common dimensionless viscoseal performance index. The relationship which exists between the net leakage flow and the sealing coefficient can best be shown by reference to Figure 16. A family of net leakage curves as a function of the seal pressure ratio for a fixed shaft speed are shown. The curves progress to the left for increasing values of pressure ratio until the $(r_p + 1)/(r_p - 1)$ factor approaches unity. When the family of net leakage flow curves are extended to the zero net flow condition, a corresponding sealing coefficient condition may be indicated for each of the pressure ratio curves. Operating the rarefied viscoseal at "negative" net leakage is simply another way of saying that the viscoseal has now become a positive flow pump.

In Figures 17 through 22 sealing coefficient data and theoretical values are presented. Figures 17, 18, and 19 show results for Viscoseal No. 1 at 5000; 10,000; and 30,000 rpm. Figure 17 presents a comparison of experimental data and theoretical values as predicted by the Modified Hodgson Model. Figure 18 shows the same type of comparison for the Slip Modified Boon and Tal Model. Theoretical values are shown for both the mean-value and variable mean free path solutions. Figure 19 is a similar comparison for the Annulus-Groove Model.

Figures 20 through 22 show experimental and theoretical values for Viscoseal No. 2. Again data and analytical values are shown for each of the three models at speeds of 5000; 10,000; and 30,000 rpm.

5. CONCLUSIONS

Examination of Figures 10, 11, and 12, for Seal No. 1, indicates that the Annulus-Groove Model gives the best agreement with the experimental data. The Slip Modified Boon and Tal Model gives the poorest agreement. All three models predict the general characteristic for this low aspect (groove width to groove depth ratio) ratio, 1.002, seal. It is concluded that none of the theoretical models are completely adequate for predicting the leakage through low aspect ratio viscoseals. The Annulus-Groove Model is recommended for low aspect ratio viscoseals and Inverse Knudsen Numbers greater than 5.

For Seal No. 2, the results shown in Figures 13, 14, and 15 indicate that the Slip Modified Boon and Tal Model gives a better correlation with experimental data than either of the other two models. The only exception is for static (zero rpm) conditions having Knudsen Numbers greater than 0.5 where the Modified Hodgson Model shows better agreement. The aspect ratio of this geometry was 11.071 as compared to 1.002 for Seal No. 1. As anticipated the Slip Modified Boon and Tal Model is much better for the higher aspect geometry than for low aspect ratio geometries. The variable mean free path solution is only slightly better than the mean-value solution to the Slip Modified Boon and Tal Model. In view of the added complexity of the variable mean free path solution, it is recommended that the mean-value Slip Modified Boon and Tal Model be used to predict viscoseal leakage for high aspect ratio geometries provided the Inverse Knudsen Numbers are greater than 5. It is of interest to note that the 2500 rpm data for Viscoseal No. 2 seem to approach a constant specific leakage value with increasing Knudsen number.

In Tables II through VII a comparison between the continuum-slip and composite type solutions are shown for the Slip Modified Boon and Tal Model and the Annulus-Groove Model. These particular cases were chosen for presentation since they are the ones which gave maximum deviation between the two solution techniques. Examination of Table II shows that the diffusion flow contributions in both the annular space and the sixteen grooves are only one percent of the total composite flow at an Inverse Knudsen Number of 7.0 and decrease rapidly with decreased rarefication. At an Inverse Knudsen Number of 0.01 it can be observed that the diffusion contributes 92 percent of the total composite solution and thus the transport is essentially free molecular. This same trend is evident for the other two static cases as shown in Tables IV and VI. In Tables III, V, and VII the negative values of specific leakage simply indicate that the viscoseal is acting as a pump, i.e., the viscous pumping flow due to the grooves is greater than leakage flow.

For the Slip Modified Boon and Tal Model the maximum deviation between the composite solution and the continuum solution is less than three percent for Inverse Knudsen Numbers greater than 5.0. The deviation increases with rarefication and has a maximum value of approximately twenty-five percent. This maximum occurs at $1/N_K = 0.01$ and zero rpm for Seal No. 2.

For the Annulus-Groove Model the maximum deviation is less than two percent for Inverse Knudsen Numbers greater than five. The maximum deviation was approximately sixty percent at $1/N_K = 0.01$ and 2500 rpm for Seal No. 2.

The good agreement between the rather complex composite solutions and the continuum-slip solutions for Inverse Knudsen Number greater than five is apparent. It is concluded that the complex composite solutions cannot be justified for Inverse Knudsen Numbers greater than 5.0.

Consideration of the results shown in Figures 17 through 22 reveals several important aspects of the three analytical models. Only the Modified Hodgson Model and the variable mean free path solution to the Slip Modified Boon and Tal Model predict the general sealing characteristics which are evidenced by the experimental data. In general the models predict better sealing performance (smaller sealing coefficients) than what actually existed. It may be observed that the experimental data indicate that the sealing coefficient parameter becomes speed sensitive as the sealant gas becomes rarefied. This sensitivity to shaft speed for the rarefied-gas viscoseal is unique from the operation in the laminar continuum regime where the sealing coefficient is independent of shaft speed (14, 15). This continuum characteristic may be seen by noting the asymptotic behavior of the experimental data for 5000 and 10,000 rpm as the continuum ($1/N_K$ > 100) regime is approached. These data may be compared since the mean radial clearance is essentially the same for both speeds.

Examination of Figures 18 and 21 reveals that the mean-value solution to the Slip Modified Boon and Tal Model can predict a seal pressure differential, ΔP, which may exceed the magnitude of the upstream pressure. This solution would imply a negative absolute value for the downstream pressure, a condition which cannot occur in reality. A limiting criteria to be applied to this theoretical solution to avoid this condition is predictable by considering the variables involved.

As stated previously, the Knudsen number

$$N_K \equiv \frac{\lambda}{c} = \frac{\mu(2\pi\frac{R_o}{M}T)^{1/2}}{2\overline{P}c}$$

is based on the average pressure in the seal

$$\overline{P} = \frac{P_T + P_b}{2} = \frac{2P_T - \Delta P}{2} .$$

As the downstream pressure approaches zero, then ΔP approaches the upstream pressure and for this limiting condition

$$\overline{P} \approx \frac{\Delta P}{2} .$$

Thus, the Inverse Knudsen Number variable may be written as

$$(1/N_K) = \frac{\Delta Pc}{\mu(2\pi\frac{R_o}{M}T)^{1/2}} .$$

The Sealing Coefficient variable is defined as

$$\Lambda = \frac{6\mu UL}{\Delta Pc^2} .$$

Solving for ΔP in the Inverse Knudsen Number relationship and substituting this into the above equation gives the limiting functional relationship

$$\Lambda_{limit} = \{\frac{6UL}{c(2\pi\frac{R_o}{M}T)^{1/2}}\}\frac{1}{(1/N_K)} . \qquad (105)$$

For a given seal geometry, gas, temperature, and operating speed, the limiting seal coefficient function varies inversely with the Inverse Knudsen Number, $1/N_K$. On a logarithmic plot such as Figure 17, this relation will plot as a straight line with a slope of minus unity.

Points which fall above and to the right of this line are possible while those which fall below and to the left are not possible in that a negative absolute pressure downstream is implied. The limiting relation of Equation (105) is speed sensitive and thus the limit condition can be established for each selected shaft speed. Limit curves for speeds of 5000, 10,000, and 30,000 rpm from Equation (105) are shown on Figures 18, 19, 21, and 22. The experimental sealing coefficient data agree well with these limit curves and all points fall within the "possible" regions. In addition, the speed sensitivity of the experimental data agrees with that indicated by Equation (105). It should be noted that the limiting function of Equation (105) results from a limit condition of the variables involved and applies to any and all viscoseal analyses using these variables.

The limiting relationship just established is shown on Figures 18 and 21 to indicate that the mean-value solution to the Slip Modified Boon and Tal Model when used in conjunction with Equation (105) is a useful technique for predicting sealing coefficient performance. This limiting relationship can also be used with the Annulus-Groove Model.

The devaiation of predicted performance from experimental results is approximately the same for each of the three analytical models when the limiting relationship is used on the mean-value Slip Modified Boon and Tal Model and the Annulus-Groove Model. Theoretical values are not presented for the composite type solutions since there is negligible difference between the composite solutions for sealing coefficient and the continuum-slip solutions.

Since most practical seal geometries will result in a high aspect ratio, near 10, it is concluded that the simplicity of the mean-

value solution to the Slip Modified Boon and Tal Model in conjunction with the limiting relationship justifies its use. For low aspect ratio geometries the Annulus-Groove Model in conjunction with the limiting relationship is recommended. The complexity of the variable mean free path solution (Slip Modified Boon and Tal Model) cannot be justified in view of the small improvement in predicted value. The composite solutions are not practical for the same reasons.

6. RECOMMENDATIONS

In general it is recommended that the mean-value solution to the Slip Modified Boon and Tal Model, Equation (55), be used to predict viscoseal leakage for rarefied conditions resulting in Inverse Knudsen Numbers greater than 5. No satisfactory analytical model has been developed in this study to predict leakage for Inverse Knudsen Numbers less than 5.

To predict sealing performance it is recommended, in general, that the mean-value solution to the Slip Modified Boon and Tal Model, Equation (50), in conjunction with the limiting relationship, Equation (105), be used.

It should be noted that the variable mean-free-path solution to the Slip Modified Boon and Tal Model is more accurate for all conditions. If use is made of a high speed digital computer its complexity becomes less important and thus its use may be justified.

7. REFERENCES

1. Milligan, M. W., "Fundamental Study in Low-Density Gas Dynamics - Progress Report," Mechanical and Aerospace Engineering Research Report AE-66-023-1, University of Tennessee, November 1966.

2. Milligan, M. W. and C. T. Mothershead, "Low-Density Gas Flow in Short Tubes," ASME Paper No. 66-WA/PID-8, November 1966.

3. Milligan, M. W.,P. W. Cowling, and H. J. Wilkerson, "Fundamental Study in Low-Density Gas Dynamics - Progress Report," Mechanical and Aerospace Engineering Research Report AE-67-023-3, University of Tennessee, November 1967.

4. Milligan, M. W., P. W. Cowling, and H. J. Wilkerson, "Rarefied Gas Flow Through Annuli," American Institute of Aeronautics and Astronautics Journal, Vol. 6, No. 5, May 1968, pp. 914-916

5. Milligan, M. W.and K. E. Patterson, "Rarefied Gas Flow Through Long Square Tubes," ASME Transactions - Journal of Engineering for Industry, Vol. 93, Series B, No. 2, May 1971, pp. 751-754.

6. Milligan, M.W., "Rarefied Gas Flow Through Passages with Static Boundaries," ASLE Transactions, Vol. 11, No. 3, July 1968, pp. 228-234.

7. Milligan, M. W., "Predicting Gas Flow Rates in Vacuum Systems," ASME Paper 68-WA/PID-5, December 1968.

8. Milligan, M.W. and T. E. Scott, "Rarefied Gas Flow Through Ultra-Fine Filtering Media," ASME Paper 69-WA/PID-8, November 1969.

9. Hodgson, J. N., "SNAP-8 Seals to Space Development Testing Program - Vol. II, Molecular Pump," NASA-CR-5434, May 1964.

10. Boon, E. F.and S. E. Tal, "Hydrodynamic Seal for Rotating Shafts," Chemie-Ingenieur-Technik, Vol. 31, No. 2, January 1959, pp. 202-212 (In German).

11. King, A. E., "Screw Type Shaft Seals for Potassium Lubricated Generators," Supplement to IEEE Transactions on Aerospace, June 1965, pp. 471-479.

12. Loeb, L. B., The Kinetic Theory of Gases, New York: Dover Publication, 3rd ed., pp. 296-300, 1961.

13. Patterson, K. E., "An Analytical Model for the Prediction of Viscoseal Performance in the Regime from Continuum to Free-Molecular Flow," Mechanical and Aerospace Engineering Research Report AE-70-023-7, University of Tennessee, August 1970.

14. Stair, W. K., "Theoretical and Experimental Studies of Visco-Type Shaft Seals," Mechanical and Aerospace Engineering Research Reports ME-65-587-4 (October 1965) and ME-66-587-5 (April 1966), University of Tennessee.

15. Hodgson, J. W. and M. W. Milligan, "Visco-Type Gas Sealing," Presented at the Fourth International Conference on Fluid Sealing, ASLE Preprint FICFS Number 34, May 1969.

16. Weber, S., "Uber Deu Zusammenhang Zwischen Der Laminaren Stromund Der Reineu Gase Durch Rohre Und Dem Selbsdiffusions-Koeffizienten." Math-Fysiske Meddelser, Band 28, No. 2, 1954. Translation, "The Connection Between the Laminar Flow of Pure Gases Through Tubes and the Self-Diffusion Coefficient," Translated by R. Ash and J. B. Sykes, Atomic Energy Research Establishment Trans. 946, April 1963.

17. Milligan, M. W., "Low-Density Gas Flow in Long Tubes," American Institute of Aeronautics and Astronautics Journal, Vol. 4, No. 4, April 1966, pp. 745-746.

18. Stair, W. K., "Analysis of the Viscoseal-Part 1, The Concentric Laminar Case," Mechanical and Aerospace Engineering Research Report ME-65-587-2, The University of Tennessee, January 1965.

19. Kennard, E. H., Kinetic Theory of Gases, New York: McGraw-Hill Book Company, Inc., 1938.

20. Present, R. D., Kinetic Theory of Gases, New York: McGraw-Hill Book Company, Inc., 1958.

21. Fryer, G. M., "A Theory of Gas Flow Through Capillary Tubes," Proceedings Royal Society, Vol. A293, August 9, 1966, pp. 329-341.

22. Pollard, W. G. and R.D. Present, "On Gaseous Self-Diffusion in Long Capillary Tubes," Physical Review, Vol. 73, 1948, pp. 762-774.

23. Knudsen, M., "Die Gesetze Der Molekular-stromung und der Inneren Reiburg-Sstromung der Gase durch Rohren," Ann. Physik, Vol. 28, 1909, pp. 75-130.

24. Lund, L. M. and A.S. Berman, "Flow and Self-Diffusion of Gases in Capillaries, Parts I and II," Journal of Applied Physics, Vol. 37, No. 6, May 1966, pp. 2489-2508.

25. Wilkerson, H. J., "Rarefied-Gas Viscoseal," Mechanical and Aerospace Engineering Research Report AE-70-023-8, University of Tennessee, August 1970.

26. Carley, J. F., R. S. Mallouk, and J. M. McKelvey, "Simplified Flow Theory for Screw Extruders," Industrial and Engineering Chemistry, Vol. 45, No. 5, May 1953, pp. 974-978.

27. Vreeburg, J. P. B., "Investigation of Laminar Flow Patterns and Pressure Generation in a Viscoseal Geometry," Ph.D. Dissertation, The University of Tennessee, Knoxville, Tennessee, 1969.

28. Berg, P. W., and J. L. McGregor, Elementary Partial Differential Equations, San Francisco: Halden-Day, Inc., 1966, pp. 102-110.

29. Ebert, W. A., and E. M. Sparrow, "Slip Flow in Rectangular and Annular Ducts," ASME Paper 65-FE-20, 1965.

30. Dushman, S., Scientific Foundations of Vacuum Techniques, New York: John Wiley and Sons, Inc., 1949.

31. Wilkerson, H. J., Experimental Investigation of Slip Flow Behavior in Constant and Varying Area Passages," Master's Thesis, The University of Tennessee, Knoxville, Tennessee, 1963.

32. Guthrie, A., and R. K. Wakerling, Vacuum Equipment and Techniques, New York: McGraw-Hill Book Company, Inc., 1949.

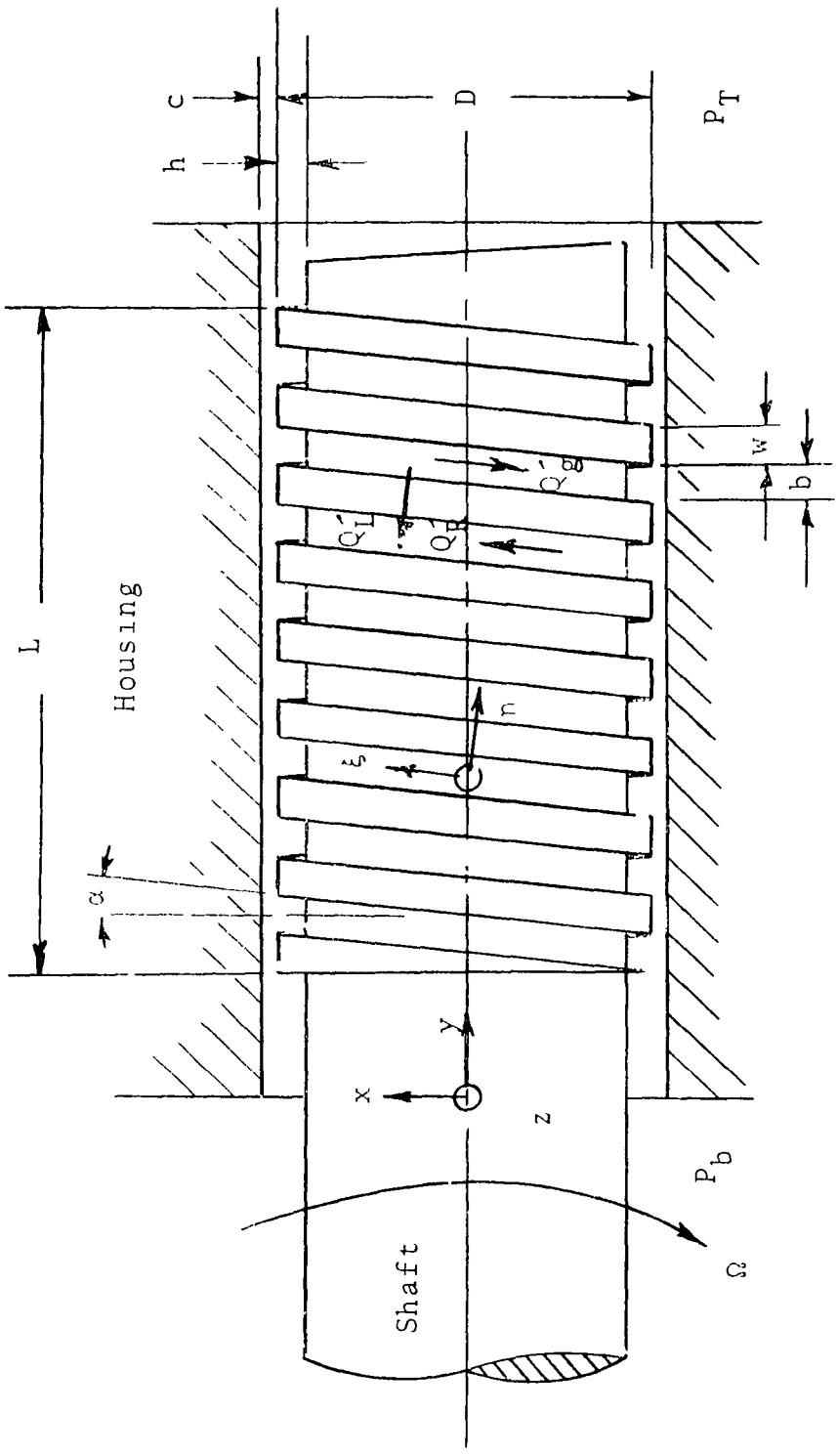

P_T = Upstream pressure

P_b = Downstream pressure

Figure 1. Basic Elements of the Viscoseal.

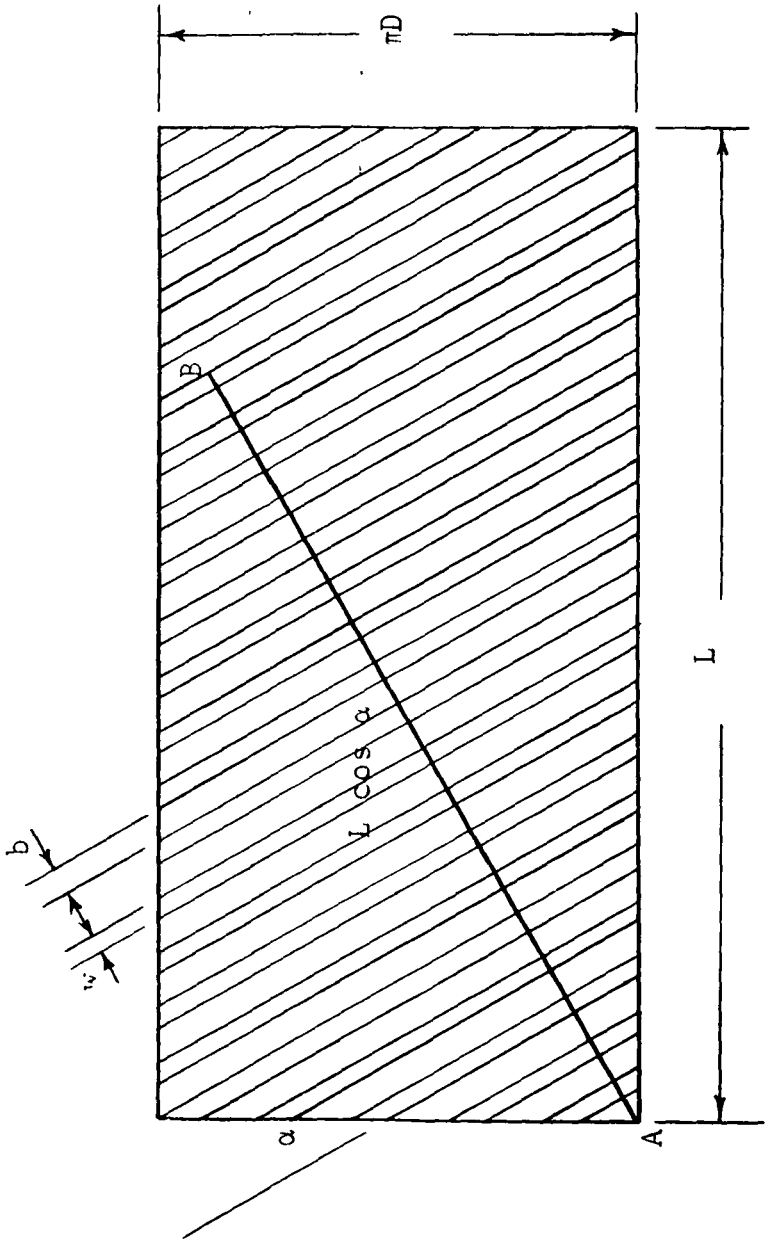

Figure 2. Viscoseal Development

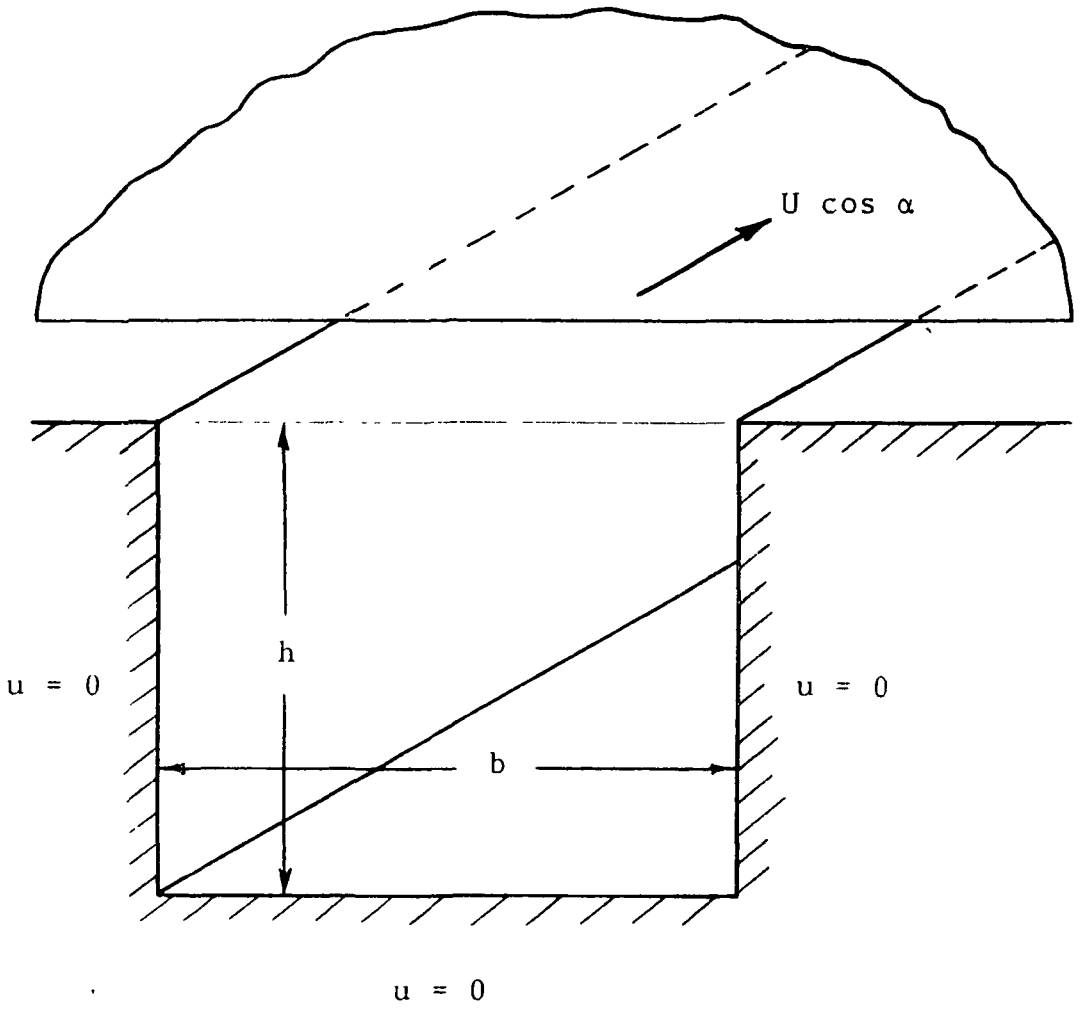

Figure 3. Groove Cross Section

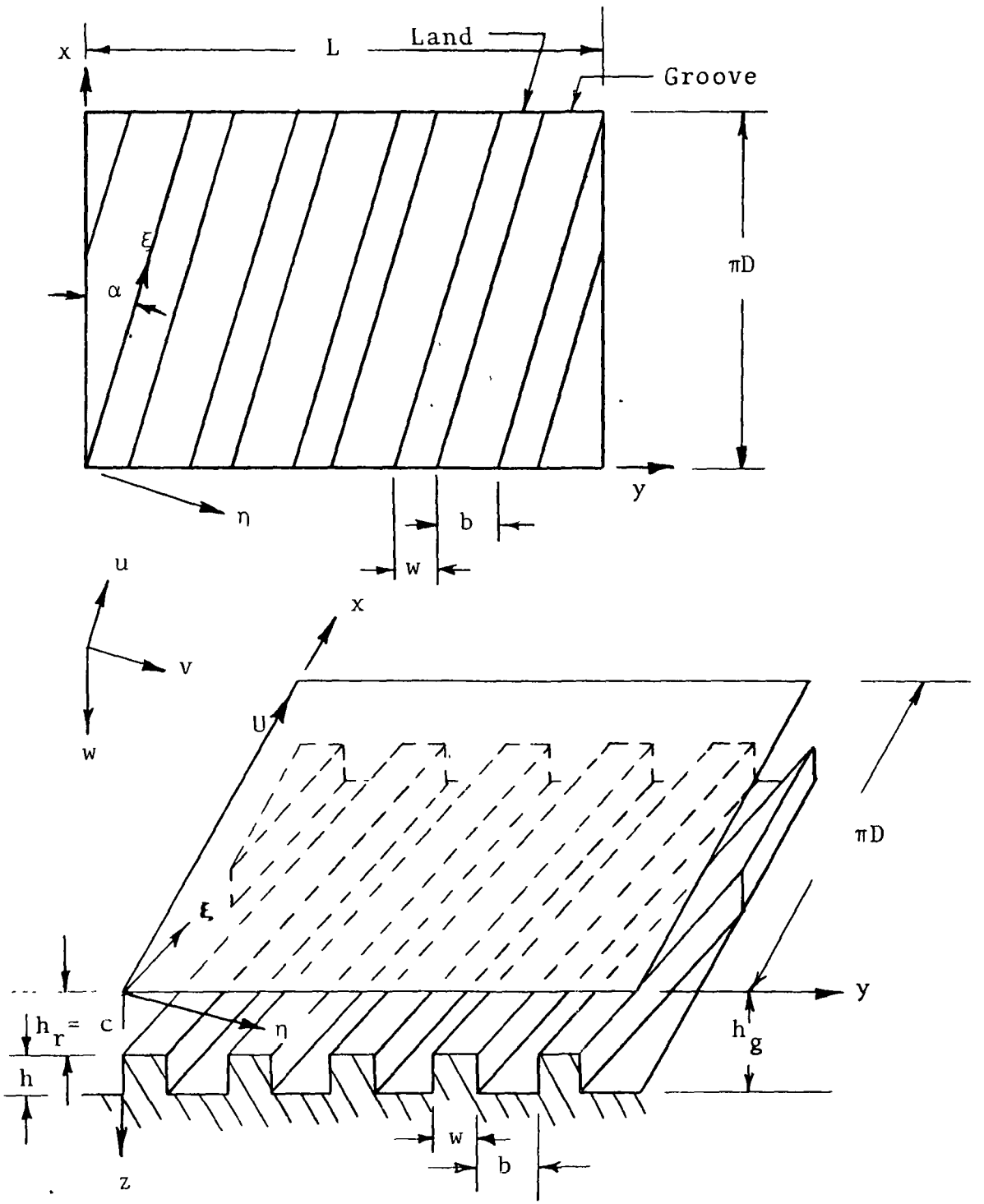

Figure 4. Developed Viscoseal Geometry.

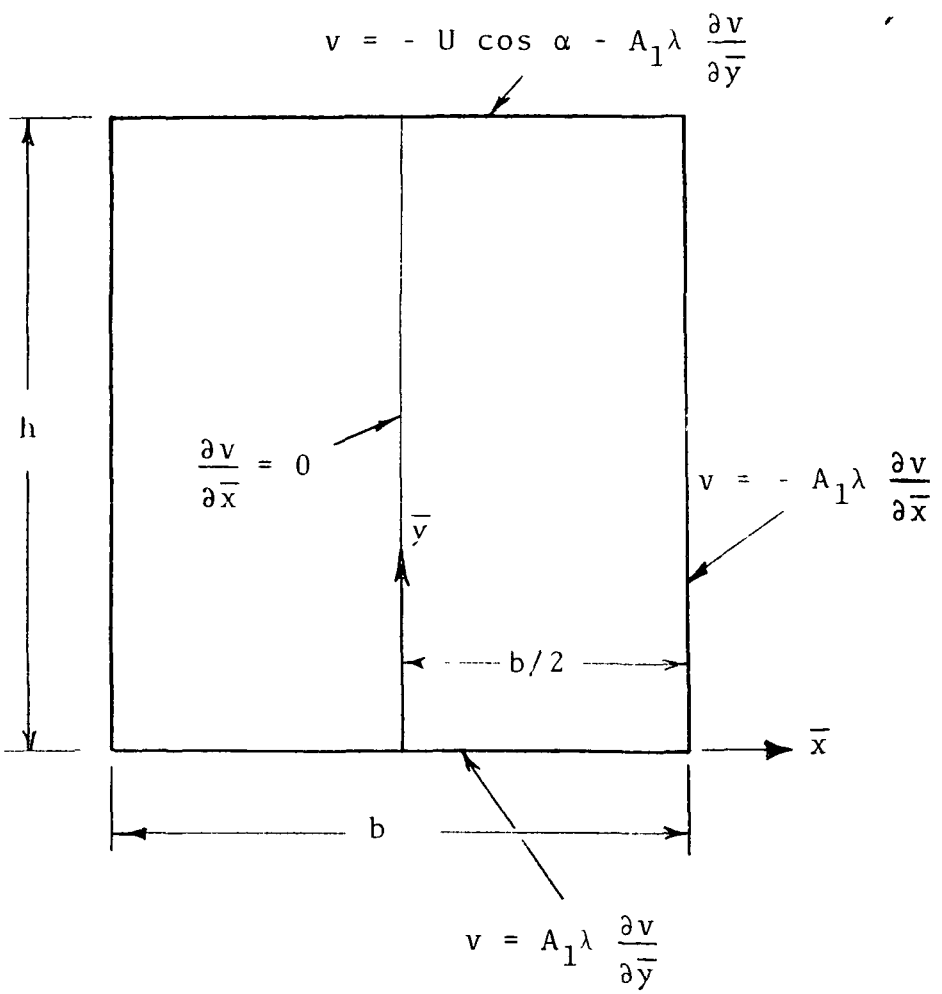

Figure 5. Groove Configuration.

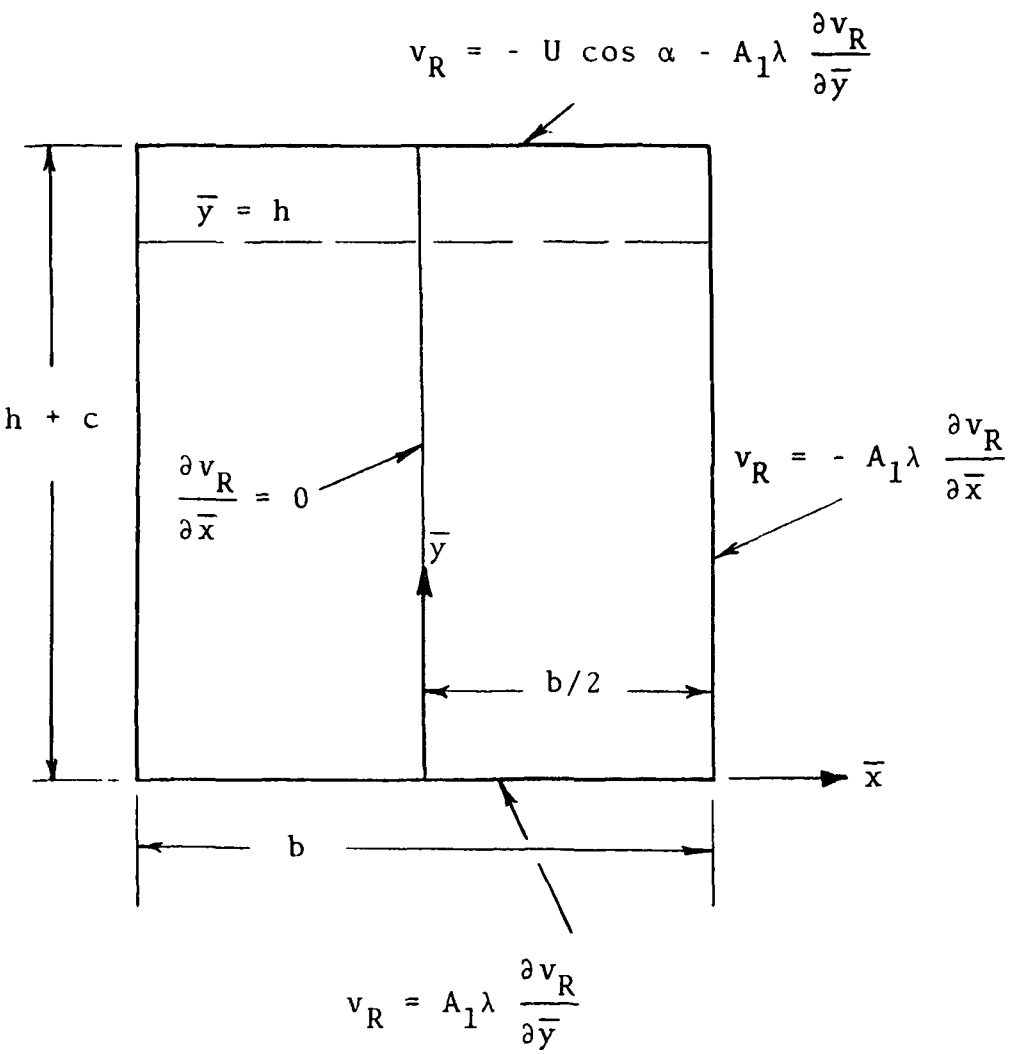

Figure 6. Hypothetical Groove.

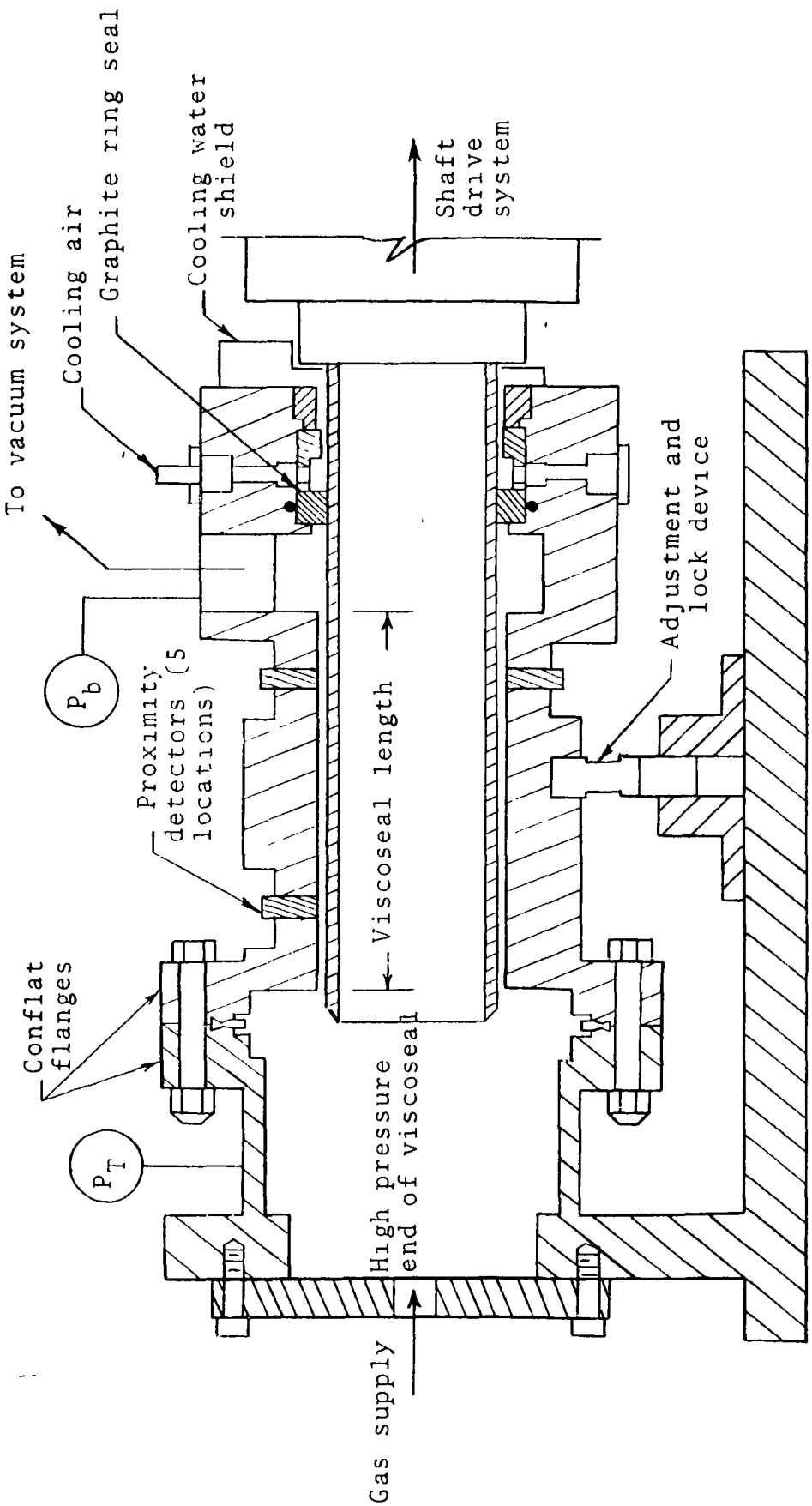

Figure 7. Viscoseal Test Section.

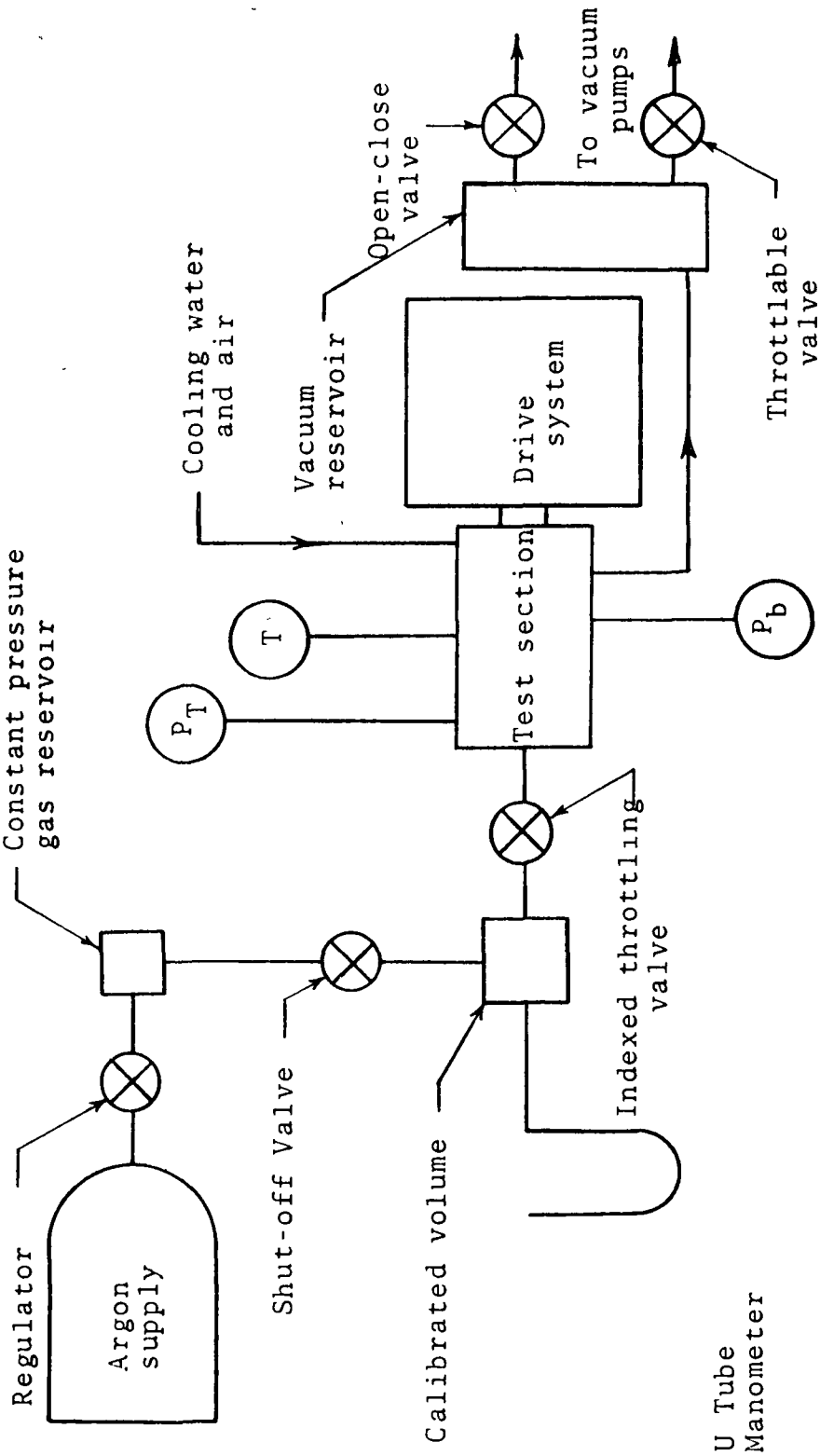

Figure 8. Schematic Diagram of the Experimental Test Apparatus.

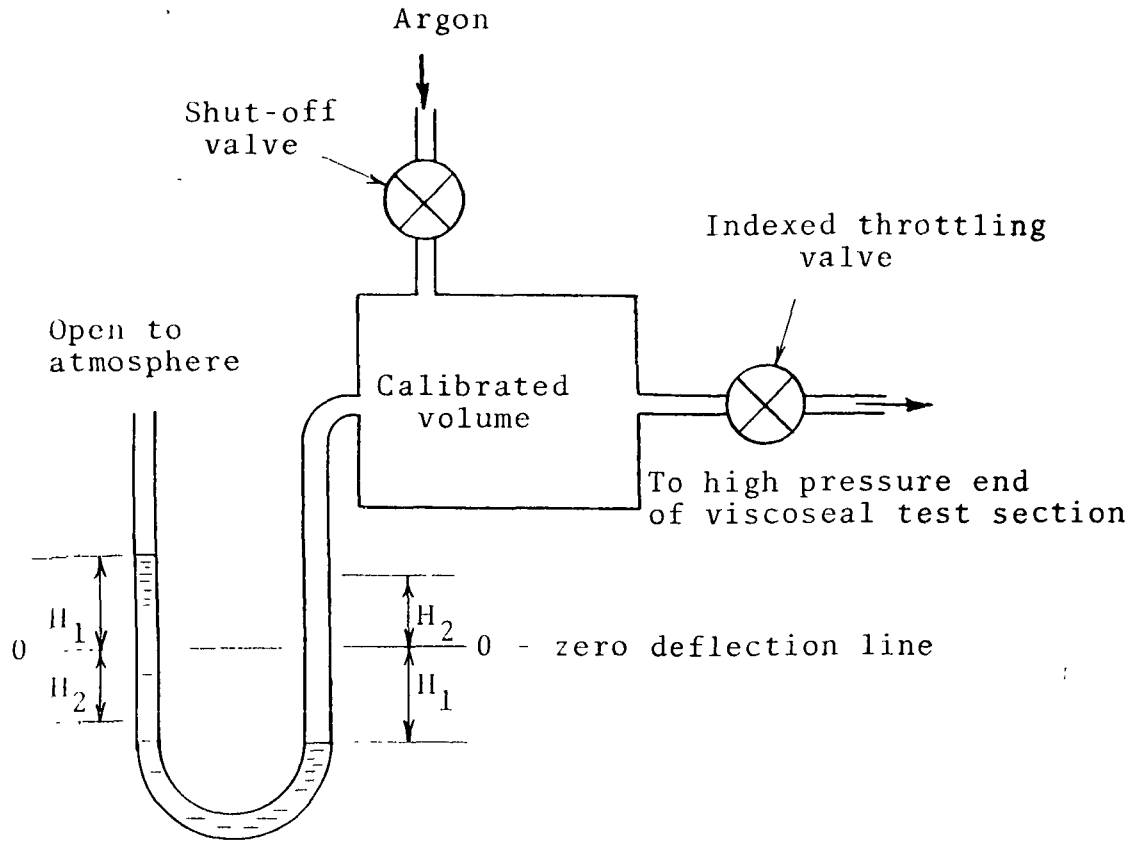

Figure 9. Flow Measurement Schematic Diagram.

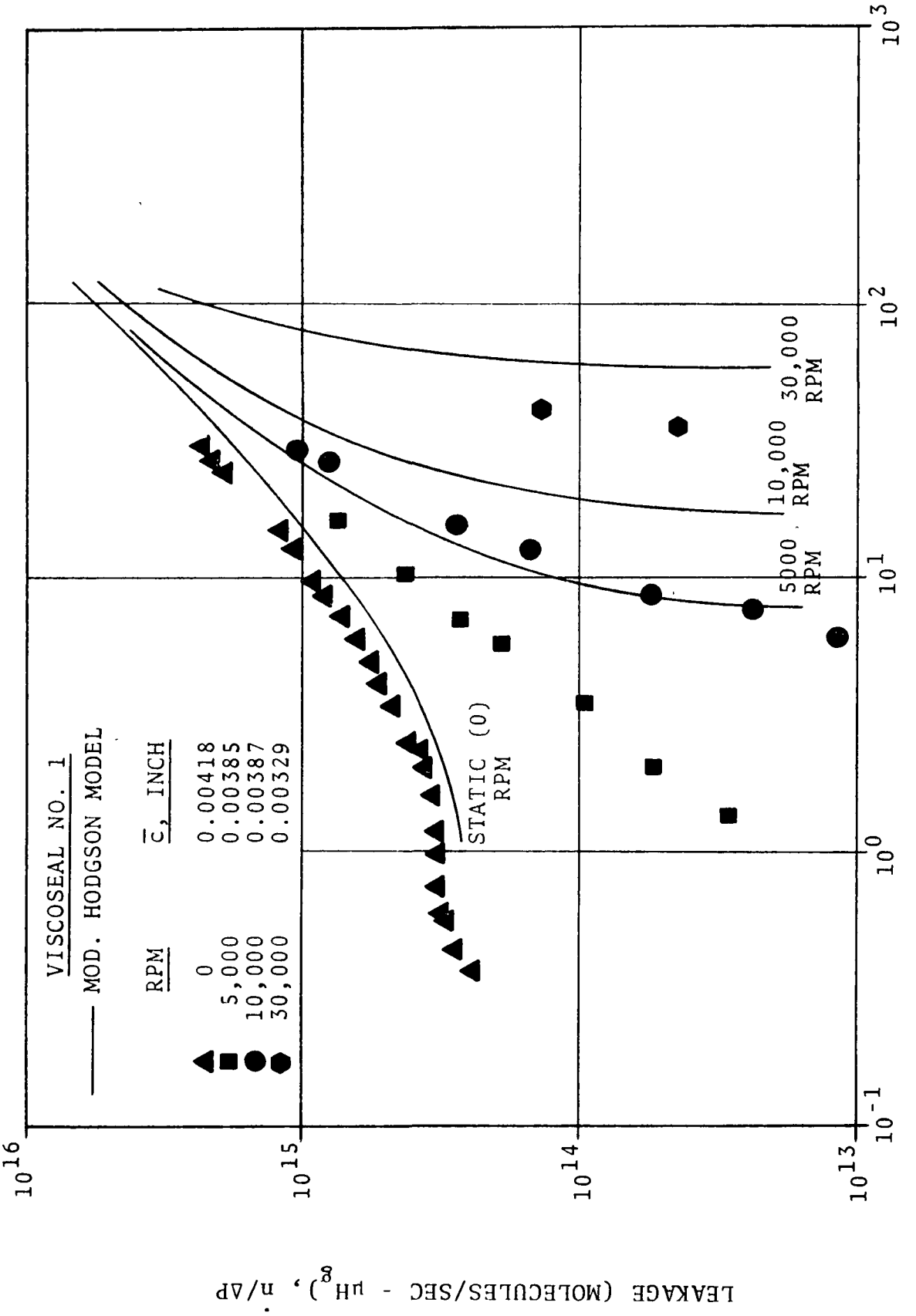

Figure 10. Net Leakage Flow Versus Inverse Knudsen Number

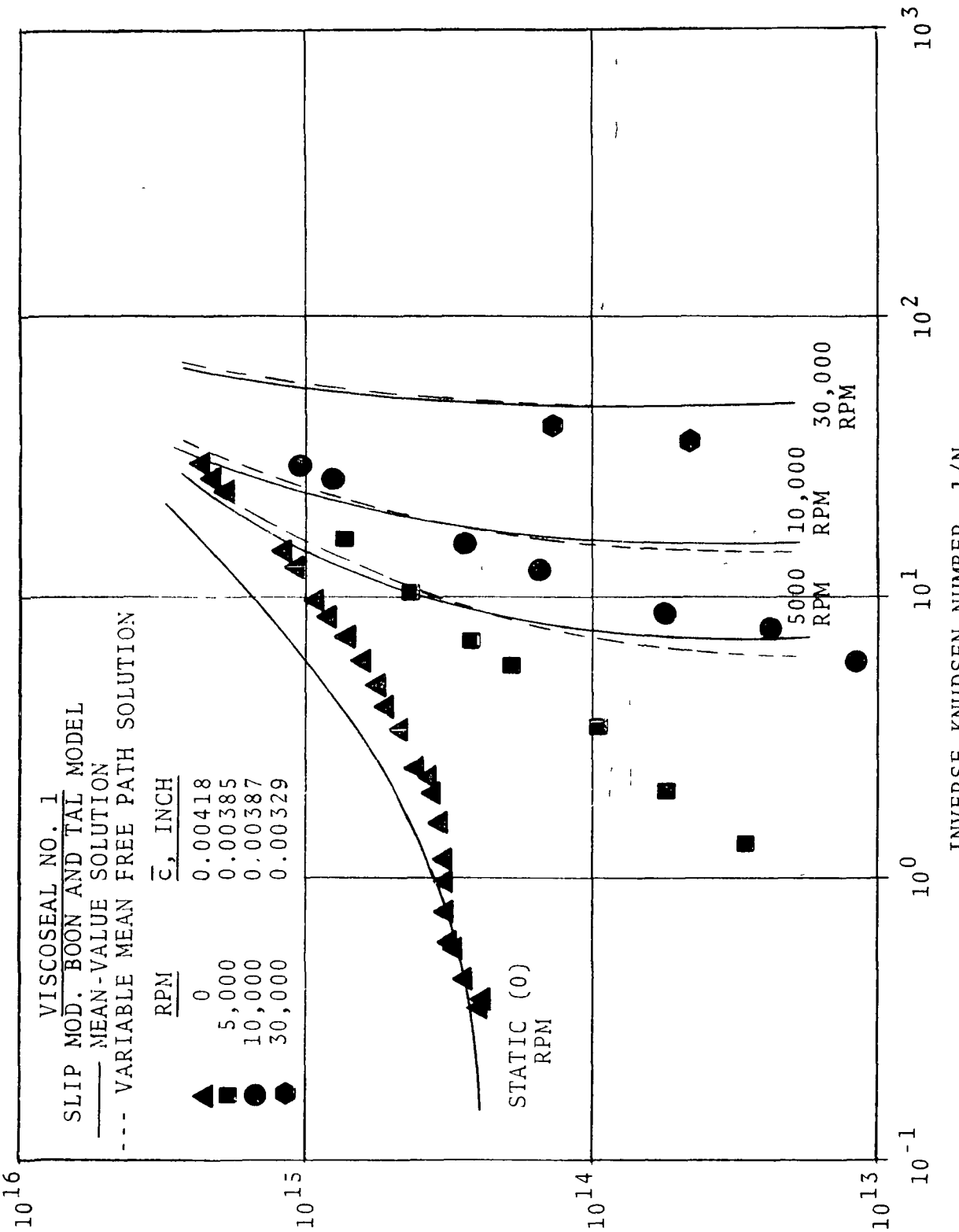

Figure 11. Net Leakage Flow Versus Inverse Knudsen Number

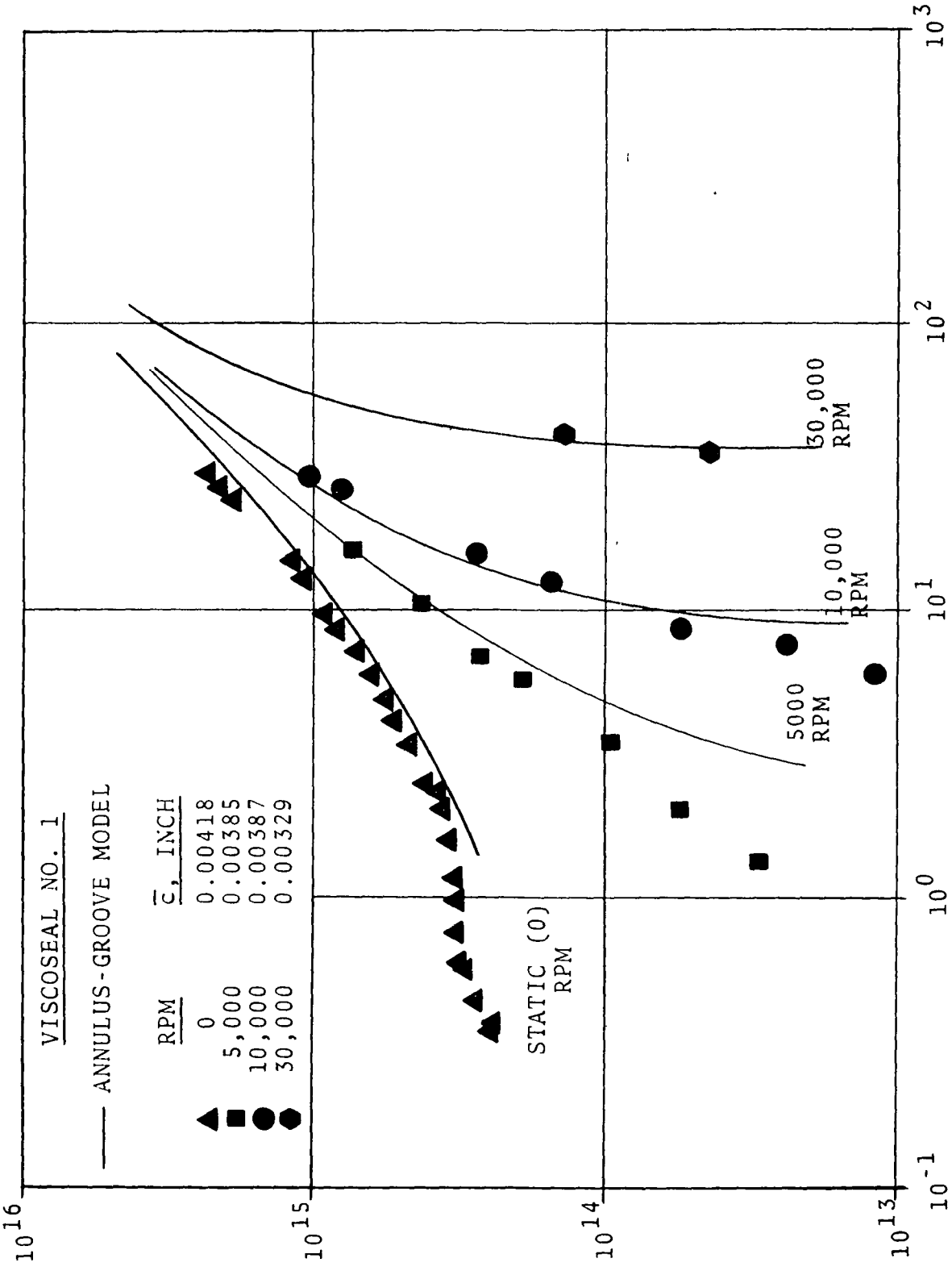

Figure 12. Net Leakage Flow Versus Inverse Knudsen Number

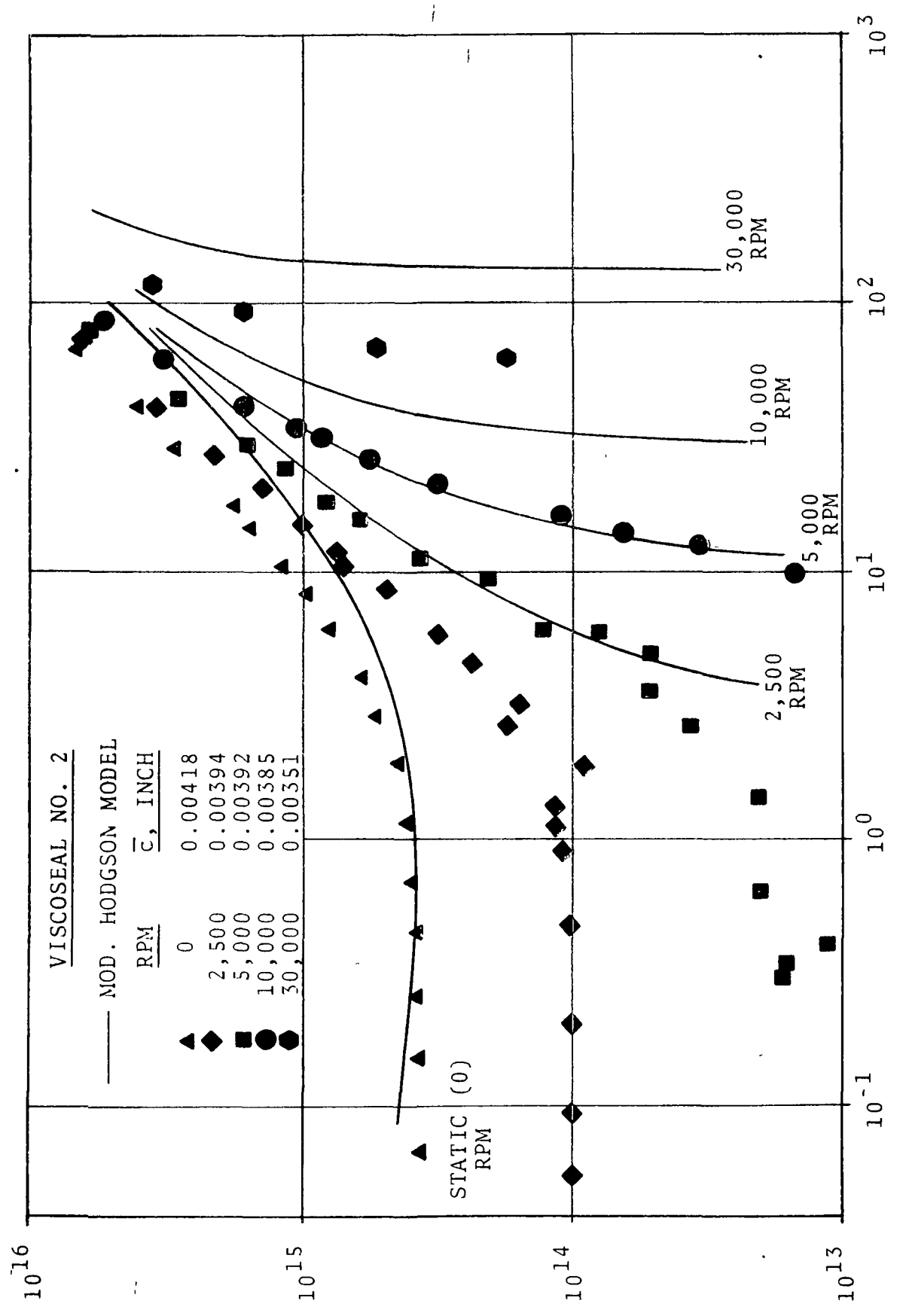

Figure 13. Net Leakage Flow Versus Inverse Knudsen Number

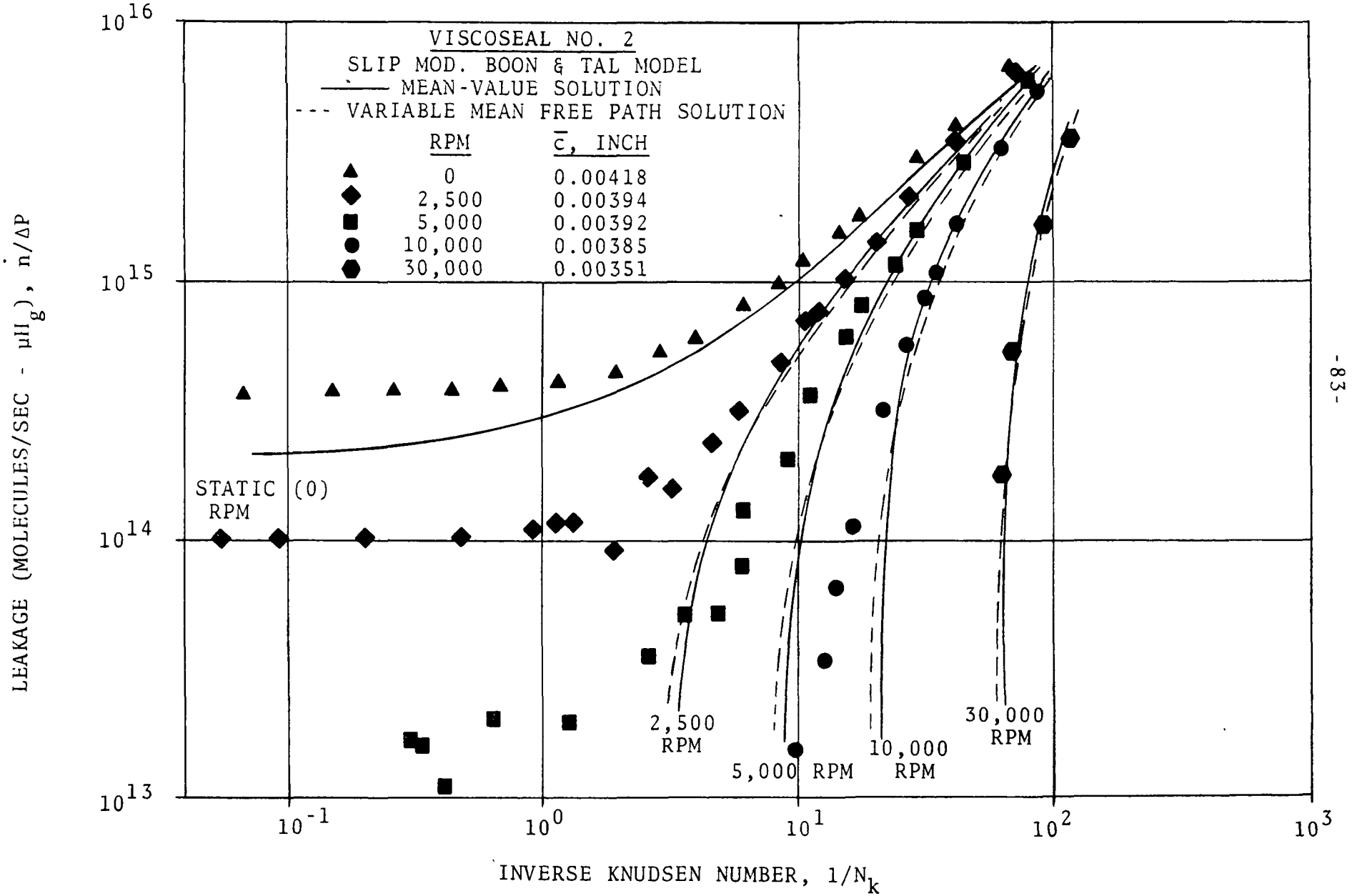

Figure 14. Net Leakage Flow Versus Inverse Knudsen Number

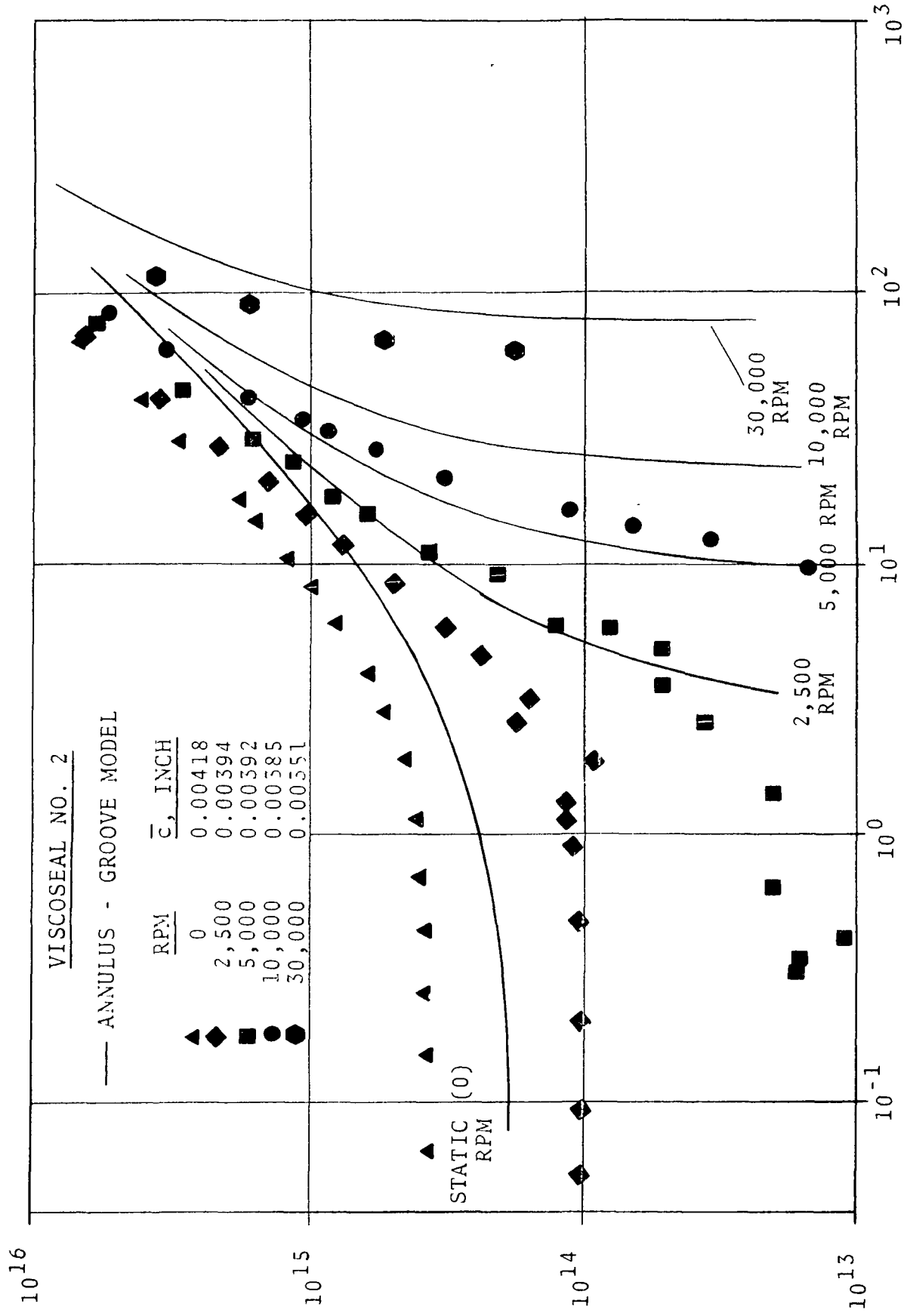

Figure 15. Net Leakage Flow Versus Inverse Knudsen Number

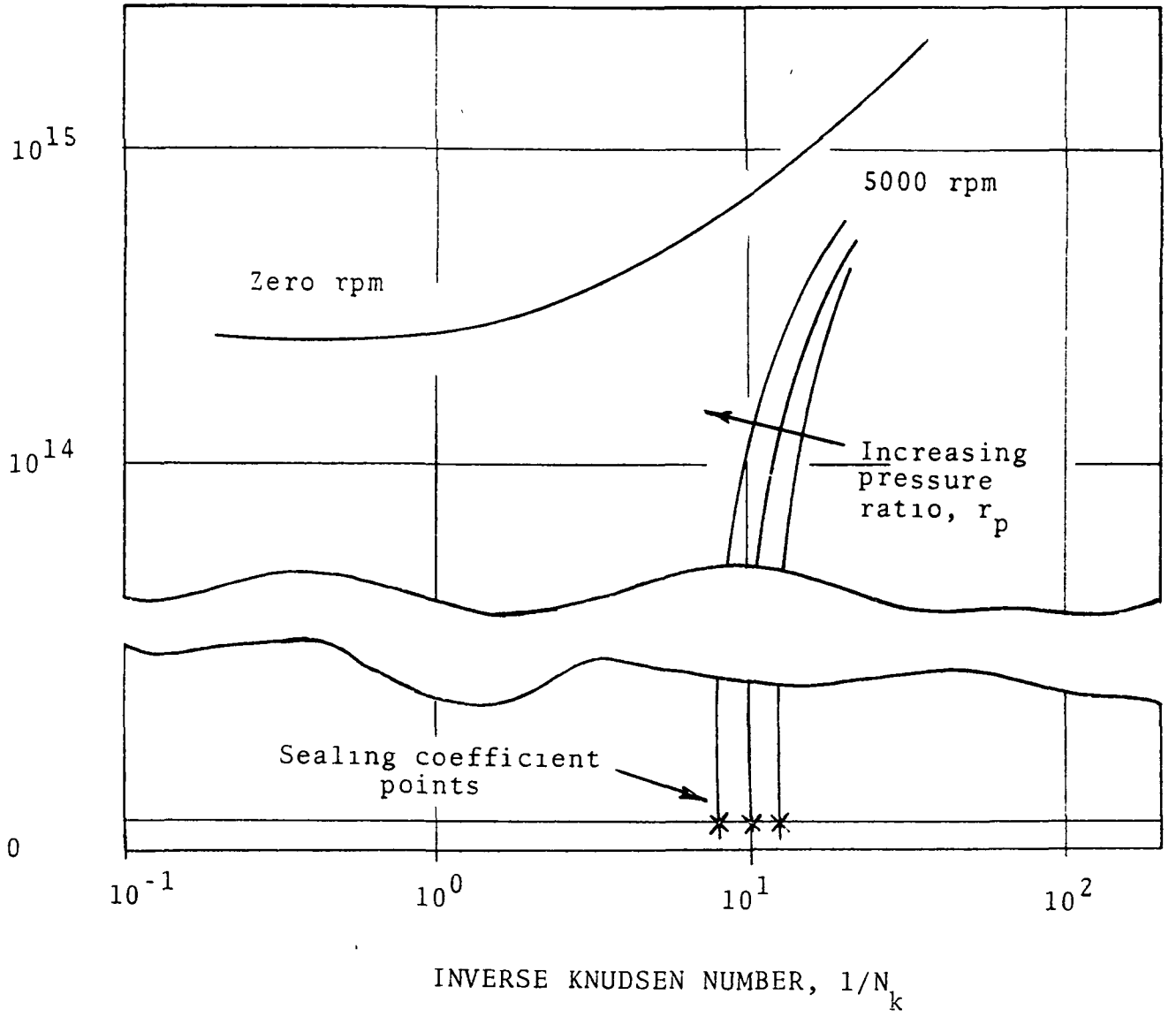

Figure 16. Relation Between the Net Leakage Flow and the Sealing Coefficients

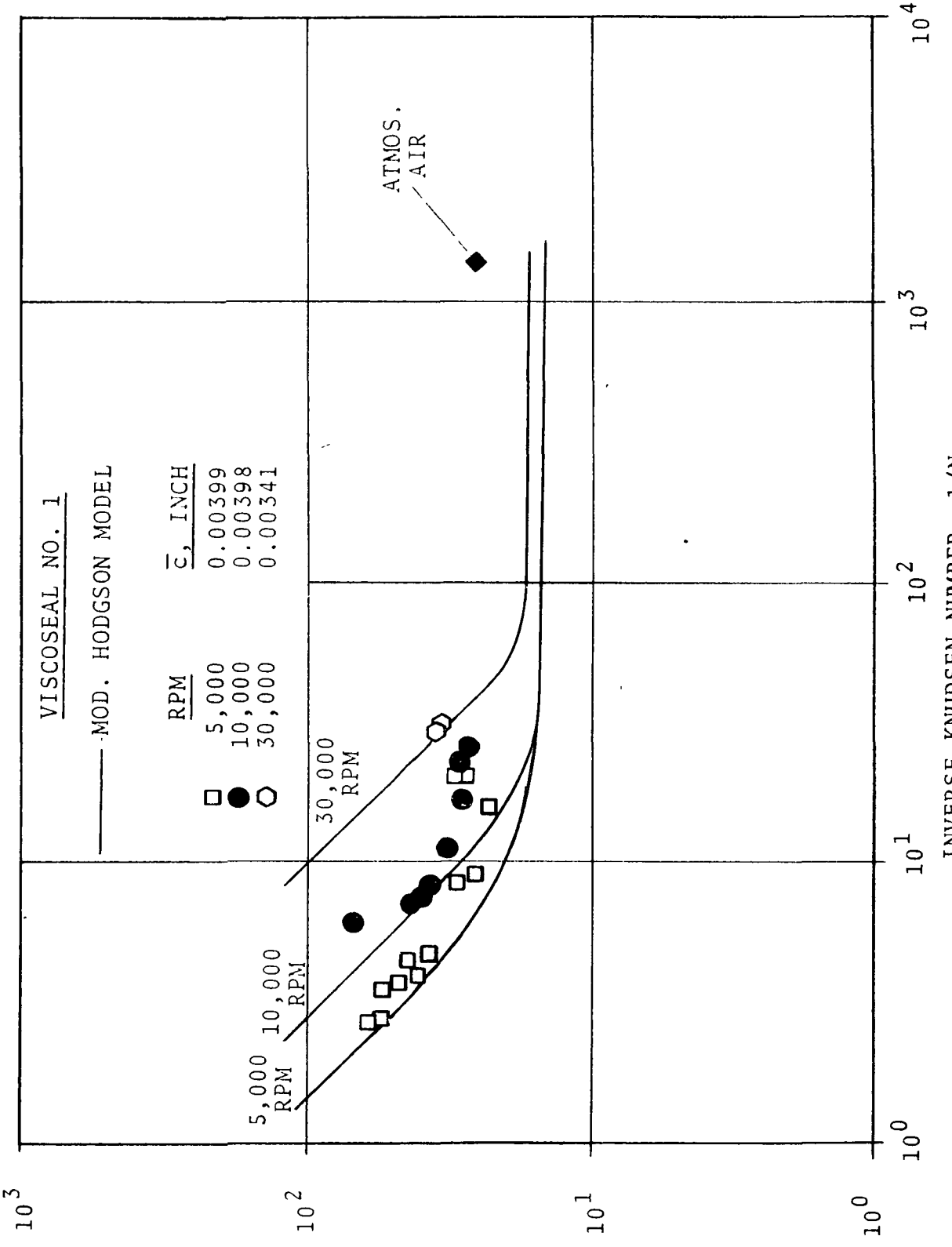

Figure 17. Sealing Coefficient Versus Inverse Knudsen Number

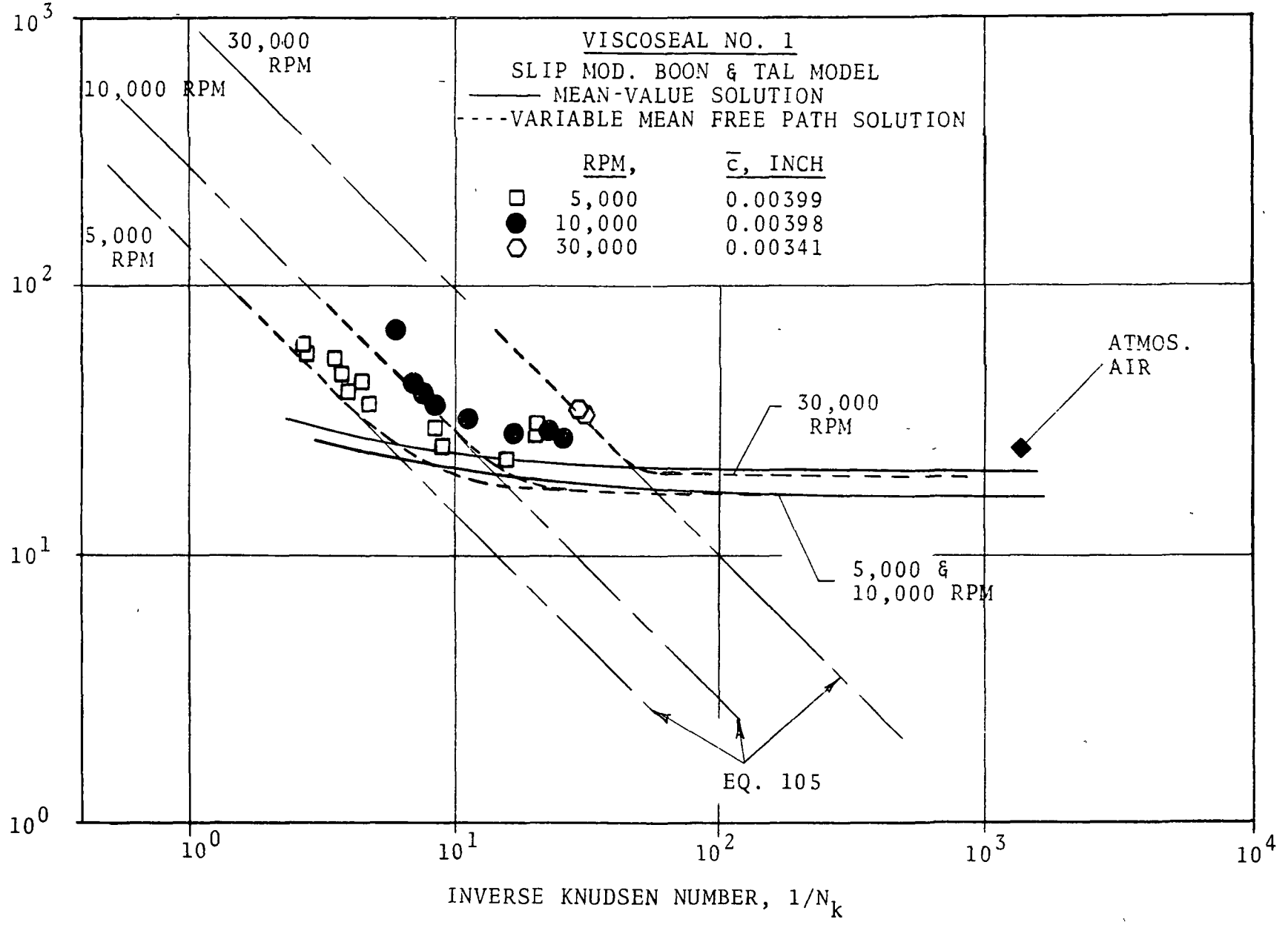

Figure 18. Sealing Coefficient Versus Inverse Knudsen Number

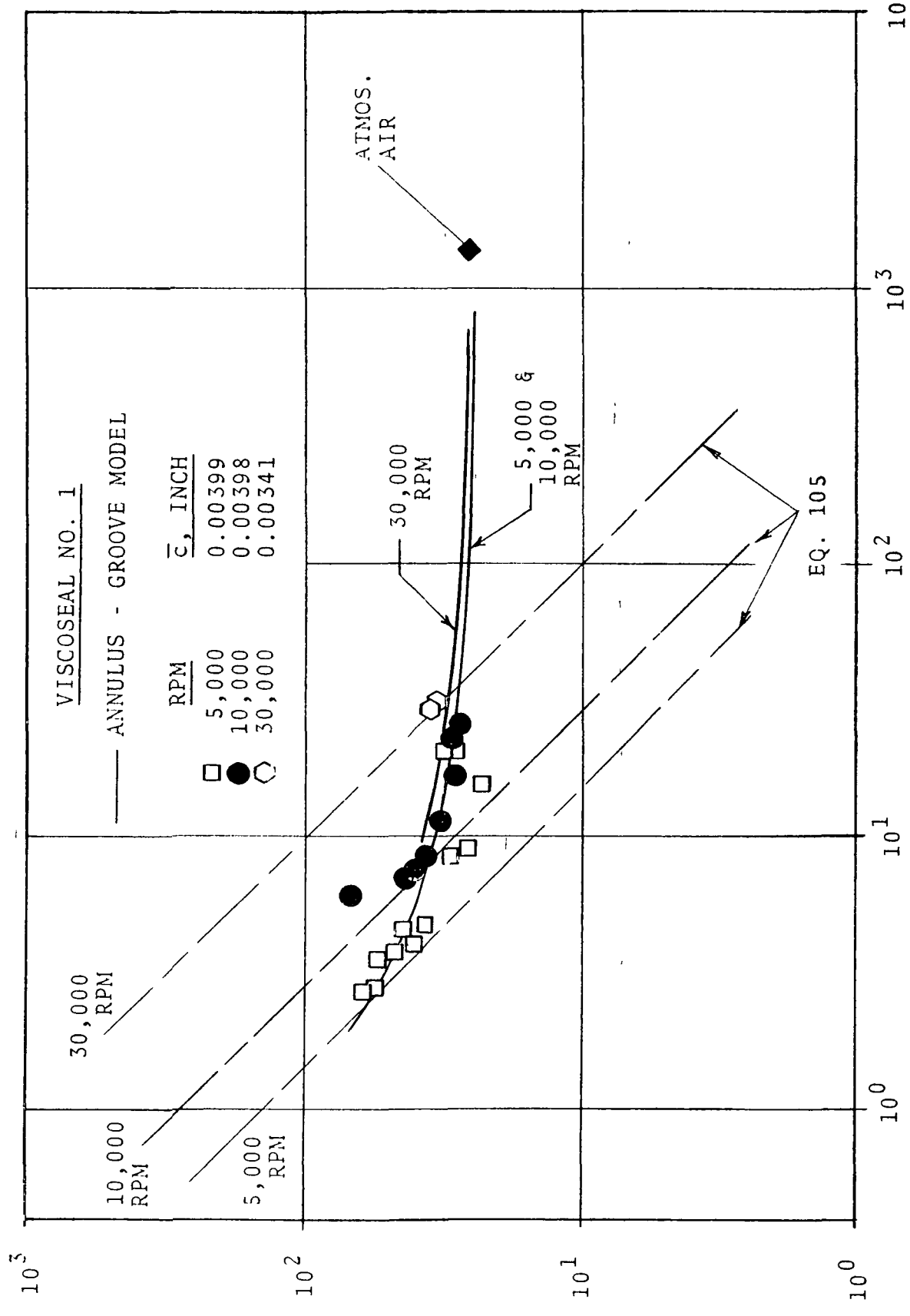

Figure 19. Sealing Coefficient Versus Inverse Knudsen Number

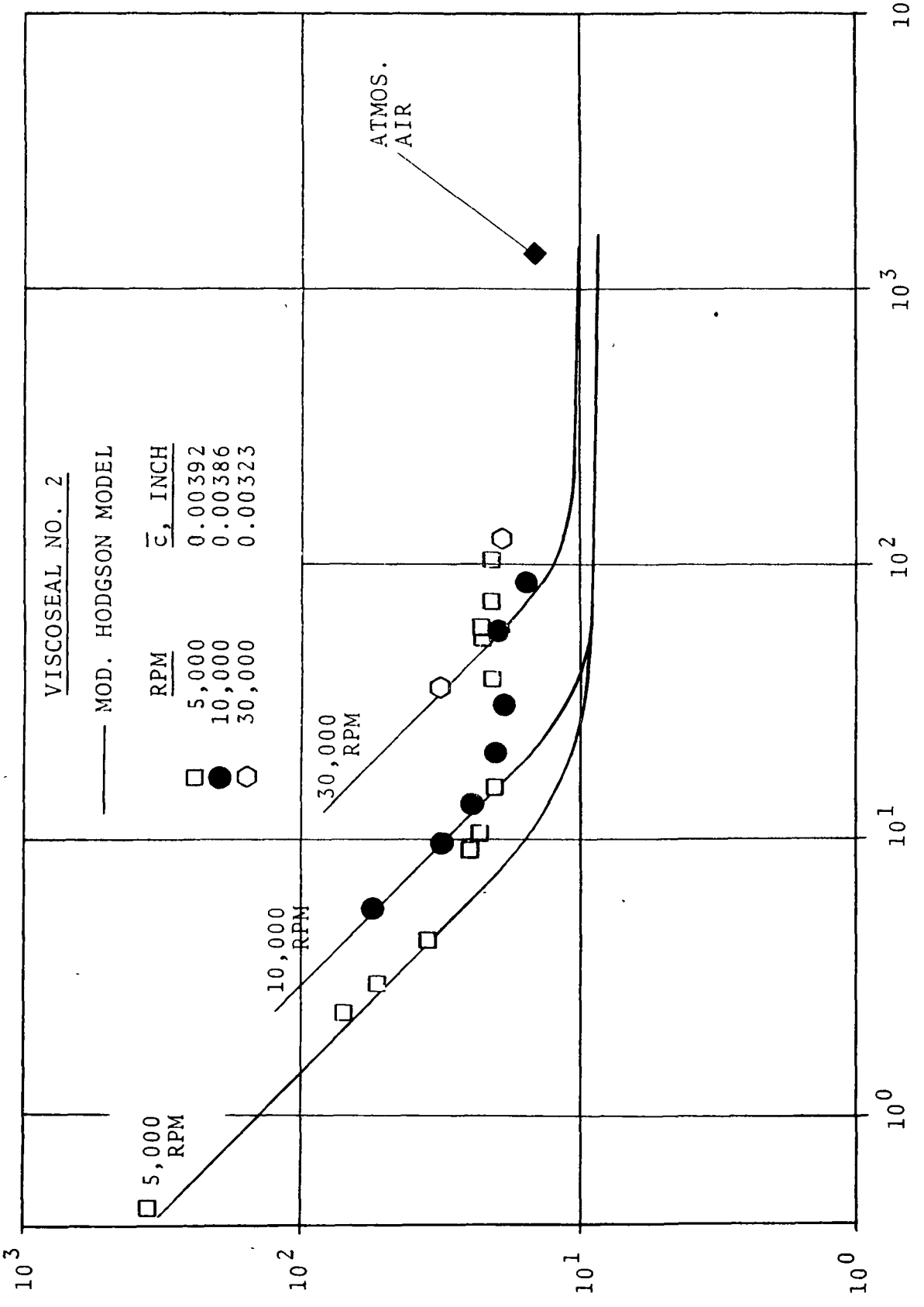

Figure 20. Sealing Coefficient Versus Inverse Knudsen Number

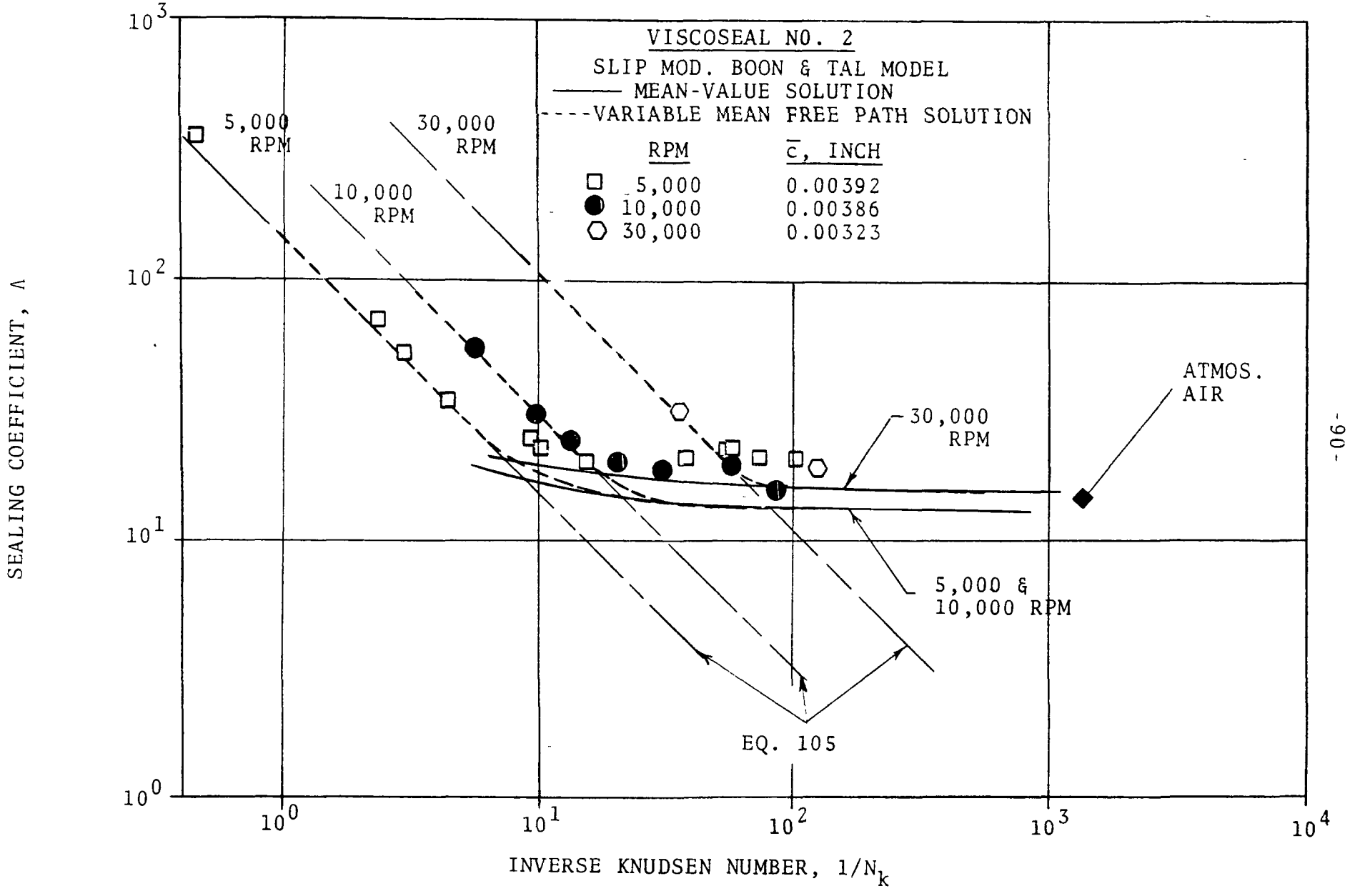

Figure 21. Sealing Coefficient Versus Inverse Knudsen Number

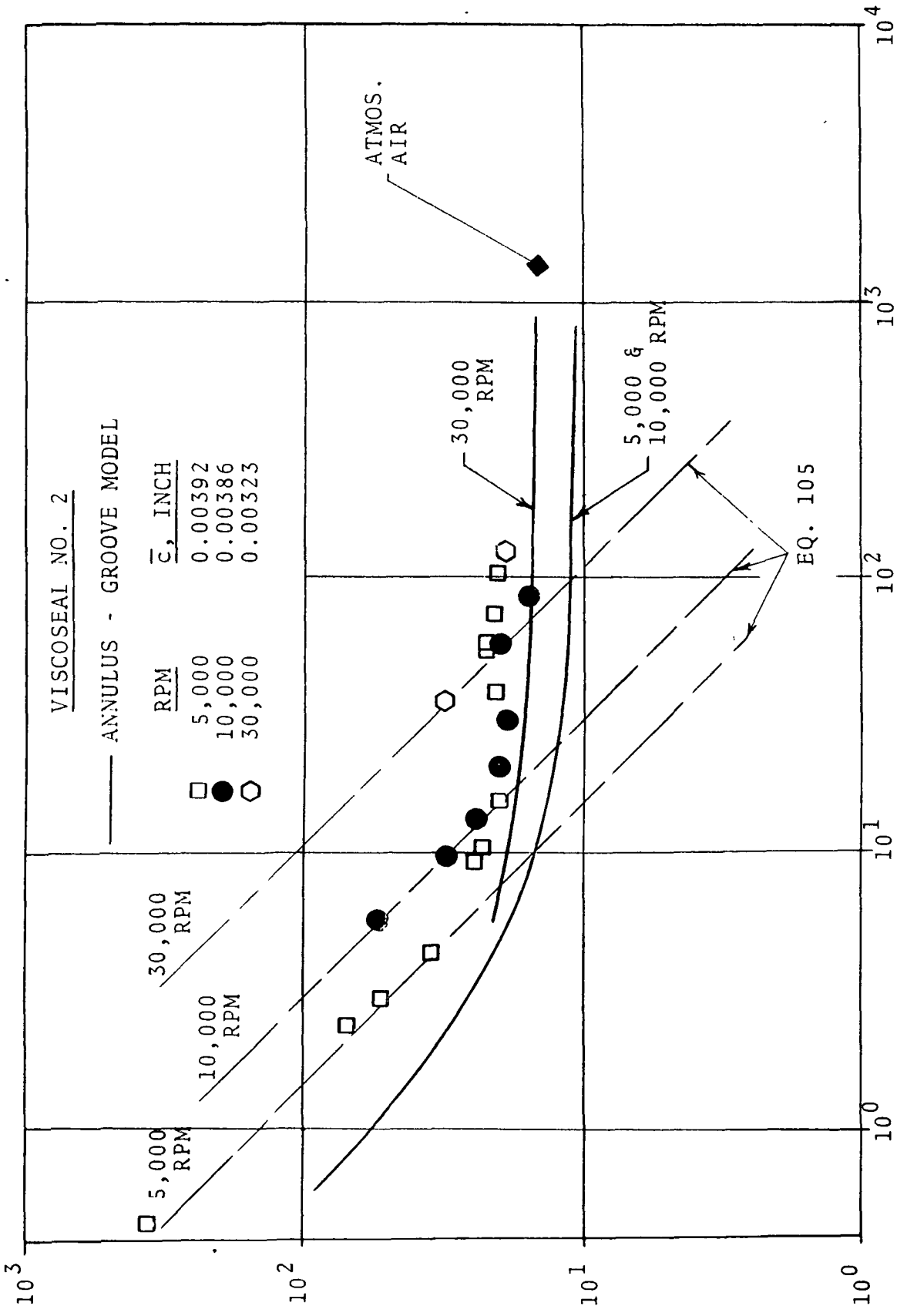

Figure 22. Sealing Coefficient Versus Inverse Knudsen Number

APPENDIX A. CONSTANTS FOR HODGSON'S MODEL

The following expressions for the coefficients in Hodgson's Model are taken from reference (9).

$$A = \frac{N\pi db^2 h}{120(b + h)} \cos \alpha$$

$$B = \frac{bh^3(b + w)K_3}{12\mu\pi d}$$

$$C = \frac{8K_1(bh)^2(b + w)}{3\pi d(b + h)} \left(\frac{kT}{2\pi m}\right)^{1/2}$$

$$D' = \frac{\pi dc^3(b + w)}{12\mu w}$$

$$E = \frac{8K_2c^2\pi d(b + w)}{3w}\left(\frac{kT}{2\pi m}\right)^{1/2}$$

$$C_1 = \frac{K_3^2(b + h)^2 h}{8K_1 b\mu\left(\frac{kT}{2\pi m}\right)^{1/2}[2K_1 b - K_3(b + h)]}$$

$$C_2 = \frac{2K_1 b}{K_3(b + h)} C_1$$

$$C_3 = \frac{c}{8\mu K_2(2K_2 - 1)\left(\frac{kT}{2\pi m}\right)^{1/2}}$$

$$C_4 = 2K_2C_3$$

$$K_1 = \frac{3(1 + a)}{8a^2}\left[a \ln (a + (1 + a^2)^{1/2}) + a^2 \ln \frac{1 + (1 + a^2)^{1/2}}{a}\right.$$

$$\left. + \frac{1}{3}(1 + a^3 - (1 + a^2)^{3/2})\right]$$

$$K_3 = 1 - 0.63 \frac{h}{b} \tanh \frac{\pi b}{2h}$$

Values of K_2

w/c	0.1	0.2	0.4	0.8	1	2	3	4	5	10
K_2	0.036	0.068	0.13	0.22	0.26	0.40	0.52	0.60	0.67	0.94

When $w/c > 10$, $K_2 = \frac{3}{8} \ln \frac{w}{c}$.

The groove flow coefficients, B, C, C_1, and C_2 are obtained from a consideration of flow in a long rectangular tube. The continuum groove flow coefficient, B, is obtained from the continuum solution for Poiseuille flow in a long rectangular tube. From a consideration of purely molecular flow, the free-molecule flow coefficient, C, can be derived. The basic free-molecule flow equation used by Hodgson is given in Reference (32) and is written as

$$Q = \frac{16}{3} K_n \left(\frac{kT}{2\pi m}\right)^{1/2} \frac{O^2}{S} \frac{dP}{d\ell} . \qquad (106)$$

Equation (106) is attributed to Knudsen (32, p. 35), but the constant K_n, which is equal to K_2, is obtained by Clausing (32, p. 40). O and S are the groove cross sectional area and perimeter, respectively. The two remaining groove flow constants, C_1 and C_2, are obtained in the same way Knudsen determined ν and ξ in Equation (1). As was pointed out in Section 2.1, the determination of the ratio ν/ξ requires knowledge of the continuum with slip solution. Hodgson does not take an exact approach at this point since he determines C_1/C_2 from the continuum with slip solution for flow between infinite parallel flat plates rather than flow in a long rectangular tube.

Hodgson obtains the land leakage flow coefficients, D, E, C_3, and C_4, from a consideration of flow in a thin slit-like tube. In this

case the continuum coefficient, D, is obtained from the continuum solution for Poiseuille flow between parallel flat plates. The same basic model, Equation (106), for free-molecule flow is used to determine the free-molecule flow coefficient, E. K_n now becomes K_1, which is also attributed to Clausing. O and S now represent the cross sectional area of the land leakage passageway and its perimeter, respectively. The constants C_3 and C_4 are also determined using the same approach Knudsen used to determine ν and ξ in Equation (1). For the continuum with slip solution, Hodgson once again uses the continuum with slip solution for flow between infinite parallel flat plates which in this case is the proper solution to use.

APPENDIX B. TABULATED EXPERIMENTAL REDUCED DATA

Net Leakage Reduced Data for Seal No. 1, Zero rpm - Argon Gas

Data Point No.	P_T μhg	P_b μhg	$1/N_K$	$\dot{N}/\Delta P$ x 10^{-14}
1	16,800	7230	24.68	18.16
2	19,150	7705	27.57	20.30
3	21,400	8155	30.32	21.60
4	22,600	8430	31.87	22.08
5	17,000	7465	25.09	17.45
6	12,150	565	13.05	10.60
7	9,370	538	10.15	9.06
8	8,100	522	8.84	8.24
9	6,850	512	7.54	7.28
10	5,450	500	6.10	6.34
11	4,180	495	4.79	5.50
12	4,200	490	4.80	5.46
13	2,950	487	3.52	4.65
14	1,870	482	2.41	3.81
15	13,800	1250	15.40	11.31
16	1,740	255	2.10	3.47
17	1,700	260	2.01	3.60
18	1,720	275	2.05	3.59
19	752	227	1.00	3.23
20	428	132	0.57	3.02
21	318	129	0.46	2.83
22	251	131	0.39	2.40
23	216	131	0.36	2.48
24	4,000	131	4.23	5.26
25	2,320	172	2.55	4.15
26	1,460	166	1.66	3.46
27	1,025	168	1.22	3.30
28	600	172	0.77	2.77
29	475	131	0.62	3.20

Net Leakage Reduced Data for Seal No. 1, Dynamic Speeds - Argon Gas

Data Point No.	P_T μhg	P_b μhg	$1/N_K$	$\dot{N}/\Delta P$ x 10^{-14}	c in. x 10^3
	10,000 rpm, $\bar{c}$ x 10^3 = 3.87 in., $\bar{r}_p$ = 146.4				
1	9,380	335	8.83	0.558	3.81
2	6,410	60	6.03	0.117	3.80
3	13,200	86	12.9	1.50	3.90
4	16,700	93	15.9	2.74	3.87
5	28,700	150	27.5	7.80	3.87
6	32,500	166	30.9	9.80	3.87
7	8,050	64	7.78	0.237	3.91
10	31,000	233	30.7	10.15	4.01
	5,000 rpm $\bar{c}$ x 10^3 = 3.85 in., $\bar{r}_p$ = 176.6				
11	16,800	63	16.6	7.29	4.01
12	11,200	42	10.6	4.14	3.84
13	7,900	33	7.18	2.61	3.69
14	6,150	30	5.88	1.88	3.88
15	3,700	27	3.51	0.953	3.84
16	1,950	26	2.03	0.540	3.76
17	1,250	29	1.32	0.290	3.94
	30,000 rpm, $\bar{c}$ x 10^3 = 3.29 in., $\bar{r}_p$ = 807				
18	44,000	53	36.0	0.451	3.33
19	49,900	64	40.9	1.36	3.33
20	39,800	49	31.4	0.038	3.20

Rarefied Sealing Coefficient Reduced Data for Seal No. 1 - Argon Gas

Data Point No.	P_T μhg	P_b μhg	$1/N_K$	Λ	Re_c	c in. x 10^3
		10,000 rpm, $\bar{c} \times 10^3$ = 3.98 in.				
SP1	7,160	267	7.47	40.2	1.01	4.18
SP2	9,860	1220	11.1	31.8	1.49	4.15
SP3	5,200	275	5.01	68.3	0.67	3.80
SP9	14,200	3495	16.9	28.3	2.28	3.98
SP10	17,200	6605	22.6	29.3	3.02	3.94
SP13	19,200	7755	25.5	27.1	3.42	3.94
SP14	8,700	44	8.29	36.4	1.10	3.91
SP19	7,350	44	6.96	43.1	0.93	3.91
		5000 rpm, $\bar{c} \times 10^3$ = 3.99 in.				
SP4	2,600	166	2.69	60.8	0.18	4.04
SP5	11,000	4730	15.6	22.5	1.03	4.11
SP6	3,880	176	3.94	39.9	0.26	4.04
SP7	3,160	407	3.47	53.7	0.23	4.04
SP15	2,850	50	2.72	56.7	0.18	3.90
SP16	13,300	8245	20.6	30.2	1.39	3.98
SP17	3,920	146	3.69	46.5	0.25	3.73
SP18	4,400	382	4.65	36.6	0.31	4.04
SP20*	4,200	559	4.47	43.6	0.30	3.90
SP21*	7,000	1835	8.44	29.6	0.57	3.97
SP22*	7,550	1710	8.94	25.5	0.60	4.01
SP23*	13,100	8145	20.7	29.8	1.39	4.04
		30,000 rpm, $\bar{c} \times 10^3$ = 3.41 in.				
SP11	35,200	104	29.3	34.7	11.8	3.44
SP12	38,100	68	30.9	33.5	12.5	3.37

*Argon blanket on graphite ring seal.

Continuum Sealing Coefficient Tabulation Viscoseal No. 1, Gas-Air

Data Point No.	Speed rpm	ΔP in.-H_2O	Λ	R_{e_c}	c in. x 10^3
		Test Date 6-25-69			
2	4,905	2.45	23.7	88.1	4.18
3	8,080	3.74	25.6	145.4	
4	11,500	5.15	26.5	207.3	
5	13,200	5.74	27.2	238.1	
6	19,600	8.49	27.4	354.7	
7	23,400	10.38	26.6	424.4	
8	25,400	11.45	26.2	461.3	
9	29,600	14.27	24.5	539.5	
10	31,800	16.50	22.8	581.2	
11	34,600	19.58	20.9	634.9	
12	21,600	9.45	27.0	391.4	
13	9,700	4.45	25.8	174.6	
15	4,800	2.40	23.7	87.1	
16	6,400	3.19	24.5	116.2	
17	7,900	3.69	25.4	143.5	
18	9,700	4.40	26.0	176.4	
19	11,600	5.12	26.8	211.1	
20	13,150	5.74	27.1	239.5	
		Test Date 7-2-69			
22	1,272	0.73	20.6	23.1	4.18
23	3,219	1.69	22.6	58.5	
24	4,644	2.34	23.5	84.5	
25	6,399	3.08	25.0	116.5	
26	7.869	3.68	25.2	143.4	
27	9,582	4.35	26.0	174.7	
28	11,562	5.13	26.7	211.0	
29	13,269	5.83	27.0	242.5	
30	7,392	3.51	24.9	134.6	
31	1,278	0.74	20.4	23.2	

Continuum Sealing Coefficient Tabulation Viscoseal No. 1, Gas-Air

Data Point No.	Speed rpm	ΔP in.-H_2O	Λ	R_{e_c}	c in. x 10^3
		Test Date 9-2-69			
32	1,566	0.87	21.5	28.1	4.18
33	3,540	1.80	23.3	63.7	
34	5,130	2.57	23.6	92.4	
35	6,690	3.17	25.0	120.6	
36	7,980	3.70	25.5	144.0	
37	9,750	4.40	26.3	176.0	
38	9,990	4.50	26.3	180.4	
39	13,800	6.01	27.2	249.7	
41	14,100	6.21	26.9	255.2	
42	19,230	8.66	26.3	349.1	
43	21,180	9.34	26.8	384.8	
44	23,400	10.41	26.6	425.7	
45	5,040	2.50	23.9	90.8	
46	1,278	0.71	21.3	23.0	
47	3,540	1.81	23.2	63.7	
48	5,010	2.46	24.1	90.2	
49	6,570	3.12	25.0	118.4	
50	7,740	3.60	25.5	139.6	
51	9,720	4.35	26.4	175.5	
52	11,490	5.04	27.0	207.6	
53	13,830	5.99	27.4	250.2	
54	2,580	1.34	22.8	46.4	
55	510	0.28	21.6	9.2	

Continuum Sealing Coefficient Tabulation Viscoseal No. 1, Gas-Air

Data Point No.	Speed rpm	ΔP in. H_2O	Λ	R_{e_c}	c in. x 10^3
		Test Date 9-17-69			
66	507	0.28	21.5	9.2	4.18
67	2,460	1.29	22.6	44.6	
68	3,600	1.84	23.2	65.3	
69	5,010	2.46	24.1	90.9	
70	6,360	3.04	24.8	115.5	
71	7,470	3.39	26.1	135.8	
72	699	0.39	21.2	12.7	
73	1,194	0.66	21.4	21.6	
74	1,338	0.74	21.4	24.2	
75	1,530	0.85	21.3	27.7	
76	1,710	0.94	21.5	31.0	
77	1,950	1.05	22.0	35.3	
78	2,190	1.17	22.1	40.0	
79	270	0.15	21.3	4.9	
80	627	0.35	21.2	11.4	
81	867	0.48	21.4	15.7	
82	762	0.42	21.5	13.8	
83	1,374	0.75	21.7	24.9	
84	1,647	0.90	21.7	29.8	
85	2,229	1.19	22.2	40.4	
86	2,970	1.54	22.8	53.9	
87	3,960	2.00	23.5	71.8	
88	4,980	2.45	24.1	90.4	
89	5,760	2.78	24.6	104.6	
90	7,140	3.35	25.2	129.8	
91	8,280	3.80	25.8	150.6	
92	9,090	4.12	26.2	165.4	
93	10,410	4.63	26.6	189.5	
94	11,640	5.12	26.9	212.0	
95	12,720	5.57	27.1	231.8	
96	13,530	5.95	27.0	246.7	

Net Leakage Reduced Data for Seal No. 2, Zero rpm, Argon Gas

Data Point No.	P_T μhg	P_b μhg	$1/N_K$	$\dot{N}/\Delta P$ x 10^{-14}
1	17,000	425	18.00	17.50
2	14,300	403	15.10	15.40
3	10,200	385	10.90	11.80
4	8,080	382	8.68	9.87
5	3,550	375	4.02	6.12
6	1,500	363	1.91	4.43
7	770	360	1.16	4.05
8	2,460	355	2.89	5.26
9	5,800	355	6.31	8.13
10	440	3.0	0.45	3.81
11	145	1.8	0.15	3.68
12	251	2.2	0.26	3.81
13	680	4.0	0.70	3.92
14	65,500	920	68.10	6.76
15	40,500	420	42.00	3.97
16	28,900	265	29.90	2.93
17	64	1.6	0.067	3.58

Net Leakage Reduced Data for Seal No. 2, Dynamic Speeds, Argon Gas

Data Point No.	P_T μhg	P_b μhg	$1/N_K$	$\dot{N}/\Delta P$ x 10^{-14}	c in. x 10^3
	2500 rpm, $\bar{c}$ x 10^3 = 3.94 in., $\bar{r}_p$ = 212.5				
1	21,200	140	20.70	13.90	3.95
2	15,700	101	15.20	10.00	3.91
3	11,000	83	10.40	6.88	3.83
4	9,000	77	8.62	4.81	3.87
5	6,200	70	5.95	3.10	3.87
6	4,670	68	4.68	2.35	4.03
7	3,240	66	3.27	1.55	4.03
8	1,850	65	1.89	0.888	4.03
9	29,200	235	28.50	21.10	3.95
10	42,900	395	42.40	33.90	3.99
11	73,000	978	72.40	63.70	3.99
12	1,180	2.1	1.11	1.14	3.83
13	222	0.6	0.20	1.02	3.71
14	97	0.45	0.093	1.017	3.90
15	59	0.40	0.055	1.014	3.79
16	12,450	53	12.10	7.63	3.95
17	2,840	6.0	2.67	1.77	3.83
18	1,410	2.4	1.33	1.15	3.83
19	952	1.7	0.92	1.09	3.95
20	505	1.0	0.48	1.01	3.83
	30,000 rpm, $\bar{c}$ x 10^3 = 3.51 in., $\bar{r}_p$ = 246.8				
21	132,500	1050	120.5	35.7	3.68
22	103,700	530	94.1	16.1	3.68
23	74,000	150	62.6	1.73	3.44
24	88,500	515	70.3	5.19	3.22

Net Leakage Reduced Data for Seal No. 2, Dynamic Speeds, Argon Gas

Data Point No.	P_T μhg	P_b μhg	$1/N_K$	$\dot{N}/\Delta P$ x 10^{-14}	c in. x 10^3
	5000 rpm, $\bar{c}$ x 10^3 = 3.92 in., $\bar{r}_p$ = 891.9				
25	29,800	200	29.40	15.6	3.99
26	44,500	360	43.50	28.2	3.95
27	78,800	1000	77.30	59.0	3.95
28	4,100	2.9	3.61	0.509	3.59
29	2,850	1.5	2.59	0.352	3.71
30	6,660	8.5	6.20	1.25	3.79
31	1,670	0.75	1.45	0.199	3.54
32	525	0.25	0.41	0.111	3.19
33	760	0.30	0.65	0.199	3.47
34	388	0.20	0.34	0.157	3.59
35	355	0.20	0.31	0.163	3.54
36	25,100	137	24.70	11.7	3.99
37	15,800	81	15.70	5.96	4.03
38	9,500	59	9.26	2.00	3.95
39	19,100	106	18.10	8.14	3.97
40	12,000	80	11.40	3.64	3.77
41	6,330	69	6.30	0.791	3.77
42	5,200	75	4.97	0.561	3.75
	10,000 rpm, $\bar{c}$ x 10^3 = 3.85 in., $\bar{r}_p$ = 1879.2				
43	17,100	70	16.3	1.11	3.87
44	27,800	109	26.8	5.72	3.91
45	33,500	135	31.9	8.55	3.86
46	23,100	115	21.8	3.23	3.83
47	7,150	0.6	6.61	0.0251	3.77
48	14,600	5.5	12.40	0.331	3.46
49	16,500	11.0	14.20	0.648	3.51
50	10,900	2.2	9.71	0.147	3.63
51	88,100	1000	87.10	52.7	3.99
52	44,400	265	42.80	16.5	3.91
53	36,100	180	34.80	10.7	3.91
54	66,000	550	64.50	33.0	3.95

Rarefied Sealing Coefficient Reduced Data for Seal No. 2, Argon Gas

Data Point No.	P_T μhg	P_b μhg	$1/N_K$	Λ	R_{e_c}	c in. x 10^3
	5000 rpm, $\bar{c} \times 10^3 = 3.92$ in.					
SP1	4,600	90	4.41	35.0	0.296	3.91
SP2	35,000	28,000	59.80	22.2	4.006	3.94
SP3	33,000	25,800	55.77	21.6	3.739	3.94
SP4	12,000	4,400	15.70	20.0	1.053	3.98
SP5	24,000	16,600	38.90	20.6	2.608	3.98
SP6	8,950	2,330	10.80	23.0	7.245	3.98
SP7	8,250	1,670	9.24	24.4	6.195	3.87
SP8	3,180	50	2.95	53.7	0.198	3.79
SP14	42,000	34,800	73.80	21.0	4.945	3.99
SP15	56,200	49,000	102.80	20.3	6.893	4.06
SP18	2,610	66	2.36	70.7	0.158	3.66
SP19	520	3.8	0.45	364	0.030	3.58
	10,000 rpm, $\bar{c} \times 10^3 = 3.86$ in.					
SP9	39,000	23,000	58.20	19.7	7.804	3.90
SP10	14,000	695	13.54	24.6	1.817	3.83
SP11	10,700	51	9.91	30.8	1.329	3.83
SP12	19,000	3,380	20.80	20.7	2.788	3.86
SP13	24,900	8,160	31.00	18.9	4.162	3.90
SP16	54,000	36,200	87.30	16.8	11.704	4.02
SP22	4,450	3	3.87	83.1	0.519	3.61
	30,000 rpm, $\bar{c} \times 10^3 = 3.23$ in.					
SP20	111,200	42,200	123.00	18.8	49.463	3.33
SP21	50,200	1.1	36.10	32.1	14.534	2.99
SP17	63,000	205	51.1	20.3	20.564	3.36

Continuum Sealing Coefficient Tabulation Viscoseal No. 2, Gas-Air

Data Point No.	Speed rpm	ΔP in. H_2O	Λ	R_{e_c}	c in. x 10^3
1	543	0.48	13.43	9.73	4.18
2	1,148	0.99	13.77	20.6	4.18
3	4,140	3.50	14.31	73.7	4.14
4	3,480	2.98	14.13	61.9	4.14
5	2,850	2.48	13.91	50.7	4.14
6	2,310	2.00	13.98	41.4	4.14
7	1,710	1.50	13.80	30.4	4.14
8	1,110	0.99	13.57	19.7	4.14
9	570	0.52	13.27	10.11	4.14
10	4,800	4.01	14.49	85.5	4.14
11	5,430	4.49	14.70	96.6	4.13
12	6,090	5.00	14.88	108.1	4.12
13	6,690	5.46	15.04	118.6	4.11
14	7,380	6.01	15.15	130.6	4.10
15	8,040	6.51	15.31	142.0	4.09
16	8,700	7.02	15.51	153.0	4.07
17	9,300	7.47	15.90	162.0	4.03
18	10,020	8.01	16.21	173.4	4.00
19	10,590	8.48	16.51	181.5	3.96
20	11,250	9.01	16.52	193.0	3.96
21	11,790	9.46	16.48	202.4	3.96
22	12,510	10.05	16.46	214.9	3.96
23	13,110	10.54	16.45	225.3	3.96
24	14,520	11.74	15.80	254.3	4.03
25	13,680	11.07	15.78	239.4	4.03

Continuum Sealing Coefficient Tabulation Viscoseal No. 2, Gas-Air

Data Point No.	Speed rpm	ΔP in.-H_2O	Λ	R_{e_c}	c in. x 10^3
			Test Date 9-2-70		
26	4,950	4.11	14.30	89.1	4.18
27	10,200	8.00	15.28	183.6	4.16
28	14,850	11.83	15.19	267.2	4.14
29	16,440	13.31	14.95	296.4	4.14
30	18,180	15.01	14.66	328.5	4.14
31	19,590	16.54	14.33	354.6	4.14
32	21,210	18.34	14.00	384.8	4.14
33	22,650	20.14	13.61	411.9	4.14
34	23,700	21.67	13.24	431.7	4.14
35	24,930	23.26	12.97	455.0	4.14
36	25,920	24.79	12.65	474.0	4.14
37	27,000	26.55	12.31	494.8	4.14
38	27,900	28.08	12.02	512.3	4.14
39	28,890	29.94	11.66	531.7	4.14
40	29,760	31.81	11.32	549.0	4.14
41	30,510	33.41	11.05	563.9	4.14
42	31,410	35.58	10.67	582.1	4.14
43	32,130	37.32	10.41	596.7	4.14
44	32,940	39.33	10.12	613.2	4.14
45	34,110	42.43	9.72	637.3	4.14